



**UNIVERSIDAD
DE ANTIOQUIA**

**THERMO-ECONOMIC ANALYSIS OF ENERGY
RECOVERY FROM MUNICIPAL SOLID WASTE
IN AN INTEGRATED PLASMA GASIFICATION
COMBINED CYCLE PLANT BY MODELING IN
ASPEN PLUS®**

Autor

Néstor Darío Montiel Bohórquez

Universidad de Antioquia

Facultad de Ingeniería

Medellín, Colombia

2021



THERMO-ECONOMIC ANALYSIS OF ENERGY RECOVERY FROM MUNICIPAL SOLID WASTE IN AN
INTEGRATED PLASMA GASIFICATION COMBINED CYCLE PLANT BY MODELING IN ASPEN
PLUS®

By:

Néstor D. Montiel Bohórquez, Mech. Eng.

Research work submitted as partial fulfilment of requirements for
MSc. Degree in Engineering

Advisor:

Juan Fernando Pérez Bayer, Ph.D.

Line of research:

Biomass as a Renewable Resource

Research group:

Group of Efficient Management of Energy

University of Antioquia

Engineering School

Medellín, Colombia

2021

A mis padres

A mis hermanas

A mi Carolina

Hay que tener mucho cuidado con lo que se cree saber, porque por detrás se oculta una cadena interminable de incógnitas, la última de ellas, probablemente sin solución.

Ensayo sobre la lucidez

Esta vez seré breve. Gracias UdeA, gracias Juan Fernando, gracias Francia, gracias Pedro Juan, gracias Esmeralda. Lo que han hecho por mí, lo llevaré en el corazón hasta el último latido.

Contents

1	<i>Municipal Solid waste and Plasma Gasification Overview</i> -----	8
1.1	INTRODUCTION -----	8
1.2	CONCEPTUAL FRAMEWORK -----	10
1.2.1	Municipal Solid Waste definition-----	10
1.2.2	Energy Recovery from MSW -----	11
1.2.3	Plasma gasification-----	13
1.3	OBJECTIVES -----	16
1.3.1	General objective-----	16
1.3.2	Specifics objectives -----	16
1.4	IMPACTS OF THE MASTER RESEARCH WORK -----	16
2	<i>Techno-economic assessment of syngas production by plasma gasification of municipal solid waste</i> -----	18
2.1	INTRODUCTION -----	18
2.2	MATERIALS AND METHODS -----	21
2.2.1	Municipal solid waste -----	21
2.2.2	Plasma gasification model of MSW.-----	23
2.2.3	Thermodynamic performance-----	26
2.2.4	Model validation-----	29
2.2.5	Simulation plan -----	30
2.2.6	Levelized costs of syngas as substitute gaseous fuel -----	31
2.2.6.1	Tax incentives for renewable energy projects in Colombia-----	32
2.3	RESULTS AND DISCUSSION -----	33
2.3.1	Model Validation -----	33
2.3.1.1	Validation with experimental data -----	33
2.3.1.2	Validation with numerical data -----	34
2.3.2	Strategy-1: Effect of plasma temperature and feedstock composition-----	35
2.3.2.1	Air mass flow and torch power consumption -----	35
2.3.2.2	Heating value, thermal power, and exergy of raw syngas-----	36
2.3.2.3	Cold gas (CGE) and exergy efficiencies (ExE)-----	38
2.3.3	Strategy-2: The maximum efficiency of Plasma-G process-----	40
2.3.4	Levelized costs of syngas as substitute gaseous fuel -----	43

2.3.4.1	Cost estimation of plasma gasification technology	43
2.3.4.2	Levelized cost of syngas production	45
2.4	CONCLUSIONS	49
3	<i>Exergoeconomic analysis of an integrated plasma gasification combined cycle for MSW energy recovery by modeling in Aspen Plus</i>	52
3.1	INTRODUCTION	52
3.2	METHODOLOGY	56
3.2.1	IPGCC power plant description	57
3.2.2	IPGCC power plant model description	58
3.2.2.1	Plasma Gasification model	60
3.2.2.2	Syngas treatment system model	60
3.2.2.2.1	Syngas cooling system	60
3.2.2.2.2	Fabric filter	61
3.2.2.2.3	Wet scrubber	61
3.2.2.2.4	Syngas compressor and syngas preheater	63
3.2.2.2.5	COS-hydrolysis unit and LTGC	64
3.2.2.2.6	MDEA absorption and sour water stripping system	64
3.2.2.3	Combine cycle and power generation model.	66
3.2.2.3.1	Gas turbine	66
3.2.2.3.2	HRSG and Steam cycle	68
3.2.3	Exergoeconomic assessment	71
3.2.3.1	Exergy analysis.	71
3.2.3.2	Exergoeconomic model	74
3.3	RESULTS AND DISCUSSION	78
3.3.1	Plasma gasification operative parameters	78
3.3.2	Exergy analysis	79
3.3.3	Exergoeconomic analysis.	83
3.4	CONCLUSIONS	90
Appendix A.	<i>Productive structure of the IPGCC power plant and the four propositions of TEC methodology.</i>	93
Appendix B.	<i>Properties of streams in the IPGCC power plants.</i>	95
Appendix C.	<i>Rate of exergy destruction, exergy cost and unit exergy cost in the IPGCC power plants.</i>	100

Appendix D. Cost equations and results from exergoeconomic analysis. -----106

4 References-----110

Municipal Solid waste and Plasma Gasification Overview

1.1 INTRODUCTION

Currently, the management of municipal solid waste (MSW) is an important issue for the worldwide population due to its continued increase in generation rate. The global generation of MSW was ~1300 million tons in 2012, with an average per-capita generation rate of 1.2 kg/inhabitant-day. Furthermore, estimations indicate that the global production of MSW will reach ~2200 million tons in 2025 [1][2]. The increase in the generation rate of MSW is directly linked with the urban population and richness. Likewise, more than half of the global population occupies urban areas and its annual increase is ~1.5% [3][4]. Although the per-capita MSW generation rate in developed countries is higher than that of developing ones, the estimations indicate that both generation rates will be similar in the coming decades [5]. To face the problems associated with MSW disposal, the efforts have been focused on developing comprehensive programs of MSW management, in which the waste is considered as a resource or feedstock, but not a problem [2]. According to European strategy, an adequately waste management must accomplish with a group of hierarchy activities such as (i) reduce (ii) reuse (iii) recycle, (iv) recovery, and (v) landfill to manage efficiently MSW disposal (Figure 1) [6], [7].

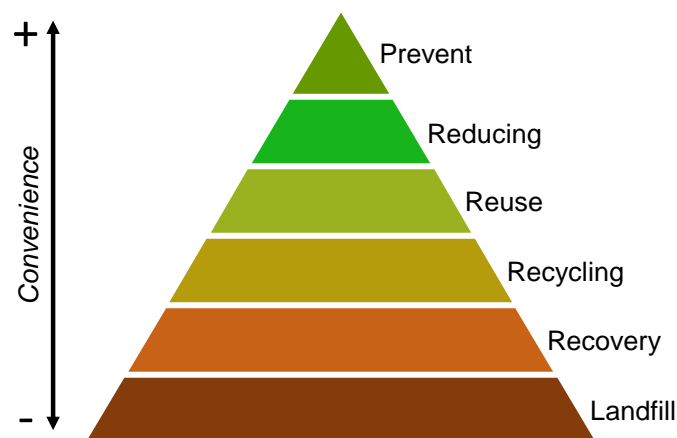


Figure 1. Activities hierarchy to manage efficiently MSW disposal [6], [8]

In Colombia, MSW generation reached ~30100 tons/day in 2017, which represents an increase of 13% with regard to 2010. Thereby, the average rate has increased at ~2% yearly [9]. The country recycles only 17% of total MSW and this recycled material is used in the productive system. The remaining 83% is disposed in landfills and other inappropriate disposal-sites or methods (open dump, waterbody, water streams, burial, open burning, etc.) [10]. The growth and development level of the main Colombian cities in recent years has led to enhance MSW management and disposal. Public policies have been created to promote MSW integrated management programs, leading to an increase in the amount of well-design and less environmental-harmful sanitary landfills, as well as to decrease the use of open-dumps. Nevertheless, according to international standards, some new landfills can only be considered as controlled dumps, because they have an operating deficiency and do not match the requirements to be a landfill [2], [10], [11]. Landfills are land areas in which MSW are safely disposed, to reduce environmental impact by means of biogas and leachable recovery [12]. Complex and expensive emissions control, large land areas requirement, long-time degradation of waste, and low acceptance of the population due to the social problems and health risks are some of the main disadvantages of sanitary landfills [13].

The trends of MSW production in Colombia (~30100 t/day) and the lack of space for landfills indicate that management dynamics of MSW must be improved by increasing recovery strategies, seeking to avoid sanitary emergencies by 2030, as well as high greenhouse gases (GHG) emissions [10]. Currently, 39% of licensed sanitary landfills of the country have expired or have less than 3 years lifespan [9]. The first alternative to counteract the low life span of landfills is to open new ones. Nevertheless, opening new landfills involve negative impacts, such as water source contamination and human health affectation [14]. Therefore, the government entities must design new policies seeking to diminish the MSW disposal in sanitary landfills. Consequently, the implementation of sustainable technologies with a high MSW recovery rate are favoured [14], [15].

In the United Nations Climate Change Conference (COP 21) carried out in 2015, Colombia committed to reducing by 20% the projected GHG emissions for 2030. A driver of this goal is looking for reducing the environmental negative impact of cities associated with MSW production and its disposal [10]. A strategy to improve the waste management is the energy recovery by means of incineration or gasification, which has lower environmental affectation than landfill disposal [13], [16], [17], and contributes to employment generation [17]. Furthermore, the energy recovery contributes to diversifying the national power generation mix, which mainly depends on hydroelectric power plants (~70%) which capacity is susceptible to weather events, such as *El Niño* phenomenon [18].

The power potential of MSW produced in Medellin city (the second most important city of the country) is from 27.7 MWe to 44.4 MWe. This power could satisfy the needs of 53000-85000 homes [19]. The waste to energy (WtoE) projects are driven by governmental policies such as National Power Plan from Colombia proposed by the Mining-Power Planning Unit (UPME, Spanish acronym). The aim is to diversify the national energy mix [20]. Another driver is the 1715 renewable energies law, approved in 2014, in which tax incentives for renewable energy projects are defined. The energy content of non-recyclable MSW is considered as a renewable energy source in the 1715 law. Therefore, WtoE projects using MSW could profit from these tax incentives [21]. Nevertheless, the energy recovery from MSW by thermochemical processes has the highest specific cost (98-130 USD/t of MSW) [22], whereas landfill disposal has the lowest one (68 USD/t of MSW¹). This difference is related to the fact that the landfill is still the main pathway to MSW disposal in the country [2], [10]. However, by analysing the WtoE projects feasibility using MSW as a feedstock under tax incentives and exemptions of 1715 renewable energies law, the incineration, and gasification technologies reached a lower levelized cost of electricity (38.73 and 58.17 USD/kWh, respectively) than anaerobic digestion (108.85 USD/kWh) or landfill gas (118.83 USD/kWh)[18].

In this research work it was studied the techno-economic performance of an integrated plasma gasification combined cycle plant (IPGCC) using MSW as a feedstock, due to the increasing production of MSW in the country, the low availability of land for landfills, as well as the need to diversify the energy mix, During the development of the work, the following research questions were answered:

- Is it possible to model an IPGCC plant using the thermochemical equilibrium approach in order to assess its techno-economic performance?
- How accurate is the proposed model regarding reported data in specialized literature?
- What is the techno-economic performance of an IPGCC plant processing MSW, as a function of operating parameters and Colombian economic legislation?

1.2 CONCEPTUAL FRAMEWORK

1.2.1 Municipal Solid Waste definition

MSW is any non-liquid substance derived from human activity, which is discarded as a useless product [23]. MSW is a heterogeneous product whose composition and properties mainly depend on the socioeconomic and climatic factors of the place where it is produced [24]. MSW term covers organic and inorganic

¹ Estimated as average value from [157].

compounds, such as food waste, plastic, gardening waste, textile, leather, glass, paper, metals, etc. [25], [26]. The highest fraction of MSW comes from the residential sector, although MSW is also produced from industrial, commercial, and institutional sectors [27]. Physical and chemical properties of MSW are crucial factors that affect the performance of energy recovery processes. MSW small particulate size and high density are desired since they result in small system size and short conversion time. Furthermore, other MSW properties such as high calorific value, low moisture, and ash contents, as well as low content of polluting compounds precursors (such as sulphur and chlorine) have a positive effect on the energy recovery process performance [26], [28]. In order to enhance MSW properties as feedstock for WtoE projects, upgrading pre-treatments are a common practice. Those pre-treatments can involve separation, drying, shredding, and even densification to produce refuse-derived-fuel (RDF) for energy recovery via thermal conversion [29].

1.2.2 Energy Recovery from MSW

MSW recovery could be achieved by means of energy and non-energy pathways. Non-energy routes include reusing and recycling, while the energy routes cover biochemical and thermochemical processes (Figure 2). The organic matter of MSW is broken down by microorganisms and/or enzymes in biochemical processes. Generally, the biochemical conversion is applied to process wastes with high contents of degradable organic matter and moisture [8], [12]. There are two widely used biochemical methods, anaerobic digestion (AD) and ethanol fermentation (EF) [26]. In AD processes, the organic matter is decomposed in absence of oxygen, with the aim to produce a gas mixture known as biogas, which is typically composed of 50-75% CH₄, 25-50% CO₂, and 1-15% other gases (H₂O, NH₃, H₂S, etc.). The microbial reaction involved in AD processes has typical times of 20-40 days [12]. Meanwhile, EF process is a biochemical reaction involving sucrose hydrolysis and sugars fermentation, whose target is bioethanol production by means of several food wastes processing [26].

Through thermochemical processes of MSW, such as incineration, gasification, and pyrolysis, MSW can be transformed into heat, electricity, fuels or chemical products by applying high temperatures [8]. Thermal conversion is typically applied to process feedstocks with low moisture content and high fraction of non-biodegradable organic matter [12]. The main advantages of thermal process application for energy recovery from MSW is the high volume and mass reduction in a relatively short time [26]. Incineration is the most widely used process for MSW energy recovery [12] due to its capability to process waste with heterogeneous composition [30]. Incineration technologies have lower pollution, higher energy potential, and higher waste volume reduction than landfill disposal [31]. According to results presented by Kaplan *et al.* [32], the CO₂ equivalent emission from land fill gas energy recovery ranges from 3.40 to 8.25 MTCO₂.

eq/MWh , while that of incineration is $0.64 \text{ MTCO}_{2\text{-eq}}/\text{MWh}$. Nevertheless, some disadvantages have been attributed to an incineration process, such as residuals ashes with potentially damage soil and water, and release of dangerous pollutants for public health (NO_x , SO_x , HCl , particulate matter, dioxins, and furans) [12], [30].

The gasification process transforms the organic matter and fixed carbon of MSW into a gaseous mixture known as syngas, which is mainly composed of H_2 , CO , CH_4 , and CO_2 . Also, tars ($<0.1 - 10 \text{ g/Nm}^3$), inorganic compounds (H_2S , HCl , NH_3 , HCN , HF , alkaline), and particulate matter ($0.01 - 100 \text{ g/ Nm}^3$) are produced in a negligible amount. The gasification process is recognized as a flexible process concerning incineration since the produced syngas can be used as a gaseous fuel to produce electricity, heat, or raw material for the chemical industry [30], [31], [33]–[36]. Besides, syngas can be burned in high-efficiency devices such as internal combustion engines (ICE), gas turbines, or fuel cells. Thus, this technology has a great adaptation capability for power generation in isolated areas in developing countries [30], [36]. Currently, MSW gasification can be achieved by several types of autothermal reactors, known as the fixed bed (downdraft and updraft), fluidized bed (bubbling and circulating), or entrained flow gasifier. Moreover, the plasma gasification is a novel allothermal process, that is increasingly considered for MSW gasification [30], [34], [37]. The main disadvantage of autothermal gasification is its limited control on syngas quality and tars production rate [38].

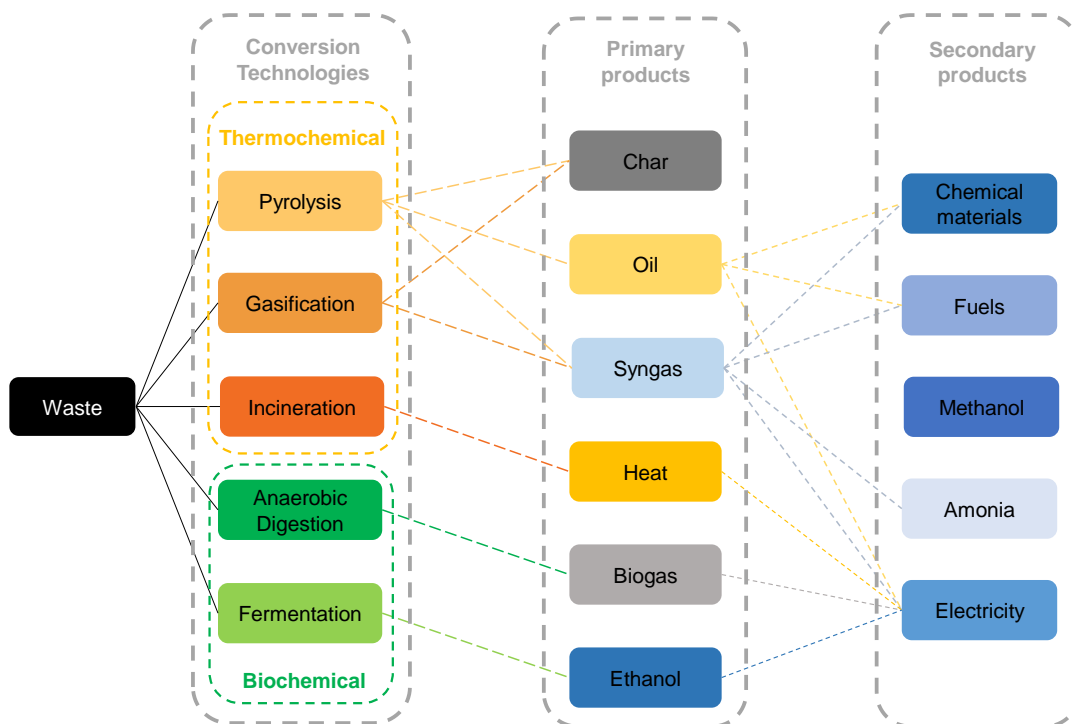


Figure 2. Energy recovery routes and possible products [8], [12], [26].

1.2.3 Plasma gasification

Plasma gasification (Plasma-G) is an advanced and eco-efficient thermochemical process, in which organic matter is thermally decomposed by a plasma jet in useful syngas and inert slag [39], [40]. Comparing Plasma-G to autothermal gasification, Plasma-G is advantageous due to its high material yield, dynamic response, compactness, and flexibility [41]. Plasma-G process consists of four stages, namely i) fast solid particulate heating by plasma jet, ii) “explosive” volatile compound release, iii) fast gasification of homogeneous phase, with mass and heat exchange, and iv) char gasification by reaction with gaseous species [42]. The external power source of Plasma-G allows reaching high temperatures, giving a set of important features to the process, such as: a) high syngas quality due to high concentration of CO and H₂, as well as low tars production; b) low production of human health-harmful emissions, such as dioxins and furans; c) high syngas composition control and high flexibility, and d) inorganic matter melted and converted into inert and non-toxic slag [41], [43], [44].

Plasma, commonly known as the fourth state of matter, is an ionized gas created when enough amount of energy is supplied to a gas stream increasing the gas temperature and its kinetic energy, which leads to release electrons from atoms and molecules [43], [45], [46]. The most common sources to supply the energy required for the plasma are electricity, thermal energy, UV light, and microwaves [44]. The plasma is classified into two groups as a function of temperature values: high-temperature plasma (HTP) and low-temperature plasma (LTP). In HTP, ions, electrons, and neutral molecules are in thermodynamic equilibrium. On the other hand, LTP involves two subcategories known as cold plasma and thermal plasma. The latter being the most suitable for MSW treatment. The thermal plasma reaches a quasi-equilibrium state with a high density of electrons and temperatures between 2000 and 30000 °C [44], [47]. Thermal plasma can be generated by energy transfer to gas through direct current (DC plasma), alternating current (RF plasma), or microwaves (McW plasma) [42], [44]. Additionally, several reactor types have been developed for plasma gasification, such as fixed/moving bed, entrained flow, and spout/spout fluid bed plasma reactors. Further information about plasma gasification reactors is presented by Tang *et al.* [42].

For DC plasma generators, the gas stream flows between two electrodes (cathode and anode). A direct current (up to 10000 A) is applied to gas-plunged electrodes generating a high voltage difference. The energy applied as electricity is transfer to the gas stream increasing its temperature and kinetic energy, which leads to the ionization of the gas and the formation of the plasma jet. [44]. The, the plasma jet is used to thermally decompose the organic matter into syngas and slag. Plasma jet stabilization is carried out by two methods, by the use of an external magnetic field or by controlling the gas flow rate [48]. DC plasma generators are classified in two kinds, DC transferred generators and DC non-transferred generators

(Figure 3). In DC transferred generators, one of the electrodes (usually anode) has a large separation with respect to the cathode. This configuration allows working with extremely high thermal flux towards the material melting and slag vitrification processes. At the same power level, DC transferred plasma generator needs a lower plasma gas flux than DC non-transferred generator. Further, DC transferred generator has heating efficiencies higher than 90% [49]. Conversely, the electrodes (cathode or anode) of DC non-transferred generators are not involved in the material processing, the electrodes just have the function of plasma generation. DC non-transferred generators are popular because of their capability to generate a high-temperature and high-speed plasma jet (up to ~ 12000 K and 600 m/s, respectively) [48], [49].

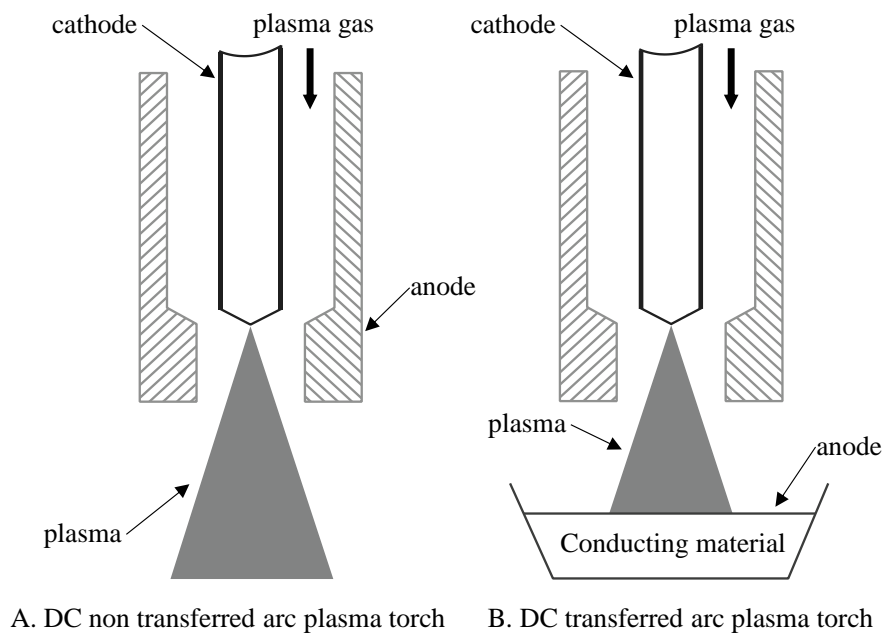


Figure 3. Schemes of DC plasma generators [48].

RF (Radiofrequency) plasma generator is shown in Figure 4. The electrodes in the RF plasma reactor are on the outside surface as a coil, and the gas is sent into the reactor. Energy applied to coil ionizes the gas and plasma is formed inside the reactor [44]. Since plasma gas is not in contact with electrodes, the contamination possibility is avoided and, consequently, the electrode erosion is minimized [42]. RF plasma generators are able to work with different nature gases, such as inert, oxidizing, or reducing atmosphere, with input power ranges from 30 kW to 1 MW [49]. The main disadvantages of RF plasma generators are the difficulty to ignite the plasma and the effect of solid material feeding on plasma stability [48].

McW plasma generator creates plasma by injection of microwave power. This method does not need electrodes and its voltage requirement is lower than the ones for DC or RF plasma generators.

Electromagnetic radiation in the frequency range of 300 MHz – 10 GHz (typically 2.45 GHz) can be considered for McW plasma generation. The main advantages of McW plasma generation are low power and low voltage requirements, high effectiveness and ionization level, and simple and robust reactor design.

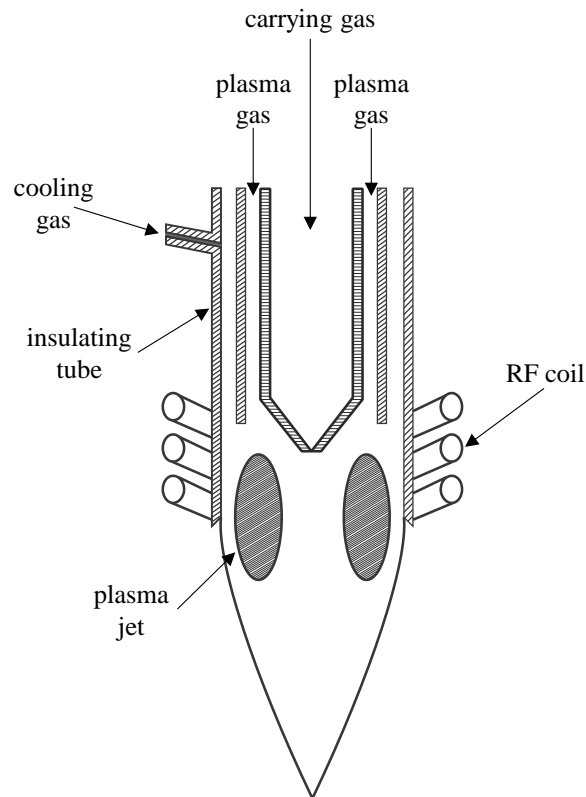


Figure 4. RF plasma generator scheme [42]

There are several configurations of McW plasma generators, such as the cavity induced plasma, the free expanding atmospheric plasma torches, the electron cyclonic resonators, and the surface wave discharges [42], [44]. A scheme of cavity induced plasma torch is presented in Figure 5. Although all above plasma technologies have been studied in the last time for MSW treatment, at the pilot/commercial level the predominant one is the updraft moving bed reactor using DC non-transferred torches [42], due to the fact that this reactor has a simple design and manufacturing, high stability of torches, and torch availability with input power up to 6 MW [42], [45], [49].

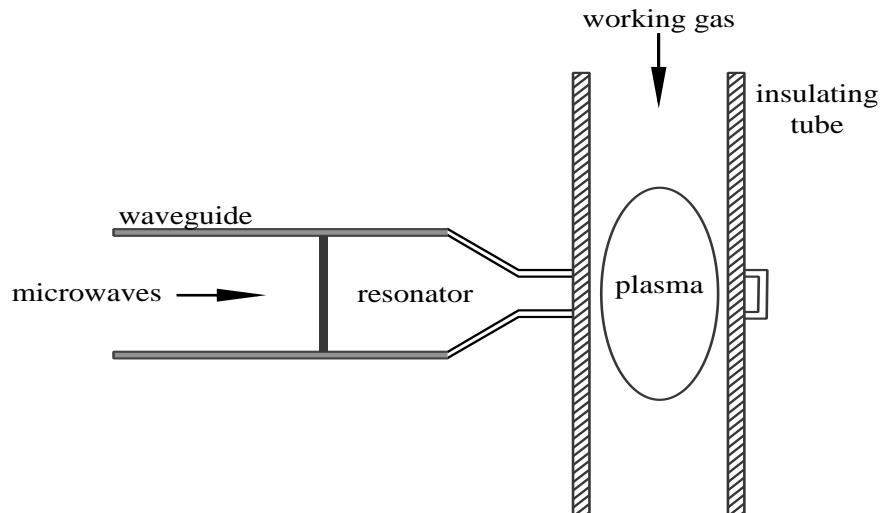


Figure 5. Schematic diagram of McW plasma generator [42].

1.3 OBJECTIVES

This master's research work, in which the techno-economic performance of an IPGCC planta processing MSW was studied, ties in with the energy and solid waste management policies that are implanted and proposed in Colombia; moreover, this process has operating and environmental advantages regarding autothermal gasification and incineration of MSW. Since techno-economic assessment of IPGCC plant has not been carried out in the national context the following objectives are proposed.

1.3.1 General objective

To assess from a techno-economic point of view the energy recovery from MSW through IPGCC plant by modelling in Aspen Plus™ software.

1.3.2 Specifics objectives

- To implement a model of IPGCC plant using the Aspen Plus™ software.
- To determinate the model accuracy by comparing with reported data in specialized literature.
- To assess the effect of critical parameters on the IPGCC plant performance.
- To carry out an exergoeconomic analysis on the IPGCC plant.

1.4 IMPACTS OF THE MASTER RESEARCH WORK

This work is developed looking for impact on the following aspects:

Scientific: A professional with a Master's degree in Energy with solid knowledge about energy systems and renewable resources is formed to help the university and the country to overcome current energy issues.

Environmental: Energy recovery from MSW through IPGCC plant contributes to the elimination of a huge volume of MSW having a lower environmental impact than other options such as incineration or landfill.

Social: Energy recovery from MSW through IPGCC plant avoids the landfilling and associated social problems such as bad odour and human health risks.

Technological: The development of accurate models allows obtaining reliable preliminary results, which are very important for initial studies on the techno-economic feasibility of advanced systems for MSW treatment.

Techno-economic assessment of syngas production by plasma gasification of municipal solid waste

Abstract

The energy recovery from different municipal solid wastes (MSW) by updraft plasma gasification process to produce syngas as substitute gaseous fuel is assessed from a techno-economic viewpoint. This study is conducted with an implemented model under a thermo-chemical approach using Aspen Plus. The model has been validated with experimental data reaching an average relative error of 17.86%. The plasma torch power consumption is one of the main process parameters that affect the energy and exergy efficiencies. Despite the moisture content of MSW increases (26.61% to 57.9%), the energy and exergy efficiencies increase on average 1.5% and 5.4%, respectively, which is ascribed to the reduction of torch power consumption; this behavior was because MSW dry fraction to be thermally degraded by the torches decreased. Whereas, if plasma temperature increases (2500°C to 4000°C), the gasification efficiencies diminish because of the torch power consumption increases by 28.3%. Furthermore, the process parameters combinations (air flow and plasma temperature) are found, which allow reaching the highest process efficiency, which is ranged from 79.22% to 83.46%, highlighting the plasma gasification flexibility. The levelized cost of syngas production varies from 13.19 to 22.95 ¢US\$/kWh. Therefore, a waste disposal charge is proposed to make these projects feasible, which must be ranged between 11.25 and 23.56 ¢US\$/kWh.

2.1 INTRODUCTION

The increasing production rate of municipal solid waste (MSW) is directly linked to urban populations and their incomes. Currently, more than a half of the global population occupies urban areas and its annual increase is ~1.5% [4]. Although per-capita the MSW generation rate in developed countries is higher than that of developing ones, the estimation indicates that both generation rates will be similar in the coming decades [5]. To face problems associated with MSW disposal in landfills, such as large land use, greenhouse gas (GHG) emissions, groundwater pollution, and environmental risk to human health [50], efforts have been focused on developing integral MSW management programs, where the waste is considered as a

resource or feedstock instead of a problem [2]. Nevertheless, in most of the developing countries the main MSW disposal pathway is still the landfill.

In Colombia, the average production rate of MSW was ~30100 tons/day in 2017, with an increase of 13% as to 2010 [9]. In 2020, only 17% of total MSW produced in the country is being recycled, while the remaining 83% is disposed in landfills. The actual and projected waste production trends indicate that if the dynamics of waste production and its management do not change, the useful life of landfills will end by 2030 leading sanitary emergencies in the big cities of the country [10]. Furthermore, in the frame of COP21 conference, Colombia has committed to reduce by 20% the projected GHG emissions by 2030. One of the driver of this reduction agreement is to diminish the negative environmental impact of cities attributed to MSW production and final disposal [10]. The waste to energy processes are pathways for energy recovery of MSW with lower environmental negative impact than landfill disposal [13], [16], [17]. Furthermore, energy recovery by MSW contributes to generate employment [17], and to diversify the national energy mix [18].

Energy recovery from MSW can be achieved by means of biochemical and thermochemical pathways. Long-standing waste-to-energy processes involve fermentation, digestion, incineration and gasification [51]. Incineration is the most widely used process for recovering energy from MSW [12], because of its processing capacity of waste with heterogeneous composition [30]. The performance of incineration technologies has associated lower pollution, higher energy potential, and higher waste volume reduction than landfill disposal [31]. Nevertheless, some disadvantages have been attributed to incineration processes, such as residuals ash with soil and water damaging potential, and release of dangerous pollutants emissions for public health such as NO_x, SO_x, HCl, particulate matter, dioxins, and furans [12], [30]. A novel pathway to reclaim energy from MSW is the plasma gasification. Plasma gasification (Plasma-G) is an allothermal process where the plasma jet is produced by an external energy source. Plasma-G thermally breakdowns organic matter in a limited-oxygen environment to produce a gaseous fuel, which is known as syngas [43]. The use of the external energy source provides important features to Plasma-G such as syngas quality improvement, low concentration of tars, high flexibility to feedstock properties (heterogeneous solid fuels), low release of dioxins and furans, and capability to transform the inorganic matter in a non-leachable and non-toxic slag [43], [44], [52].

Thermodynamic analyses of Plasma-G process as a pathway for energy recovery from MSW and biomasses, using thermochemical equilibrium models, have been presented in previous works. Minutillo *et al.* [43] reported a maximum thermal efficiency of Plasma-G process of 69%, using refused derived fuel (RDF) and air as gasifying agent. This assessment was conducted by a thermochemical equilibrium model using Aspen Plus software, considering heat and mass exchange phenomena between solid and gaseous phases. That

model has been used subsequently for several researches as a study base or starting point for analysing the Plasma-G process [53]–[57]. Janajreh *et al.* [55] by comparing the thermodynamic performance between Plasma-G and conventional air gasification processes reported that the average process efficiency of Plasma-G was 42%, while the one of conventional gasification was 72%. The lower Plasma-G efficiency than that of air-gasification is associated to power supplied to the plasma torches. Mazzoni and Janajreh [56] characterized the Plasma-G of MSW with plastic solid waste (PSW) using as plasma-gas mixtures of air-oxygen or air-steam on Integrated Plasma Gasification Combined Cycle plant (IPGCC). The better performance of MSW Plasma-G was reached when air was used as plasma gas. Whereas, the highest performance of IPGCC plant was reached using pure oxygen as plasma gas and feeding as feedstock a 70%MSW-30%PSW mixture. Zhang *et al.* [58] carried out energy and exergy analyses of solid waste treatment by Plasma-G. A steady state model was implemented, considering four sub-models to simulate drying, pyrolysis, char gasification and plasma melting. Analysing the raw syngas with tars as output parameter, the energy and exergy efficiencies were 98.4% and 86.5%, respectively. While, analysing the clean syngas (without tars), the efficiencies were 50.8% and 44.9%, respectively. The high yield reached with the raw syngas is ascribed to heating value of tars, which is not accounted in the clean syngas. The performance of hydrogen production from biomass Plasma-G with steam injection was studied by Favas *et al.* [59]. The low reactor temperature and steam injection were found as favourable conditions to rich-hydrogen content in syngas, whilst, an adverse condition was the increase of the equivalence ratio.

Works that address the fuels production via Plasma-G processes from the techno-economical point of view are scarce [60]–[62]. Galvita *et al.* [60] assessed the rich-hydrogen syngas production by pulverized coal plasma gasification at laboratory scale. The better quality of syngas was reached using steam as gasifying agent, where H₂ plus CO concentration varies from 30% to 40%. Furthermore, the cost of syngas production obtained in this study was ~189 ¢US\$/t of syngas, which was 8.6% lower than the cost of synthesis gas from natural gas reforming. Clark and Rodoff [61] carried out a feasibility study of a Plasma-G plant fed with MSW in Marion city. For a feedstock feeding rate of 300 t/day and producing syngas as a substitute fuel, the selling price estimated for the substitute gaseous fuel was ~0.01 ¢US\$/kWh, which was 30% lower than that of natural gas. Meanwhile, Byun *et al.* [62] analysed a system integrated by plasma gasifier of solid waste, and by H₂ recovery unit to produce high-purity H₂. The plant was able to process 1.2 t/day of paper mill waste, and to produce 20 Nm³/h of high-purity H₂ (>99.99%). The production cost of H₂ was about ~0.58 ¢US\$/kWh, which was higher than the one reached by using coal as feedstock (0.03 ¢US\$/kWh). In this work, this deep production cost difference is obtained because the cost of coal as feedstock was not considered, nor the size difference between two systems. On the other hand, the levelized cost to produce syngas (LCOS) from waste tire/wood co-processing was assessed by Zang *et al.* [63]. LCOS values were from

0.33 to 0.60 ¢US\$/kWh, that were lower than the market price of natural gas. Furthermore, fixed bed gasification showed better economic indicators with respecting fluidized bed, even though the worse energy performance of the former.

In this work, the assessment from technical and economical viewpoint of syngas production through MSW plasma gasification is carried out. A new equilibrium model of Plasma-G process is proposed using Aspen Plus software, with the aim of analysing the effect of five types of MSW produced in Medellin-Colombia on the thermodynamic performance of the Plasma-G, and on the levelized cost to produce syngas as a substitute gaseous fuel in the Colombian context.

2.2 MATERIALS AND METHODS

The methodological pathway followed to carry out the thermo-economic assessment of syngas production via MSW Plasma-G is presented in this section. First, the amount and estimations of generation rate of MSW produced in Medellin-Colombia is described; as well as the physical and chemical composition of MSW is determined based on information from academic and government institutions, and specialized literature. Second, the detailed model description to simulate MSW Plasma-G process in a fixed bed updraft reactor is described. The model is implemented in Aspen Plus following the process sequence by using Aspen Plus built-in blocks. Moreover, the main operative features and hypothesis considered for developing the model approach are described. Third, the thermodynamic parameters (energy and exergy analyses) that characterize MSW Plasma-G process are described. Fourth, a detailed description of the model validation is presented. And finally, the simulation plan is described in order to carry out the thermodynamic assessment, as well as the economic analysis associated to the levelized energy costs of syngas production as a gaseous fuel substitute.

2.2.1 Municipal solid waste

Five types of MSW produced in Medellin-Colombia were taken into consideration to study the thermo-economic performance of syngas production by Plasma-G. In this city (the second most important of the country), the average generation rate of MSW was ~1970 t/day (TPD) in 2019 [64]. MSW is composed by wastes from different sectors, such as residential (74.5 wt%), commercial (11.8 wt%), industrial (7.9 wt%), and institutional (5.8 wt%). Only about 16% of produced MSW is recycled, and the remaining waste is disposed in the landfill named “*La Pradera*”, which is located 57 km from the city [65]. According to Center for Clean Air Policy [2] the collection coverage of MSW in Medellin is 100%. In general, the chemical and physical composition of MSW are different for each sector [64]. In Table 1 the physical composition of MSW

from each sector that makes up MSW from the city is presented. Herein, the inert wastes as glass, metal, and dangerous wastes were excluded from the waste to energy project (MSW Plasma-G) [50], [66]. The physical composition of MSW fraction suitable for energy recovery, and the ultimate and proximate analyses presented in Zhou *et al.* [67] have been considered to estimate the dry base ultimate and proximate analyses of the four wastes types (sectors) and MSW mixture produced in Medellin city.

The properties of urban solid wastes, for instance, physical composition and moisture content, depend on factors such as income level, habits, weather, and recycling actions. The moisture content of MSW from Medellin neither has been determined nor reported. Therefore, in this work, the moisture content of wastes produced in Sao Jose dos Campos-Brazil as the moisture content of MSW from Medellin are considered [68]. This hypothesis is suitable due to the similarities between both cities and considering that they belong to the same region (South America). The ultimate and proximate analysis on dry basis, and the moisture content of MSW from Medellin are presented in Table 2.

Table 1. Physical composition of MSW from Medellin for each sector [wt%] (Adapted from [69], [70]).

Component	Residential	Institutional	Commercial	Industrial
Ordinary waste	17.96	42.10	38.41	43.7
Organic matter	59.60	32.55	29.84	20.53
Plastic	8.23	12.15	13.40	14.57
Cardboard	2.16	2.16	4.15	6.01
Textile	2.42	0.19	0.97	3.12
Wood	0.41	0.79	1.96	2.88
Paper	3.38	4.58	2.77	2.87
Dangerous	0.69	0.81	0.98	2.82
Glass	2.77	3.25	5.26	1.53
Especial	1.59	0.73	0.70	1.17
Metal	0.82	0.72	0.60	0.79
Total	100	100	99	100

Table 2. Ultimate and proximate analyses of MSW produced in Medellin-Colombia.

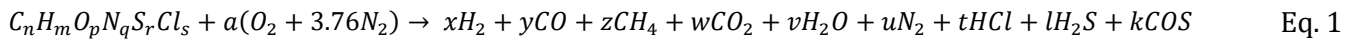
MSW type (by sector)	HHV _{wb} [MJ/kg]	Ultimate analysis (wt% dry base)						Proximate analysis (wt% dry base)			MC (wt%)	O/C [mol. rat.]	(F/A) _{stq}
		C	H	O	N	S	Cl	FC	VM	Ash			
Residential	8.55	53.01	6.91	36.85	2.65	0.34	0.24	12.36	77.53	10.11	57.90	0.52	0.146
Mixture	10.12	53.64	7.03	36.37	2.38	0.32	0.26	11.90	78.49	9.61	51.33	0.51	0.143
Institutional	13.42	55.04	7.04	36.16	1.41	0.26	0.09	10.93	80.73	8.35	37.92	0.49	0.140
Commercial	15.10	56.05	7.47	34.61	1.47	0.26	0.15	10.19	81.38	8.43	32.95	0.46	0.134
Industrial	16.41	54.98	7.43	34.70	1.87	0.35	0.67	10.82	81.58	7.60	26.61	0.47	0.136

wb: wet base

The approach to calculate the chemical composition of MSW is presented by Montiel-Bohórquez and Pérez [19]. It is worth note that the composition on dry basis of the different types of wastes is similar. Nevertheless, the main difference is the moisture content, which reaches values up to 57.9% for residential sector, 51.33% for mixture of all wastes, 37.92% for institutional sector, 32.95% for commercial sector, and 26.61% for industrial sector.

2.2.2 Plasma gasification model of MSW.

The relatively high temperatures involved in the Plasma-G process allows the hypothesis that the kinetic barriers are minimized and the syngas composition approaches to the equilibrium [43], [71]. Therefore, the Plasma-G process can be successfully modeled under a thermo-chemical equilibrium approach, whilst the hydrodynamic phenomenon of reactor is neglected [53], [57], [59], [72], [73]. Here, the syngas composition and torch power consumption associated to MSW Plasma-G, as well as energy and exergy efficiencies of the process are estimated. To this aim, a thermochemical equilibrium model of a moving bed updraft plasma gasifier, which works at atmospheric pressure (see Figure 6) is implemented using Aspen Plus software® - v10. The model is based on the following hypothesis: steady state process, perfect-insulated reactor [55], perfect mixing inside the reactor [74], no tar formation due to the higher reaction temperature [43], the gasification reaction reaches the thermo-chemical equilibrium due to the long residence time of both phases (solid and gas) [53], the global gasification equation modelled is presented in Eq. 1 [43].



In the moving bed updraft plasma gasifier, the solid waste is fed through an input port located at the top of the reactor. Thus, the solid absorbs energy from the gaseous phase (syngas) as the waste travels from the top to the bottom, while the syngas flows from the bottom to the top (Figure 6). The drying process of MSW is conducted when its temperature reaches 110 °C, which leads to evaporate the moisture that is mixed with the syngas [43], [53], [55]. Downstream (from top to bottom), the dried solid continues being heated by the gaseous phase until the waste reaches the stage of high energy-density (plasma), where plasma jet impacts the solid phase, and consequently, it is thermally degraded for producing the syngas and slag. Considering the temperature distribution inside plasma reactor, the gasifier can be classified in two gasification zones [43]; for instance, high temperature zone (HTZ) and low temperature zone (LTZ). This approach has been used in previous plasma gasification works [43], [53]–[55], [75]. Nevertheless, in this work, a new model is proposed and developed. Regarding the previous models presented in above-mentioned works, some modifications were implemented seeking a closer representation of the real process. The contributions implemented to the model in this work are listed, as follows: 1) The energy required to dry MSW has been

included in the process energy balance. This drying energy is composed by heating process of MSW up to the drying temperature (110 °C) for evaporating the moisture. 2) The convective heat transfer (heating) between gaseous phase and MSW after the drying process has been considered up to MSW reaches the plasma zone. 3) The inorganic fraction of MSW has been considered for thermochemical equilibrium calculations of Plasma-G process.

The flowsheet implemented in Aspen Plus is depicted in Figure 7. The Peng-Robinson equation of state have been used to estimate thermal and physical properties of conventional components and streams involved in the model [73], [74], [76]. Furthermore, HCOALGEN and DCOALIGT were used to estimate thermal and physical properties of non-conventional components, which are not included in the Aspen Plus’s database (e.g. MSW) [57]. Stream of raw (wet) MSW is fed to an RYield reactor as a non-conventional component (DRYER) to simulate the drying process of MSW [77].

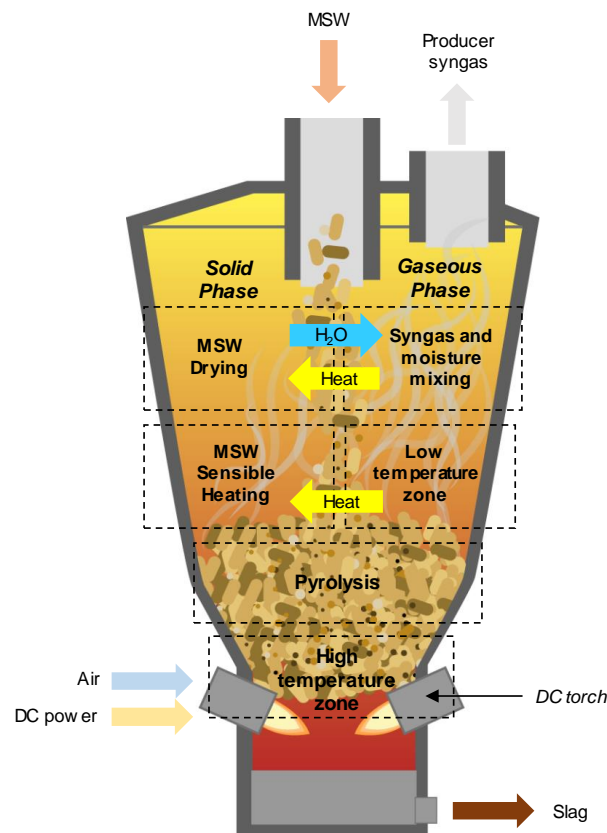


Figure 6. Moving bed plasma gasifier scheme with considered solid phase-gaseous phase interactions.

In DRYER block, the yield distribution is specified according to moisture content of raw feedstock given by the proximate analysis. The heat transfer between solid and gaseous phases to simulate the drying process of MSW is modelled by a Heater block (HEX-3). HEX-3 uses the heat stream (HEAT-DRY) as energy source,

which is produced by reclaiming the thermal energy to the syngas before the mixing with the moisture (MIXER). This first model stage simulates MSW feeding process and its drying, which is favoured by the thermal energy of the syngas before leaving the reactor (Figure 6). A separator block (SEP-1) is used to separate the moisture content (MOISTURE) and the dry MSW (MSW-DRY1). Two heater blocks (HEX-1 and HEX-2) are used to simulate sensible heat exchange between dry MSW and syngas stream (SYNGAS-2) taking place after drying process. This sub-process simulates the convective heat transfer process between dry MWS and the gaseous stream (syngas) as the solid goes down into the reactor, whilst the syngas goes up from bottom to top. MSW is a non-conventional component for Aspen Plus; therefore, it must be decomposed into its elemental and conventional constituents for the software. Thus, a RYield reactor (DECOMP) is used to simulate the breakdown of dry MSW (MSW-DRY2) into C, H, O, N, S, and Cl, by defining a yield distribution according to proximate and ultimate analysis of MSW [71].

The plasma torch is simulated by a heater block (TORCH) that increases the air temperature up to plasma temperature. Decomposed waste stream (MSW-DEC) and plasma stream (PLASMA) are fed to an RGibbs block (HTZ reactor) where organic fraction reacts to produce the syngas, while inert fraction is transformed into inert and non-leachable slag. Here, the syngas composition and reaction temperature are estimated by the direct minimization of the Gibbs free energy and energy conservation equation, respectively [43], [71]. The heat associated with MSW decomposition (pyrolysis) is considered in the energy balance of Plasma-G process [53]. Thereby, the heat stream associated with MSW (HEAT-DEC) is supplied from DECOMP block to HTZ block.

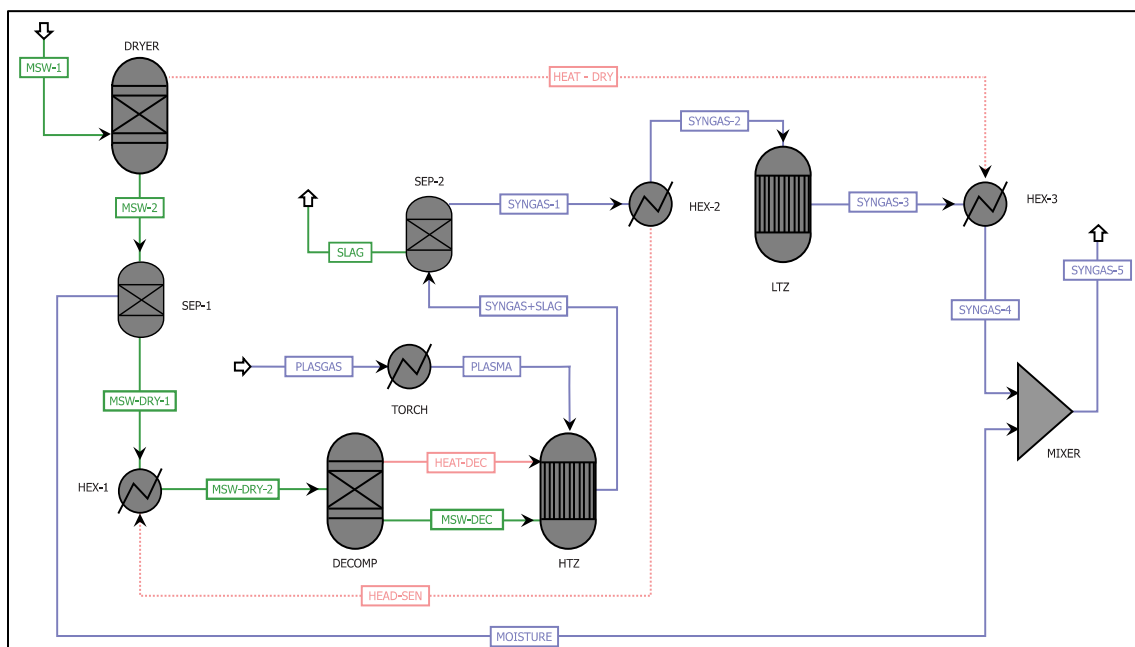


Figure 7. Flowsheet of Plasma gasification model

Syngas (SYNGAS-1 stream) and slag produced in HTZ reactor are separated by a separator block (SEP-2). The syngas (SYNGAS-2) is fed to a RGibbs block (LTZ reactor) for completely reacting in syngas species, such as CO, H₂, CH₄, CO₂, HCl, H₂S, and COS (Eq. 1) [43]. This syngas composition is also estimated by the direct minimization of the Gibbs free energy. Finally, by using a mixer block (MIXER), the moisture (MOISTURE) from the drying process is mixed with the syngas (SYNGAS-4) to simulate the raw-syngas produced in the process (SYNGAS-5). The detailed descriptions of Aspen Plus blocks used to develop our Plasma-G model are presented in previous works [12, 13, 16–18, 21, 22].

2.2.3 Thermodynamic performance

In thermo-chemical processes such as gasification or combustion, the equivalence ratio (Eq. 2) is defined as the ratio between the actual fuel/air ratio and the stoichiometric fuel/air ratio. In gasification processes the equivalence ratio is lower than 1.0 indicating that the amount of air is lower than the stoichiometric air required.

$$ER = \frac{(\dot{m}_{air}/\dot{m}_{fuel})_{actual}}{(\dot{m}_{air}/\dot{m}_{fuel})_{stoich}} \quad \text{Eq. 2}$$

The performance assessment of MSW Plasma-G process is carried out by determining the first and second thermodynamic laws efficiencies associated to the thermo-chemical process. The energy efficiency is defined as the ratio between the usable energy output and the energy required as input [78]. In Plasma-G process energy required as input is associated with feedstock's energy content and with the electrical energy consumed by the torches. On the other hand, the usable energy output is associated to syngas energy content, which includes chemical and sensible energy forms. Nevertheless, to analyse the energy performance of Plasma-G process, the cold gas efficiency (CGE) (Eq. 3) is usually analysed [43], [53], [75], [79], considering the chemical energy of the syngas [79].

$$CGE = \frac{\dot{m}_{syngas} \cdot HHV_{syngas}}{\dot{m}_{MSW} \cdot HHV_{MSW} + \dot{W}_{torch}} \quad \text{Eq. 3}$$

The syngas is assumed as an ideal gas mixture; therefore, its higher heating value can be calculated by means of Eq. 4. Where y_i (dimensionless) and HHV_i (kJ/kmol) are the molar fraction and the higher heating value of each gaseous species with chemical energy (i -component), respectively. Where $i = \text{CO, H}_2, \text{ and CH}_4$.

$$HHV_{syngas} = \sum_i y_i HHV_i \quad \text{Eq. 4}$$

The higher heating value calculation of MSW can be experimentally measured or calculated by using empirical regressions. Herein, it is used an empirical regression (Eq. 5) that is proposed by Channiwala and Parikh [79], [80]. Where C, H, S, O, N, and Ash are the mass fraction in percentage of carbon, hydrogen, sulphur, oxygen, and ash of MSW, respectively.

$$HHV_{MSW}(MJ/kg) = 0.3491C + 1.1783H + 0.1005S - 0.1034O - 0.0151N - 0.0211Ash \quad \text{Eq. 5}$$

The torch power consumption is the ratio between the effective energy transferred to the air and the torch efficiency (Eq. 6). The torch efficiency is considered here of 80% [81]. The energy transferred to air is the energy required to increase the temperature of a specific air mass flow (plasma gas) from ambient to plasma temperature (Eq. 7).

$$\dot{W}_{torch} = \frac{\dot{W}_{plasma}}{\eta_{torch}} \quad \text{Eq. 6}$$

$$\dot{W}_{plasma} = \frac{\dot{m}_{air}}{MW_{air}} \cdot \left[\int_{T_{air}}^{T_{plasma}} \bar{c}_p(T) dT \right] \quad \text{Eq. 7}$$

With reference to the exergy analysis of the Plasma-G process, generally, total specific exergy of a stream includes physical and chemical exergy (Eq. 8) [47], [79]. The physical exergy arises from temperature and pressure difference between stream conditions in relation to the dead state [47], [79]. In a general way, physical exergy can be calculated using Eq. 9. However, considering the syngas as an ideal gas mixture, Eq. 10 can be used instead Eq. 9.

$$e_T = e_{ph} + e_{ch} \quad \text{Eq. 8}$$

$$e_{ph} = (h - h_0) - T_0(s - s_0) \quad \text{Eq. 9}$$

$$e_{ph} = \int_{T_0}^T \bar{c}_p(T) dT + T_0 \left[\int_{T_0}^T \bar{c}_p(T) \frac{dT}{T} - R \ln \left(\frac{P}{P_0} \right) \right] \quad \text{Eq. 10}$$

The exergy is the maximum quantity of usable work obtained when a system undergoes a process from a specific state up to the dead state, involving heat transfer and substances exchange only with the environment [82]. The chemical exergy of syngas is calculated by Eq. 11.

$$e_{ch} = \sum_i y_i e_i^0 + RT_0 \sum_i y_i \ln(y_i) \quad \text{Eq. 11}$$

MSW compositions can be inaccurate, which stem from the variation of wastes and leads to difficult chemical exergy calculation [47]. As a consequence, statistical correlations presented by Kotas (Eq. 12) [82] are used to determine chemical exergy of MSW. Where β is calculated by Eq. 13, which is suitable for fuels with mass ratio O/C < 2.67 [79].

$$e_{MSW}^0 = [LHV + 2.442MC] \cdot \beta + 9.417 \cdot S \quad \text{Eq. 12}$$

$$\beta = \frac{\left(1.0412 + 0.2160 \left(\frac{H}{C} \right) - 0.2499 \left(\frac{O}{C} \right) \left[1 + 0.7884 \left(\frac{H}{C} \right) \right] + 0.045 \left(\frac{N}{C} \right) \right)}{1 - 0.3035 \left(\frac{O}{C} \right)} \quad \text{Eq. 13}$$

The exergy efficiency of Plasma-G process (Eq. 14) relates the exergy content of syngas with MSW exergy content and the torch power consumption. Exergy input is associated to the feedstock's exergy content and the electric exergy consumed by torch. Whilst, the exergy output is associated with syngas, but only considering its chemical exergy. Here, it is only considered the chemical exergy of syngas because it is analysed as a substitute gaseous fuel.

$$\eta_{Ex} = \frac{\dot{m}_{syngas} \cdot e_{syngas}}{\dot{m}_{MSW} \cdot e_{MSW} + \dot{W}_{torch}} \quad \text{Eq. 14}$$

2.2.4 Model validation

The validation of the proposed model was carried out by comparing numerical results obtained in this work regarding experimental and numerical data of RDF Plasma-G reported in literature. The aim is to assess the model accuracy for simulating MSW Plasma-G and the syngas production as a gaseous fuel. To validate the model, it is required to know operation conditions, such as feedstock composition, temperature, pressure, and mas flow rates. These parameters have been taken from two previous works where numerical and experimental data have been reported [43], [73]. In the case of experimental data, the operating conditions of the Solena Plasma Gasification and Vitrification (SPGV) reactor [83] reported by Perna *et al.* [73] were used for our validation purpose, which are presented in Table 3. SPGV reactor is fed with refuse derived fuel (RDF) with the aim to produce syngas with high CO and H₂ contents. Moreover, Coke (4.76 wt.%) and CaO (0.04 wt%) were fed to the reactor for enhancing the heat distribution through the reactor cross-section, and seeking to keep a proper slag chemistry, respectively. Air was used as plasma gas, and oxygen (O₂ 97 %vol., N₂ 3%vol.) was additionally fed to the reactor for reducing the plasma torch consumption, while RDF Plasma-G was improved. Furthermore, the operative conditions of two simulation cases carried out by Minutillo *et al.* [43] were chosen because it has been used in previous works as reference numerical data for validation processes. The feedstock gasified under plasma regimes is RDF (Table 4), and the high temperature zone was 2500°C. In Case A only air was used as plasma gas, while in Case B enriched air (O₂ 40%vol., N₂ 60%vol.) was supplied instead of air. To carry out the validation process of the model proposed here, the ultimate and proximate analyses of RDF, as well as the other operating conditions were specified in this work. The model accuracy is evaluated by means of the relative error (Eq. 15) [37] [84].

$$RE [\%] = \left| \frac{X_{reference,i} - X_{model,i}}{X_{reference,i}} \right| \times 100 \quad \text{Eq. 15}$$

Table 3. Operative conditions for experimental validation process [73].

Parameter	Unit	Value
Feedstock mass flow rate	kg/h	21004
Gasification pressure	bar	1.013
O ₂ /RDF mass ratio	kg/kg	0.468
Plasma gas/RDF mass ratio	kg/kg	0.0648
Thermal torch power	MW	3
<i>RDF ultimate analysis, wt%</i>		
C	43.48	S
H	5.76	O
N	0.56	Ash
Cl	0.21	MC

Table 4. Simulations conditions for numerical validation process [43].

Parameter	Unit	Case A	Case B
Plasma gas type	-	Air	Enriched air
Plasma temperature	°C	4000	4000
Gasification pressure	bar	1.013	1.013
HTZ temperature	°C	2500	2500
RDF mass flow rate	kg/s	1	1
Plasma gas mass flow rate	kg/s	0.782	0.643
<i>Feedstock composition</i>			
<i>Ultimate analysis (wt.%, d.b.)</i>		<i>Proximate Analysis (wt.%)</i>	
C	48.23	MC	20
H	6.37	VM (d.b.)	75.96
O	28.48	FC (d.b.)	10.23
N	1.22	Ash (d.b.)	13.81
S	0.76		
Cl	1.13		
Ash	13.81		

2.2.5 Simulation plan

The thermodynamic assessment of MSW Plasma-G is carried out by means of two sensitivity analyses, labelled here as Strategy-1 and Strategy-2. The aim of Strategy-1 is to assess the effect of plasma temperature and the type of MSW produced in Medellin-city (feedstock properties) on key answer parameters such as air requirement, plasma power consumption, and cold gas and exergy efficiencies. Operating conditions of Strategy-1, based on previous research works [43], [53], [55], [56], were assumed and summarized in Table 5.

Table 5. Assumed operation conditions for Strategy-1 simulations.

Parameter	Value
HTZ temperature [°C]	2500
LTZ temperature [°C]	1250
Plasma temperature [°C]	2500 – 4000
Reactor pressure [bar]	1.013

The air requirements (air mass flow) is set ensuring a temperature of 2500 °C in HTZ reactor (Figure 7), while model calculations were carried out based on a MSW mass flow of 1.0 kg/s for all simulation plan of this sensitivity study. The temperature of HTZ was set to 2500 °C because the maximum work-temperature of refractory materials, with which the gasifier is built is about 3000 °C [85] . A temperature of 1250°C was

set for LTZ reactor, which is higher than minimum temperature needed to prevent dioxins formations (1000 °C) inside the reactor [39], [53]. Although, plasma produced in torches has an extremely high temperature, when plasma jet interacts with feedstock, its temperature decreases to temperatures between 2500 °C and 4500 °C [72]. This plasma temperature range allows studying the effect from middle to high temperature of plasma on Plasma-G process.

The second sensitivity analysis, Strategy-2, is carried out seeking to determinate the air mass flow and plasma temperature conditions at which the cold gas efficiency (or exergy efficiency) is the highest for each MSW type (residential, commercial, industrial, institutional, and their mixture). In this simulation plan, the cold gas efficiency is analysed as a yield thermodynamic parameter because of the exergy efficiency (chemical exergy) has the same trend. As mentioned above, typical plasma temperature ranges from 2500 °C to 4500 °C; however here, temperatures between 1500 °C and 4500°C are considered in order to investigate the performance of MSW gasification process when relatively low plasma temperature is used. The analysed range of air mass flow is between 0.1 and 1.5 kg/s. Furthermore, temperature in HTZ reactor (Figure 7) must be higher than LTZ temperature (set at 1250°C), and lower than 3000 °C seeking to avoid excessive refractory material corrosion [85]. As in Strategy-1, MSW mass flow is set at 1.0 kg/s for all simulations of this second sensitivity assessment.

2.2.6 Levelized costs of syngas as substitute gaseous fuel

In this section, the levelized cost of syngas (LCOS) production by Plasma-G of the five different types of MSW produced in Medellin city is calculated. Calculations of LCOS are carried out based on the optimal conditions for each waste found from the sensitivity analysis (Strategy-2) described in section 2.2.5. Furthermore, the effect of the tax incentives promoted by Law 1715 of 2014 (Colombian law of renewable energies) on LCOS is evaluated.

The Levelized Cost of Syngas (LCOS) is the cost per unit of energy that includes all costs of an energy (gaseous fuel) generation project during its lifetime. Therefore, LCOS determines the constant price at which the energy must be sold to guarantee that the net present value is equal to zero as well as to obtain a minimum acceptable rate of return. LCOS considers the investment costs, the fixed and variable costs for operating and maintenance, the fuel costs, externalities, and tax incentives. LCOS is calculated according to Eq. 16 and Eq. 17 [63], [86]–[88].

$$LCOS = LCOS_I + LCOS_V + LCOS_F + LCOS_G + LCOS_E \quad \text{Eq. 16}$$

$$LCOS = \frac{I_0 + \sum_{t=1}^n \frac{C_t}{(1+i)^t}}{\sum_{t=1}^n \frac{E_t}{(1+i)^t}} \quad \text{Eq. 17}$$

Technology cost (¢US\$/kW) and operating and maintenance costs reported in the literature have been updated for the year of the investment. The former by the Producer Price Index (PPI), and the second one by the consumer Price Index (CPI), which are annually reported by the National Department of Statistics from Colombia [89]. Eq. 18 and Eq. 19 show the expressions for the PPI and CPI, respectively.

$$\text{Technology cost, year (b)} = \text{Technology cost, year (a)} \frac{\text{PPI, year (b)}}{\text{PPI, year (a)}} \quad \text{Eq. 18}$$

$$\text{O\&M, year (b)} = \text{O\&M, year (a)} \frac{\text{CPI, year (b)}}{\text{CPI, year (a)}} \quad \text{Eq. 19}$$

2.2.6.1 Tax incentives for renewable energy projects in Colombia

In 2014, the Colombian government issued the Renewable Energy Law 1715, which encourages investment in Non-Conventional Energy Sources (NCES) projects through four tax incentives [21], such as: 1.) Deduction of up to 50% of the investment through income tax during the first five years of operation; 2.) Exemption from VAT on national or imported equipment, elements, machinery, and services that are destined to the pre-investment and investment of NCES; 3.) Exemption from the payment of import on the components previously named; 4.) Accelerated depreciation on assets, which will not be greater than 20% per year as a global rate. Nevertheless, under the National Development Plan 2018-2022, the first tax incentive (The Investments Tax Credit) can already be exercised during the first fifteen years of operation. The concept of the tax factor (Δ) is applied to evaluate the effect of tax incentives on LCOS. Eq. 20 and Eq. 21 show the modified LCOS considering tax incentives [90].

$$LCOS = \Delta LCOS_I + LCOS_V + LCOS_F + LCOS_G + LCOS_E \quad \text{Eq. 20}$$

$$\Delta = \frac{1}{1-t} \left[1 - t \left(\sum_{j=1}^{j=t_1} \frac{I_j}{(1+i)^j} + \sum_{j=1}^{j=t_2} \frac{d_j}{(1+i)^j} \right) \right] \quad \text{Eq. 21}$$

2.3 RESULTS AND DISCUSSION

2.3.1 Model Validation

2.3.1.1 Validation with experimental data

The operative conditions of the SPGV reactor (Table 3) were mimicked in the proposed model. However, it was not possible to obtain enough information about RDF (proximate analysis) and coke composition needed to perform the Aspen Plus simulations. Therefore, a typical proximate composition of RDF was obtained from a previous work where the Plasma-G of RDF was studied [15]. Similarly, the ultimate and proximate analyses of coke were taken from Song & Guo [91], which focused on the autothermal gasification of coke in a fixed bed reactor.

The contrasted results between simulations and the operative experimental data reported in the literature are shown in Table 6. The contrasted parameters are syngas temperature, syngas composition, and lower and higher heating values of syngas. The model accuracy is analysed based on the relative error -RE- between experimental and numerical data, this parameter had been used to analyse the model's precision by other researchers [84]. By comparing operative and numerical values for syngas temperature, a slight underestimation for this parameter was found. Nevertheless, the syngas temperature estimated by the model is in good agreement with the corresponding operative value, which leads to a low RE (3%).

Table 6. Comparison between proposed model and experimental data from literature [73].

Parameter	Exp. [73]	Model	RE (%)
Syngas temperature (°C)	965	936	3.00
<i>Syngas composition (%vol.)</i>			
H ₂	36.30	31.50	13.22
CH ₄	0.00	0.00	0.00
CO	43.90	46.98	7.02
CO ₂	6.10	2.73	55.25
H ₂ O	9.80	15.60	59.18
N ₂	3.70	3.05	17.57
H ₂ S	0.05	0.06	20.00
HCl	0.07	0.08	14.29
LHV _{raw} (MJ/kg)	11.40	11.16	2.13
HHV _{raw} (MJ/kg)	12.50	11.89	4.85

Regarding to syngas composition, a good prediction for H₂, CO and CH₄ was reached, favouring to an acceptable RE values associated to the prediction of these species, where RE is 13.22%, 0%, and 7.02%, respectively. Conversely, RE values attained for CO₂ (55.25%) and H₂O (59.18%) are relatively high; these REs (CO₂ and H₂O) are attributed to their low concentration in the syngas (< 10 %vol). Therefore, in spite of RE being high, these variations do not significantly affect the energy parameters of the Plasma-G process, such as syngas heating value; this is confirmed by the suitable RE reached by the model for LHV_{syngas} (2.13%) and HHV_{syngas} (4.85%). The average RE obtained from experimental validation was 17.86%. Nevertheless, it is worth noting that this result is affected by the high RE for CO₂ and H₂O, which stems from the low concentration of these species in the syngas, as stated earlier. Besides, the low REs for LHV_{syngas} and HHV_{syngas} indicate that the proposed model can adequately represent the conversion of RDF into syngas through plasma gasification. Therefore, the good agreement between results obtained by our proposed model and SPGV operative data is highlighted. Other parameters that contributes to the results uncertainties of the model are the composition of RDF and coke considered for simulation, which were not presented in the experimental work [73], nevertheless, the model can be used as a computational tool to study Plasma-G process.

2.3.1.2 Validation with numerical data

Table 7 shows the comparison between the simulated and reference data related to the main variables that characterize the Plasma-G process of RDF using air and oxygen enriched air as plasma gas (Table 4). The contrasted parameters are HTZ temperature, syngas composition, and lower and higher heating values of syngas. Respecting HTZ temperature, the model slightly underestimates this parameter in Case A, while in Case B, HTZ temperature is lightly overestimated. However, the model results agree with the values of reference data. This is associated with acceptable RE obtained in both cases for HTZ temperature, 5.68% for Case A and 10.32% for case B. Concerning the syngas composition, a similar trend is obtained comparing CO concentration. CO is weakly underestimated for Case A, while CO difference for case B is mild. Therefore, according to the low RE (2.04% and 0.75% for Case A and case B, respectively) the good behaviour of our model is highlighted. In both simulation cases (A and B), the model underestimates the fraction of H₂ in the syngas. Conversely, the model overestimates fractions of CH₄, H₂O, and N₂. In Case A, RE for CH₄ is relatively high (40.7%), whilst in case B, RE for CH₄ and CO₂ reaches 100%. The high RE reached for CH₄ and CO₂ species is related to the low concentration of these gaseous species in the syngas (< 6 %vol). Thus, although RE is high, the low concentrations do not significantly affect the energy parameters of the process, such as syngas heating value. This is confirmed by the low RE values reached by the model for LHV_{syngas} (3.98% for Case A, and 2.38% for Case B) and HHV_{syngas} (6.38% and 4.25%, for case A and B, respectively). Furthermore,

it is worth note that the results obtained by the model proposed here, follow the trends of reference data. When oxygen enriched air is used instead air as plasma gas, the mass flow rate of plasma gas decreases, while CO and H₂ yield, as well as LHV and HHV increase. Therefore, it is highlighted the good agreement between results obtained by our proposed model and those reported by Minutillo *et al.* [43]. In summary, according to the low global RE (5.18%), excluding CH₄ and CO₂, the accuracy of the model is highlighted, confirming that the proposed model can be used as tool to simulate Plasma-G process of MSW.

Table 7. Numerical validation of RDF plasma gasification process, reference data adapted from Minutillo et al. [43].

Parameter	Case A			Case B		
	[43]	<i>This work</i>	<i>Error (%)</i>	[43]	<i>This work</i>	<i>Error (%)</i>
HTZ temperature (°C)	2500	2358	5.68	2500	2758	10.32
<i>Syngas composition (%vol.)</i>						
H ₂	21.04	15.48	26.42	31.49	29.60	6.00
CO	33.79	33.10	2.04	38.73	39.02	0.75
CH ₄	5.97	8.40	40.70	0.00	0.63	100
CO ₂	0.00	0.00	0.00	0.42	0.00	100
H ₂ O	11.68	14.34	22.77	12.50	13.71	9.68
N ₂	26.97	28.12	4.26	16.32	16.52	1.22
HCl	0.32	0.33	3.12	0.31	0.31	0.00
H ₂ S	0.22	0.22	0.00	0.22	0.22	0.00
COS	0.02	0.02	0.00	0.01	0.01	0.00
LHV _{raw-syngas} (MJ/kg)	9.55	9.17	3.98	10.10	9.86	2.38
HHV _{raw-syngas} (MJ/kg)	10.50	9.83	6.38	11.06	10.59	4.25

2.3.2 Strategy-1: Effect of plasma temperature and feedstock composition

Here, the effect of waste type (composition) and plasma temperature of the plasma gasifier on thermodynamic behaviour of Plasma-G process is characterized. The plasma temperature is related to the energy supplied to the plasma gas, which thermally decomposes the solid waste into the reactor. Whilst, the waste type is associated with the most representative five sectors that produce waste in big cities, whose composition and heating value are quite different. The response variables used for this sensitivity analysis are the torch power consumption, the syngas heating value, and the cold gas and exergy efficiencies.

2.3.2.1 Air mass flow and torch power consumption

Figure 8 shows the air mass flow (a) and torch power consumption (b) for each waste type as a function of plasma temperature. a significant effect of waste type on the air mass flow and the torch power supplied to the process were found. At plasma temperature of 2500 °C, as the moisture content (MC) of waste increases,

from Industrial waste (26.61%) up to Residential waste (57.90%), the air mass flow rate and torch power consumption decrease by 46.8% and 47.3%, respectively. While for 4000 °C of plasma temperature, the airflow and torch power also decrease by 47.7% and 48%, respectively. The reduction of air supplied to the Plasma-G process as MC of MSW-sector increases is attributed to the simulated technology (updraft plasma gasifier), where MSW is dried by the syngas stream, and MC is mixed with the gaseous phase at the top section of the reactor (Figure 6), leaving the remaining dried fraction of waste to be processed by plasma torch at the bottom of the gasifier.

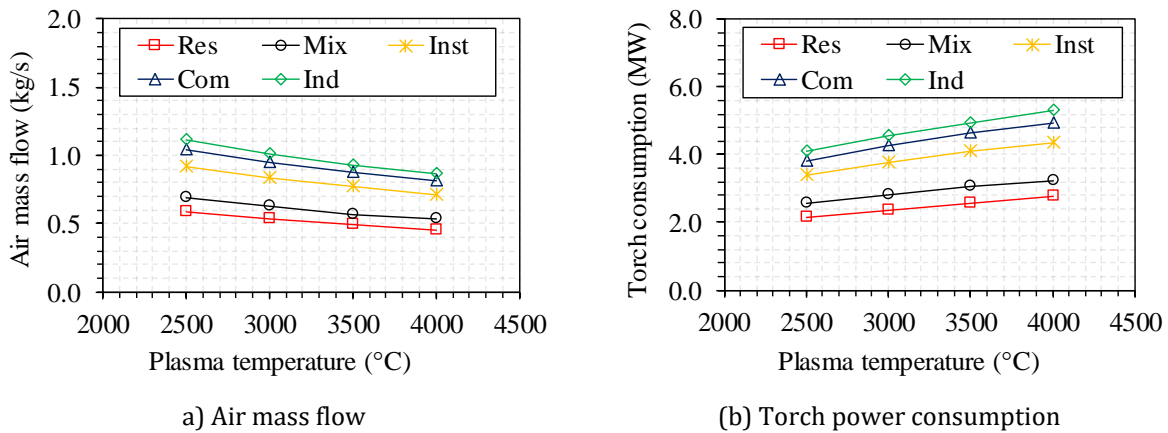


Figure 8. Air mass flow and torch power consumption vs plasma temperature for the five types of wastes.

The energy supplied to the plasma gasifier under allothermal conditions is affected by plasma temperature and the air mass flow (plasma gas). These two process parameters must accomplish the energy balance to reach the high temperature zone (T_{HTZ}) set in the reactor. Therefore, if the plasma temperature increases, the torch consumption rises, while the air mass flow, needed to reach T_{HTZ} temperature, decreases. Figure 8b shows that if MC of waste increases (from Industrial to Residential), the dried fraction of waste to be gasified diminishes, decreasing the torch consumption required to reach T_{HTZ} . The torch consumption decreases by 47.89% in average when MC of wastes increases. This reduction in torch stems from the low amount of air required to process a low amount of dried waste (Figure 8a). Nevertheless, regardless of waste type, if plasma temperature increases (from 2500 °C to 4500 °C), it leads to increase the torch consumption (by 28.3% in average) required to reach the plasma temperature set (Figure 8b), while the air mass flow (plasma gas) diminishes by 22.88% in average (Figure 8a). Indeed, this behaviour is ascribed to the energy balance in the gasifier accomplished to reach T_{HTZ} set at 2500 °C.

2.3.2.2 Heating value, thermal power, and exergy of raw syngas

Figure 9 shows the concentration of gaseous fuel species of syngas (H_2 , CO , and CH_4 , in vol%). As MC of waste decreases from 57.9% (Residential waste) to 26.61% (Industrial waste), CO concentration increases

on average from 21.4% up to 30.83%. Similar trends have been found for H₂ and CH₄, whose average increase is by 43.18% for H₂, while CH₄ rises from 0.92 %vol to 2.30 %vol. The high concentration of H₂, CO, and CH₄ as MC of waste diminishes leads to increase HHV of syngas by 45.01% (Figure 10a). This trend (high HHV_{syngas}) stems from the decrease of air-fuel equivalence ratio, which decreases as MC decreases leading to increase the dry fraction of waste involved in the process (Figure 10d). As the dry fraction of waste increases (from Residential to Industrial), the thermal power and exergy rate of syngas increase by 89.90% and by 92.37% on average, respectively (Figure 10b and c). The increment of output energy and exergy is due to high syngas mass flow rate produced by the increased air mass flow rate required to gasify wastes with low MC (Figure 8a). As plasma temperature increases from 2500°C up to 4000°C, disregarding waste type, slightly changes are obtained for CO concentration (average variation of ~1.6%), whilst H₂ decreases by 16.6% on average. For CH₄, the trend is opposite to that one of H₂. For instance, at plasma temperature of 2500°C, CH₄ concentration is very low for all waste types ranging from 0.0%vol. to 0.31%vol., whereas if the plasma temperature increases up to 4000 °C, CH₄ concentration rises up to 2.0%vol. – 4.29%vol. As stated earlier, the increase of plasma temperature leads to reduce the air mass flow rate (Figure 8a), decreasing the air-fuel equivalence ratio (Figure 10d), and thus, promoting the increase of CO yield. Furthermore, the gasification reaction is promoted if the plasma temperature increases, because of the reduction reactions of gasification are favoured [53]. The water vapor is reduced by the char to yield CO and H₂ ($C + H_2O = CO + H_2$); while H₂ is reduced by the char to yield CH₄ ($C + 2H_2 = CH_4$). The activation of these reactions, at T_{HTZ}= 2500 °C, explains the reduction of H₂ at the expense of CH₄ increase [92].

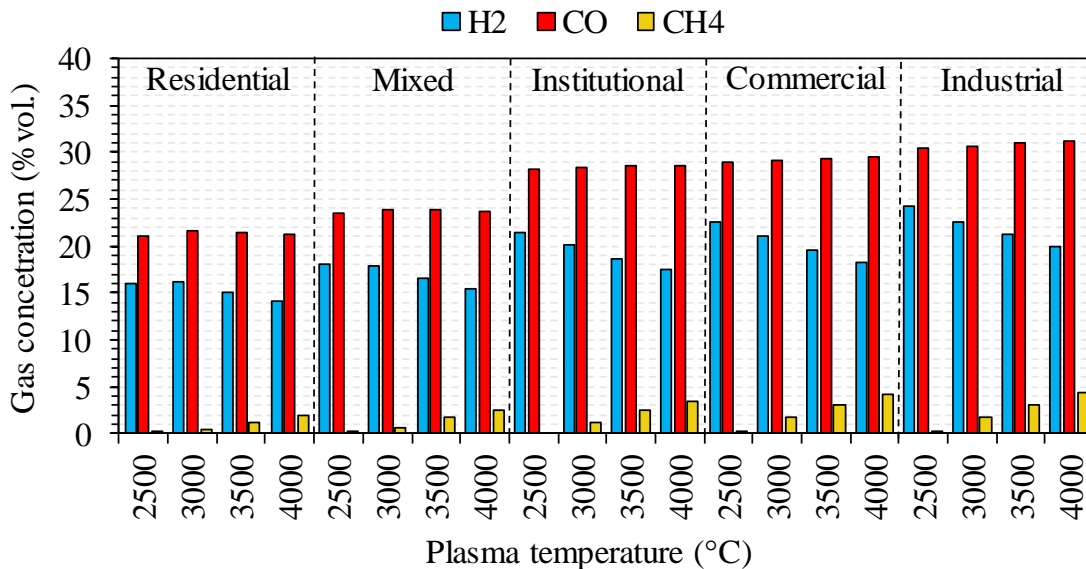


Figure 9. Syngas composition as a function of MSW type and plasma temperature.

The syngas HHV is positively affected by plasma temperature increase (Figure 10a), when plasma temperature increases from 2500°C to 4000°C, an average increase of 13.65% is obtained for syngas HHV, which is related to the high concentration of CO and CH₄ reached at high temperatures (low air mass flow supplied). However, regardless of waste type, the thermal power and exergy rate of syngas slightly increase by 1.5%, as plasma temperature increases (2500°C to 4000°C). At higher plasma temperatures, the air mass flow rate supplied to the reactor decreases (see Eq. 7), which leads to diminish the syngas mass flow rate produced (by mass conservation) counteracting the increment of HHV_{syngas}.

2.3.2.3 Cold gas (CGE) and exergy efficiencies (ExE)

The effect of waste composition on cold gas efficiency was analysed classifying the wastes in two groups: 1) Residential, Mixed, and Institutional, and 2) Industrial and Commercial. Analysing the group 1, CGE slightly increases by 1.39% on average, as MC increases from 37.92%-Institutional to 57.9%-Residential. For those waste types, as MC increases, the gas quality (syngas' HHV, Figure 10a) and energy supplied to the process decrease.

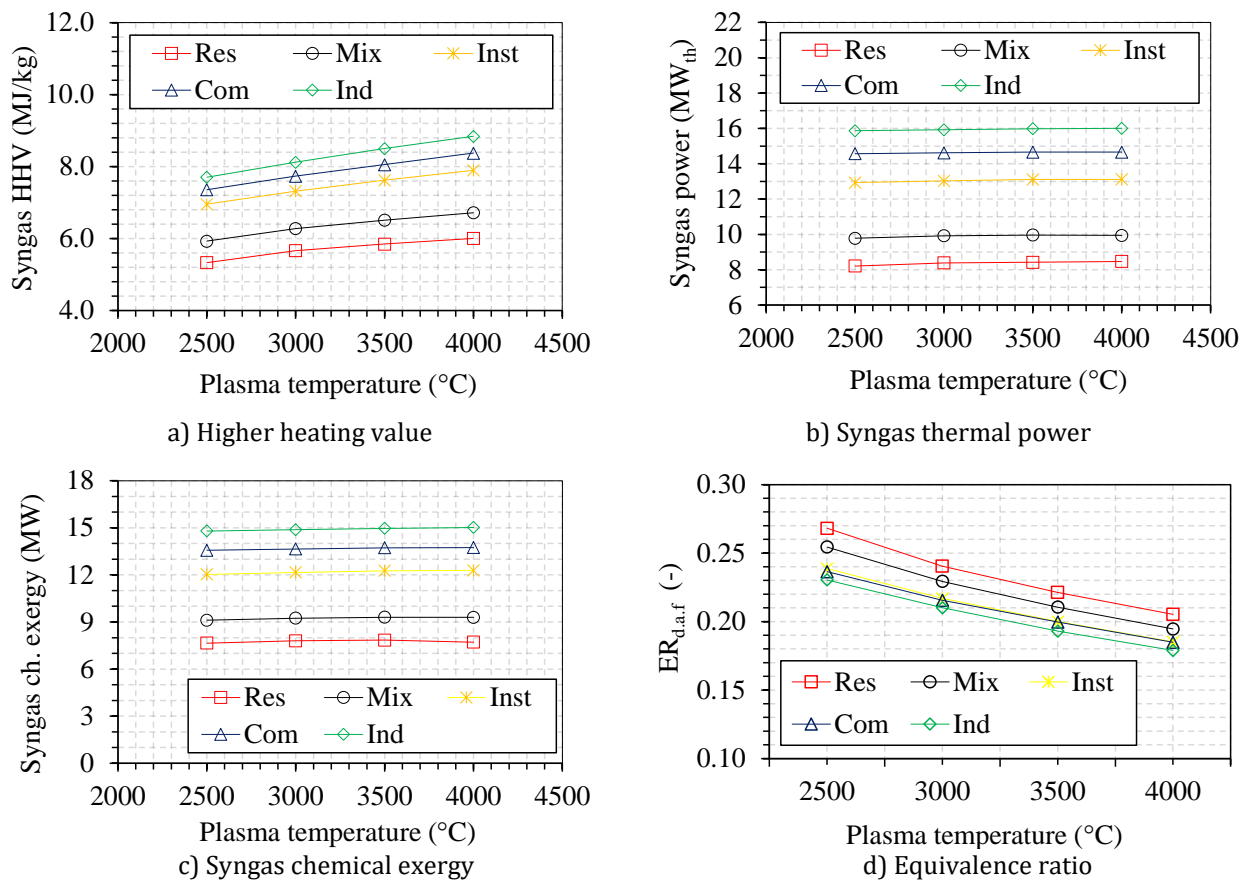


Figure 10. Effect of MSW type and plasma temperature on a) heating value, b) thermal power, c) chemical exergy of syngas, and d) equivalence-ratio.

The supplied energy is composed by HHV of waste and torch power consumption (Table 2 and Figure 8b). The thermal power of syngas decreases by 35.8% on average (Figure 10b), whilst energy supplied to the process diminishes by 36.4%. The higher reduction of energy supplied than the reduction of syngas thermal power leads to slightly increase CGE (Eq. 3). Regarding group 2 (wastes from Industrial and Commercial sectors) an opposite trend for CGE vs MC was found, i.e., CGE obtained with Commercial waste (32.95% moisture) is 0.6% lower than that of Industrial waste (26.61% moisture). This cross effect attained for Industrial and Commercial wastes is attributed to the specific torch power consumption. The average specific torch energy consumption for Commercial waste (6.58 MJ/kg_{dry MSW}) is higher than that of Industrial waste (6.43 MJ/kg_{dry MSW}). The high energy consumption of the torch to process Commercial waste is due to its lower molar O/C ratio (0.46) with regard to the molar O/C ratio (0.47) of Industrial waste. A low molar O/C ratio means a low oxygenate feedstock, which needs a high amount of oxygen to be processed and to reach the target temperature (T_{HTZ}) of 2500°C. According to Eq. 7, the torch power consumption is proportional to the air mass flow rate, and the Commercial waste requires a greater amount of air to be gasified, which leads to increase the specific energy consumption of torch, diminishing CGE. From Figure 10a, it is highlighted a positive effect of MC on CGE, this behaviour is ascribed to the updraft technology considered herein, where the raw MSW fed to the reactor is dried by the gaseous phase by convective heat and mass transfer. Thus, a high MC leads to decrease the fraction of dry MSW to be processed by the torches, and consequently, the power torch consumption diminishes.

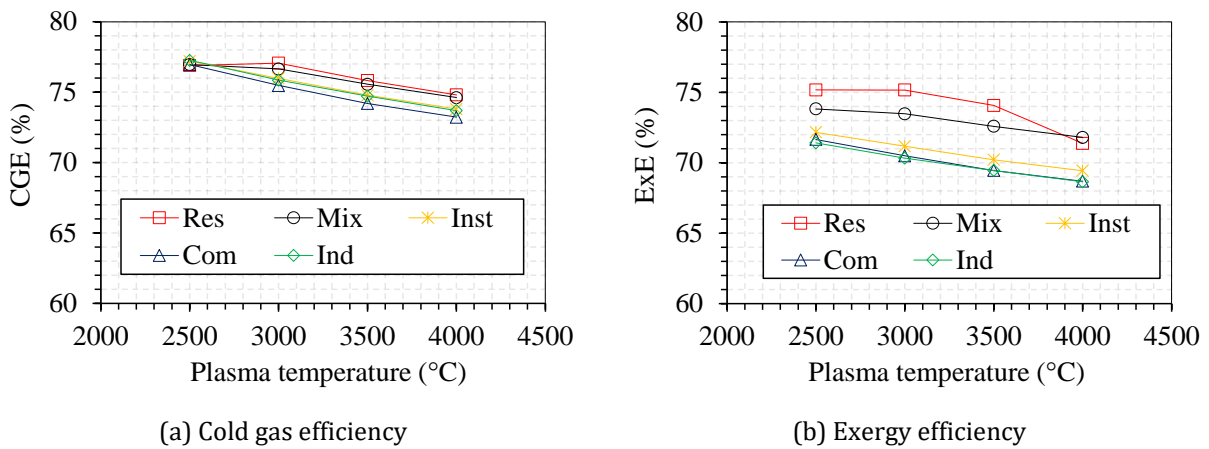


Figure 11. Cold gas efficiency and Exergy efficiency.

For the exergy analysis, ExE slightly increases by 5.83% as MC increases from 26.61% up to 57.9%. The improved ExE obtained for processing a waste with high moisture content is related to the effect on the terms of Eq. 14, namely, syngas chemical exergy (recovered exergy, $\dot{m}_{\text{syngas}}e_{\text{ch,syngas}}$) and supplied exergy ($\dot{m}_{\text{MSW}}e_{\text{ch,MSW}} + \dot{W}_{\text{torch}}$). As moisture content increases from 26.61% (Industrial) up to 57.9% (Residential), the syngas chemical exergy decreases by 47.93% on average (Figure 10c), which is attributed

to the low concentration of CO, H₂, and CH₄ (Figure 9); while, the supplied exergy decreases by 50.68% on average. The higher reduction of supplied exergy than the reduction of syngas chemical exergy leads to increase ExE with MC.

The plasma temperature (2500 °C – 4000 °C) adversely affects CGE and ExE of the plasma-G process. CGE decreases by 3.94% and ExE diminishes by 3.64%, on average. This behaviour is associated with the increment of torch energy consumption, which rises by 28.3% on average, as the plasma temperature increases (Figure 8b). Whilst the syngas thermal power and syngas exergy rate are slightly affected by the plasma temperature (Figure 10b and c); therefore, both thermodynamic efficiencies decrease.

The CGE values found in this work (ranged from 73.23% to 77.27%) are relatively high compared with those reported in previous works of wastes Plasma-G using air as plasma gas (42% - 66%)[43], [53], [55], [56]. This difference stems from the CGE equation used herein (Eq. 3), which is based on HHV of MSW and syngas. Besides, in those previous works, the CGE approach included a fossil-based plant efficiency for supplying the electric power to the torches and ASU [43], [53], [55], [56]. While here, it was assumed that the electric power for the plasma torches was self-generated by an internal combustion engine (ICE) fuelled with a fraction of the syngas produced in the plasma gasifier (section 2.3.4.1). Furthermore, similar values of CGE (~78%) for Plasma-G process have been reported by Paulino et al. [93].

2.3.3 Strategy-2: The maximum efficiency of Plasma-G process

A sensitivity analysis was carried out in order to determine which conditions of process parameters (plasma temperature and air mass flow) allow achieving the maximum CGE for each waste type. Ranges for plasma temperature and air mass flow were 1500°C - 4500 °C, and 0.1 - 1.5 kg/s, respectively. Furthermore, here, as thermodynamic feasibility criteria, T_{HTZ} has been set between 1250°C and 3000 °C (see Section 2.2.5). Therefore, the combinations between plasma temperature and air mass flow are considered thermodynamically feasible if T_{HTZ} reaches values between 1250 and 3000 °C as a result of simulations.

Figure 12 shows CGE for each waste type as a function of the suitable combinations between the plasma temperature and air mass flow rate. It must be clarified that in this figure, the suitable air mass flow rates are the parametric series (numbers, kg/s) at the top of each subfigure. For each waste type, in Figure 12 (a-e) only CGE associated to the feasible combinations that reach the target T_{HTZ} range (1250 °C < T_{HTZ} ≤ 3000 °C) is shown. According to the number of suitable combinations found for each waste type, which increases as MC of wastes decreases, it is highlighted the flexibility of the Plasma-G for wastes with low moisture content, e.g. industrial or commercial wastes (Figure 12d and e). Whereas residential and mixed wastes are less flexible to be gasified due to the low number of combinations of suitable operational conditions (Figure 12 a and b). Furthermore, Figure 12 shows the effect of plasma temperature and air mass flow rate on CGE

for each waste type processed via Plasma-G. Regardless of air mass flow rate, an increase of plasma temperature leads to diminish CGE, which is related to the increase of the torch power consumption, it was discussed in detail in section 2.3.2.3.

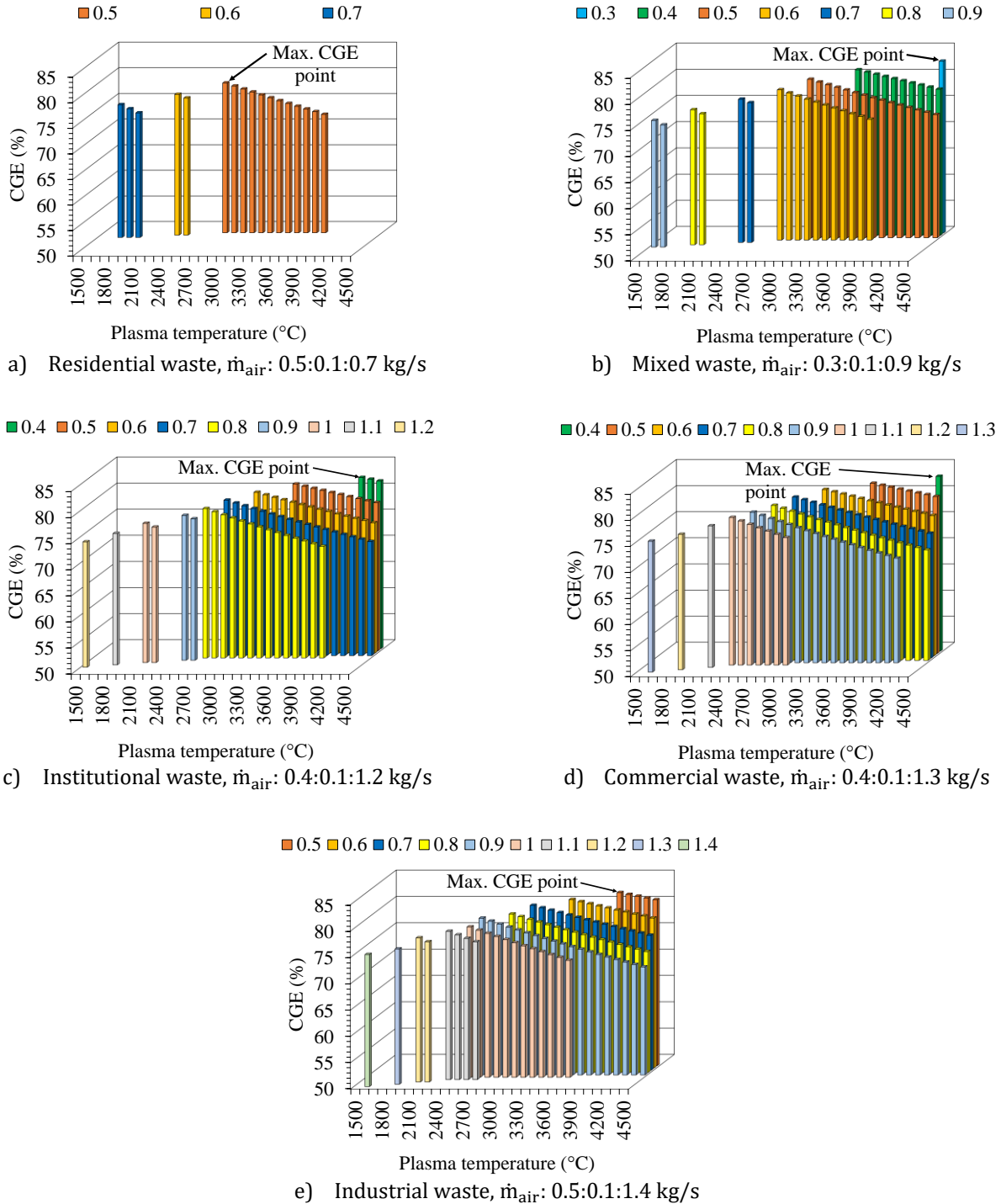


Figure 12. The maximum CGE of Plasma-G process for each MSW type as a function of suitable operational conditions (air mass flow in kg/s and plasma temperature in °C) with $1250\text{ °C} < T_{HTZ} \leq 3000\text{ °C}$.

Analysing the air mass flow rate, disregarding plasma temperature, it can be seen that CGE rises as the air mass flow rate decreases. Therefore, the increment of CGE is ascribed to the favoured yields of CO and CH₄, and the reduction of torch power consumption as the air flow decreases. For all wastes, the maximum CGE is reached with the combination between the lowest suitable air mass flow and the lowest plasma temperature associated with this air mass flow (Figure 12), since under these conditions the lowest torch power consumption, the highest HHV_{syngas}, as well as the highest syngas thermal power are reached for each waste type (Eq. 3). For instance, the maximum CGE for industrial waste is obtained with 0.5 kg_{aire}/s (the lowest suitable air mass flow) and 4100 °C, which is the lowest plasma temperature suitable for 0.5 kg_{aire}/s. The air flow supplied to the Plasma-G process was discussed in sections 2.3.2.1 and 2.3.2.3, where CGE increases if air flow diminishes due to the reduction of torch's power consumption.

The best results for each waste type are summarized in Table 8 and Table 9. The maximum CGE values have been reached for plasma temperatures higher than 4000°C, excepting the residential waste type (2800°C), and with relatively low air mass flow (≤ 0.5 kg/s). The relatively low plasma temperature for residential waste is attributed to its high MC. A large reduction of dry matter to be processed by the torches is favoured when the residential waste is fed to the plasma gasifier. This leads to a less amount of required energy by the plasma ($\dot{m}_{\text{air}} \cdot h_{\text{plasma}}$ associated to T_{plasma}) to reach the upper limit of T_{HTZ} (3000°C) into the reactor (see Figure 7). The difference between the maximum CGE reached for each waste type is mild, CGE varies from 79.22% for residential waste up to 83.46% for commercial waste. This close variation of CGE (~5%) can be analysed by CGE equation (Eq. 3). The amount of energy supplied by the solid-fuel to the Plasma-G process increases for wastes with low MC because of their high HHV (Table 2).

Table 8. The best Plasma-G behaviour (CGE) as a function of operational parameters for each MSW type.

Waste type	\dot{m}_{air} (kg/s)	fuel-air ER _{d.a.f} (-)	T_{plasma} (°C)	\dot{W}_{torch} (MW)	T_{HTZ} (°C)	\dot{W}_{syngas} (MW)	CGE (%)
Residential	0.5	4.38	2800	2.09	1287	8.43	79.22
Mixed	0.3	9.08	4500	2.08	1666	10.10	82.77
Institutional	0.4	9.60	4300	2.64	1691	14.97	82.76
Commercial	0.4	8.76	4500	2.77	1786	14.92	83.46
Industrial	0.5	9.66	4100	3.14	1681	16.04	82.84

But furthermore, the wastes with low MC need a greater torch power to be processed due to the larger amount of dry matter (Table 8). Therefore, the energy supplied to the process increases by 83.7%. Nevertheless, the syngas thermal power also increases by 90.3%, if the MC of wastes decreases, which is related to the high HHV of syngas (Table 9). Thereby, as the supplied power to the Plasma-G process (input)

and the syngas thermal power (output) have the similar trends when the MC varies from 57.9% to 26.61%, CGE is very comparable unconcerned of the waste type, although their difference regarding MC is meaningful.

Table 9. Composition (%vol.) and HHV (MJ/kg) for syngas obtained at maximum CGE conditions.

Waste type	H ₂	CO	CH ₄	N ₂	H ₂ O	CO ₂	HCl	H ₂ S	COS	HHV
Residential	15.47	21.47	0.95	18.86	43.15	0.00	0.03	0.05	0.003	5.78
Mixed	7.72	23.35	8.55	13.95	46.30	0.00	0.05	0.06	0.008	8.06
Institutional	7.95	29.43	11.64	17.71	33.17	0.00	0.02	0.06	0.010	9.86
Commercial	5.80	30.86	15.43	18.22	29.56	0.00	0.04	0.06	0.015	11.10
Industrial	10.11	32.85	13.53	21.14	22.07	0.00	0.19	0.10	0.014	11.21

2.3.4 Levelized costs of syngas as substitute gaseous fuel

The economic analysis of the syngas production as substitute gaseous fuel, produced by MSW Plasma-G, is carried out considering the Levelized Cost of Syngas Production (LCOS) as the economic indicator. LCOS indicates the selling price of syngas per energy unit (US\$/kWh) to obtain an NPV equals to 0.0 over the whole lifetime of the plant. This calculi method is similar to one of the Levelized Cost of Electricity (LCOE), which has been calculated in other works [94]. Both parameters, LCOS and LCOE, consider the investment costs, the fixed and variable costs of operation and maintenance, the fuel costs (feedstock), and externality costs.

2.3.4.1 Cost estimation of plasma gasification technology

The five types of wastes produced in Medellin city are considered as potential feedstock for plasma gasification plants. The capacity of each plant depends on the production of each waste type (see section 2.2.1.). The costs information of Plasma-G technology is scarce; therefore, it has not been possible to obtain cost information from entrepreneurs or plasma gasification plant operators. The investment cost, and operating and maintenance costs (O&M) have been estimated from economic data available in previous published works [22], [61], [95]. The capital cost of each plant was calculated based on the information presented by Clark and Rogoff [61]. There, the capital cost for a Plasma-G plant, with a capacity of 300 TPD to produce syngas, was estimated based on the capital cost of a conventional mass burning plant with the same capacity, as shown Table 10.

Table 10. Capital cost for 300 TPD Plasma-G plant (syngas only configuration), adapted from [61].

Component	Price
Cost of mass burn plant (US\$)	66,000,000
Cost of stoker and boiler (US\$)	-16,500,000
Cost of exhaust stack (US\$)	-1,200,000
Cost of scale house (US\$)	500,000
Cost of syngas compressor, treatment, and pipeline (US\$)	1,100,000
Cost of steam turbine and auxiliary (US\$)	-16,500,000
Cost of waste pre-processing (US\$)	5,000,000
Cost of the plasma torch (US\$)	27,400,000
Cost of engine generators (US\$)	1,200,000
Cost of Plasma Gasification plant (US\$)	67,000,000

Base year cost: 2014

Here, in order to estimate the capital cost of each plant, it has been considered that a reduction of 50% in the plant processing capacity leads to decrease the capital cost by a half and multiplied by 1.1 factor, which is denominated an economy scale factor (an increase of 10%). Conversely, when the plant capacity is doubled (600 TPD), the capital cost increases twice, and it is multiplied by 0.9 factor (a reduction of 10%) [61]. According to this scale model, the estimated capital costs associated to each waste type is presented in Table 11. In order to verify the suitability of capital costs estimated here, the specific capital cost ranges (US\$/TPD) for each plant capacity were obtained from Byun *et al.* [95], and those ranges have been compared with the estimated costs in Table 11. Based on the comparison, it is worth note that our estimated capital costs are within the range's suitable values [95].

In order to estimate O&M cost, information from Byun *et al.* [95] was adapted for cases 3, 4, and 5, whose capacities are 75, 150, and 100 TPD, respectively (Table 11). Where O&M specific cost for a 100 TPD plant was 101 US\$/t. Furthermore, considering that the plants for cases 3 and 4 have a similar capacity (75 and 150 TPD), the same O&M specific cost was assumed for those plants (cases 3 to 5). On the other hand, specific costs from Ducharme [22] were taken for cases 1 and 2, an O&M specific cost of 53 US\$/t was found for a 750 TPD plasma gasification plant. Therefore, as cases 1 and 2 have similar processing capacity to that of 750 TPD, here, an O&M specific cost of 53 US\$/t for cases 1 and 2 is considered. Given that O&M specific cost for a 1000 TPD plant is lower than that of for a 750 TPD plant, 53 US\$/t for O&M specific cost is a conservative value. In Table 11 cost updated to December 2019 are presented.

Table 11. Capital and O&M cost for five analysed cases.

Case	1	2	3	4	5
Processed waste type	Residential	Mixed	Institutional	Commercial	Industrial
Plant capacity (TPD)	1000	1000	75	150	100
Capital cost (US\$)	171,300,000	171,300,000	20,300,000	36,850,000	29,050,000
Specific capital cost (US\$/TPD)	171300	171300	270667	245667	290500
Specific capital cost range (MMUS\$/TPD) [95]	0.132-0.178	0.132-0.178	0.287-0.361	0.221-0.327	0.261-0.350
Updated capital cost to 2020 (US\$)	232,851,86	232,851,86	27,594,24	50,091,02	39,488,30
Updated O&M specific cost (US\$/t)	83	83	159	159	159
Updated annual O&M cost (US\$)	27,525,250	27,525,250	3,934,000	7,868,100	5,245,400

The energy behaviour and technical parameters of each plasma gasification plant were calculated and analysed in section 2.3.3. The main parameters, such as air mass flow, syngas mass flow, torch power consumption, syngas composition and its heating value are shown in Table 12. Furthermore, it was assumed that the treatment system of plasma gasification plant completely removes the undesirable compounds from the syngas (H₂S, COS, HCl, etc.); as well as that a fraction of syngas is used to produce the torch power requirements by its combustion in an internal combustion engine (ICE) with a thermal efficiency of 36% [96].

2.3.4.2 Levelized cost of syngas production

LCOS was calculated for each plant case considering tax incentives in the Colombian renewable energy law context. Thereby, the tax incentives of the Law 1715 of 2014 and the benefits of the National Development Plan 2018-2022 have been evaluated on LCOS [21], [97]. Table 12 presents additional technical and financial data of the Plasma-G plants for each case, which is used for calculating LCOS. The specific cost and O&M cost of each plant were updated to December 2019, by means of Eq. 18 and Eq. 19, respectively. O&M cost includes the fixed and variable costs. The fuel cost is set to zero because, in the business model proposed here, the plants do not have to pay for solid waste [63], [66]. The externality cost represents an income (¢US\$/kWh) for the project from disposal of solid waste. For LCOS calculation is considered a discount rate of 8.1%, which was calculated according to Weighted Average Cost of Capital (WACC). Additionally, the cash flows have been calculated considering constant the following parameters: a lifetime of 20 years, a cost of 8.7 US\$/t for solid waste disposal, a market representative rate of 3300 COP/US\$ (December 29th, 2019), an accelerated depreciation on assets of 10 years, as well as the constant prices methodology. In Table 13 LCOS is presented without and with tax incentives for each plant.

Table 12. Technical and financial parameters for each plant case.

Case	1	2	3	4	5
Processed waste type	Residential	Mixed	Institutional	Commercial	Industrial
Treated syngas HHV (MJ/kg)	9.64	13.72	13.77	14.77	13.85
Treated syngas mass flow (kg/s)	10.16	8.51	0.84	1.75	1.35
Torch power consumption (MW)	24.19	24.07	2.29	4.81	3.63
Syngas flow for selling (Sm ³ /s) - [MMSCFD*]	2.94 - [8.98]	3.34 - [10.18]	0.34 - [1.05]	0.76 - [2.33]	0.57 - [1.75]
Syngas thermal power for selling [MW _{th}]	25.92	45.1	4.76	11.54	7.89
Yearly Energy Production (GWh _{th})	205.3	357.2	37.7	91.4	62.5
Efficiency of plant (%)	26.19	38.51	40.84	44.04	41.55
Capacity Factor	0.9	0.9	0.9	0.9	0.9
O&M costs (¢US\$/kWh)	13.4	7.7	10.4	8.6	8.4
Externality Cost (¢US\$/kWh)	1.4	0.8	0.57	0.47	0.46

*MMSCFD: Million standard cubic feet per day of syngas.

According to our results presented in Table 13, LCOS of each plant is reduced (by ~4.3% on average) when the tax benefits of Law 1715 of 2014 and of the National Development Plan 2018-2022 are applied. Case 2 (mixed wastes) reached the lowest LCOS (14.37 ¢US\$/kWh) because that plant has the highest yearly energy production and the lowest O&M cost, as shown in Table 12. Case 2 has associated the highest investment cost that is compensated by the two mentioned variables (high energy production and low O&M costs). Thereby, case 2 could generate a unity of energy at a lower cost than the other plants.

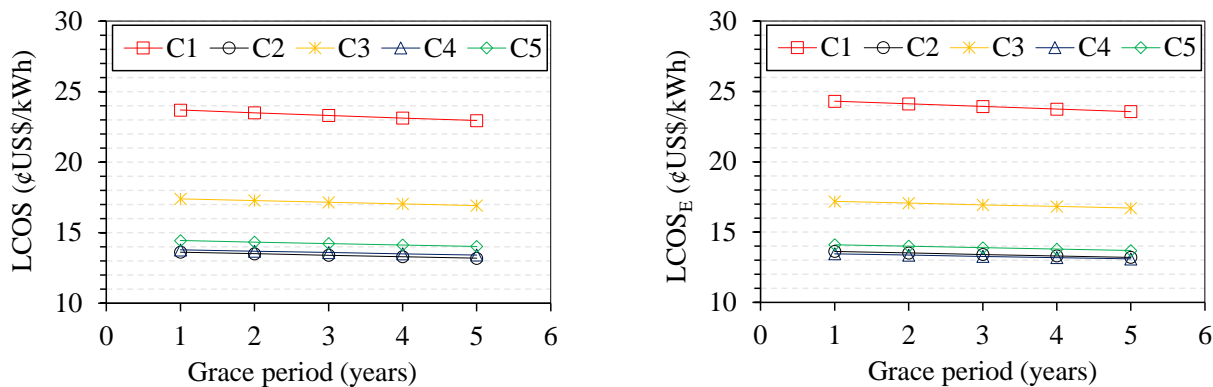
Table 13. LCOS without and with tax incentives.

Case	Waste type	LCOS without tax incentives	LCOS with tax incentives	Reduction
		(¢US\$/kWh)	(¢US\$/kWh)	(%)
1	Residential	26.21	25.01	4.59
2	Mixed	15.06	14.37	4.59
3	Institutional	19.02	18.25	4.07
4	Commercial	14.99	14.41	3.87
5	Industrial	15.83	15.17	4.22

On the other hand, the reduction percentage of LCOS increases if the investment costs and the pretax earnings of the plant increase. This is attributed to the effect of tax incentives on LCOS that depends on the investment tax credit, as shown in Eq. 17. Therefore, cases 1 and 2 reach the highest reduction on LCOS (4.59%), which is ascribed to their high investment costs and the pretax earnings. According to the highest investment costs for cases 1 and 2 (residential and mixed), these cases can take advantage to reduce LCOS.

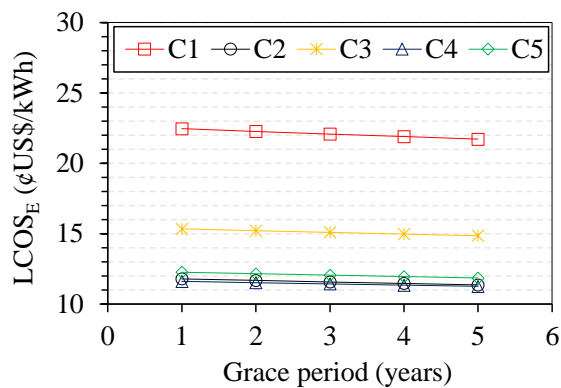
The benefits are related to the investment tax credit during the first fifteen years of operation, which allow recovering up to the 50% of the initial investment through the income tax [21], [97]. Seeking to further reduce LCOS of Plasma-G plants, here, an alternative investment plan is proposed. This alternative investment plan consists in financing 70% of the capital investment considering different grace periods, between 1 to 5 years, and the tax incentives. Figure 13a shows LCOS variation of each plant with regard to the grace periods.

LCOS of each Plasma-G plant decreases if the grace period increases (Figure 13a), this behaviour is related to the effect of the effective corporate tax income rate on the net present value. LCOS decreases when the financial interests are paid in some periods of the cash flow, where there is not deduction for accelerated depreciation. LCOS of the five cases (wastes types) for a grace period of 5 years is 22.95 ¢US\$/kWh, 13.19 ¢US\$/kWh, 16.92 ¢US\$/kWh, 13.42 ¢US\$/kWh y 14.02 ¢US\$/kWh, respectively. Consequently, case 2 reached the lowest LCOS, with a reduction by 12.43% with reference to LCOS without tax incentives.



a) LCOS variation as function of the grace period

b) International LCOS_E as function of the grace period



c) National LCOS_E as function of the grace period.

Figure 13. Effect of the grace period on LCOS and LCOS_E of each case of study associate to the five wastes types.

For this investment alternative, the effect of the tax incentives will be greater on projects with high investment costs and high pretax earnings, as well as within the projects where there is no financing.

Respecting the economic feasibility, in the international and national market, natural gas is traded at 2.3 US\$/MMBTU (LCOS=0.78 ¢US\$/kWh) [98] and 7.72 US\$/MMBTU (LCOS=2.6 ¢US\$/kWh) [99], respectively. Seeking that the syngas matches this levelized costs (LCOS), it is required that the Plasma-G plants receive an income from waste disposal charge that is represented by $LCOS_E$ externality, which is defined as the income per unit of generated energy associated (¢US\$/kWh) to the waste disposal charge. As the international and national price of the natural gas are different, one value of $LCOS_E$ must be calculated for each price of reference, finding an $LCOS_E$ for the international price and another one for the national price, named international $LCOS_E$ and national $LCOS_E$, respectively (Figure 13b and c).

Figure 13b and c show the international and national $LCOS_E$ considering tax incentives as a function of the grace period, respectively. According to these results and considering a grace period of 5 years as a reference, $LCOS_E$ of the plants 1, 2, 3, 4, and 5 must be equal to 23.56 ¢US\$/kWh, 13.20 ¢US\$/kWh, 16.71 ¢US\$/kWh, 13.1 ¢US\$/kWh, and 13.96 ¢US\$/kWh, respectively, to obtain an international natural gas price of 0.78 ¢US\$/kWh (2.3 US\$/MMBTU). For a national natural gas price of 2.6 ¢US\$/kWh (7.72 US\$/MMBTU), $LCOS_E$ of the plants must be 21.71 ¢US\$/kWh, 11.36 ¢US\$/kWh, 14.86 ¢US\$/kWh, 11.25 ¢US\$/kWh and 11.84 ¢US\$/kWh, respectively. When national and international price of natural gas (LCOS) are lower than that of the Plasma-G plants, the waste disposal charge must raise in order to obtain greater incomes from externalities and be able to reduce LCOS. On the other hand, analysing Figure 13b and c, $LCOS_E$ of each plant diminishes when the grace period increases. This behaviour stems from the effect of the effective corporate tax income rate on the net present value, since the net present value decreases when the financial interest payment is deferred to a longer time, while the tax incentives are considered. This was previously analysed in Figure 13a.

The plant of case 4 reached the lowest $LCOS_E$ for both scenarios (national and international), this is due to the highest ratio between incomes from energy generation and total incomes (sum of incomes from externalities and incomes from energy generation), and likewise the lowest LCOS without incentives, as shown in Table 13. Therefore, the incomes from the gaseous fuel (syngas) production and the low cost of the technology per unit of net power allow a greater reduction of the cost of solid waste disposal than the other plants. Finally, and according to the cash flows, the plant of case 2 (wastes mixed) presents the highest reduction percentage in $LCOS_E$, which is associated with the highest ratio between pre-tax earnings and externalities incomes, allowing it to take greater advantage of the tax incentives by means of the investment tax credit.

2.4 CONCLUSIONS

The syngas production from MSW Plasma-G has been studied from a techno-economic viewpoint. The five types of MSW generated in Medellin-Colombia (Residential, Mixed, Institutional, Commercial, and Industrial) were considered as feedstock. A new model of Plasma-G process was proposed and validated in order to investigate the effect of feedstock composition (MC from 26.6% to 57.9%) and plasma temperature (2500°C – 4000°C) on the process performance. An adverse effect of MC on raw syngas HHV was found, varying in average from 8.3 MJ/kg for Industrial waste to 5.71 MJ/kg for residential waste. Conversely, CGE and ExE were positively affected by a high MC since a feedstock with a high MC requires a lower torch energy consumption to be processed, this is ascribed to the updraft technology considered herein, where the gaseous phase dries MSW fed to the process by convective heat transfer. Therefore, the average CGE varies from 76.15% for residential waste to 74.97% for commercial waste; meanwhile, average ExE varies from 73.94% for residential waste to 70.07% for commercial waste. On the other hand, a high plasma temperature was related to a greater torch energy consumption, which leads to decrease CGE and ExE values. The suitable combinations of plasma temperature and air mass flow, that allow reaching the highest CGE, were found for each waste type. Thus, the maximum CGE reached was 79.22% for Residential waste, 82.77% (Mixed), 82.76% (Institutional), 83.46% (Commercial), and 82.84% (Industrial).

In order to assess the economic feasibility of the syngas production by means Plasma-G of MSW, LCOS was estimated and used as economic indicator. The five plant cases were considered according to the studied waste types, 1-Residential, 2-Mixed, 3-Institutional, 4-Commercial, and 5-Industrial. LCOS found without tax incentives is 26.21, 15.06, 19.02, 14.99, 15.83 ¢US\$/kWh for cases from 1 to 5, respectively. Nevertheless, when the tax incentives of Renewable Energy Law 1715 of 2014 and Development National Plan 2018-2022 are applied, LCOS is reduced up to 22.95, 13.19, 16.92, 13.42, and 14.02 ¢US\$/kWh for cases from 1 to 5, respectively. These reduction values on LCOS were reached considering the following statements: an accelerated depreciation on assets of 10 years, a financing of 70% of the initial investment, and a grace period of 5 years. It is highlighted that the plants 1 and 2 achieved the greater reduction percentage of LCOS (12.43%), which is attributed to their high investment costs and the pretax earnings, allowing them to exercise in a greater proportion the investment tax credit during the first fifteen years of operation. However, these projects of syngas production (as a substitute gaseous fuel) from solid waste are not yet financially feasible in Colombia, LCOS for each case is higher than the average national price of natural gas 2.6 ¢US\$/kWh (7.72 US\$/MMBTU – December 29th, 2019). Therefore, although the Plasma-G process of MSW is thermodynamically feasible, it is necessary to implement new tax policies and incentives in order to diminish LCOS ensuring financial feasibility and competitiveness of Plasma-G plants in our country. As it was proposed here, an increase in the waste disposal charge through $LCOS_E$ that must be

ranged between 11.25 and 23.56 ¢US\$/kWh on average contributes to the economic feasibility of the project.

Nomenclature			
<i>Abbreviations</i>		E_t	Yearly energy production, kWh
		ExE	Exergy efficiency, %
		i	Discount rate, %
		I_j	Investment tax credits, %
CPI	Consumer price index	I_0	Initial investment, US\$
DC	Direct current	\dot{m}	Mass flow rate, kg/s
HHV	Higher heating value, MJ/kg	MW	Molecular weight, kg/kmol
HTZ	High temperature zone	n	Lifetime of the project, year
LCOS	Levelized cost of syngas, US\$/kWh	P	Pressure, bar
LHV	Lower heating value, MJ/kg	R	Universal gas constant, kJ/kmol-k
LTZ	Low temperature zone, °C	t	Effective corporate tax income rate, %
MC	Moisture content, %	T	Temperature, °C
MSW	Municipal solid waste	t_1	Maximum time to apply the investment tax credits, years
O&M	Operative and Maintenance cost, ¢US\$/kWh	t_2	Lifetime of the project facility for accelerated depreciation purposes, years
PPI	Producer price index	\dot{W}	Power, MW
RDF	Refuse derived fuel	y	Molar fraction, dimensionless
RE	Relative error, %	η_{torch}	Torch efficiency, %
TPD	Ton per day, t/day	Δ	Tax factor
vol.%	Volume percentage, %	<i>Subscripts</i>	
WACC	Weighted average cost of capital	ch	chemical
wt.%	Weight percentage, %	E	externalities
<i>Symbols</i>		F	Fixed operating and maintenance
β	Ratio of chemical exergy to lower heating value	G	fuel
CGE	Cold gas efficiency, %	I	investment
\bar{c}_p	Specific molar heat capacity, kJ/kmol-K	ph	physical
C_t	net costs for operating, maintenance and externalities in year t	T	Total
d_j	Accelerated depreciation rate, %	th	thermal
e	Specific exergy, MJ/kg	V	Variable operating and maintenance
e^0	Standard chemical exergy, MJ/kmol	wb	Wet basis
ER	Equivalence ratio, dimensionless	0	Standard state

Exergoeconomic analysis of an integrated plasma gasification combined cycle for MSW energy recovery by modeling in Aspen Plus

Abstract

Herein, the energy recovery from different MSW through an integrated plasma gasification combined cycle (IPGCC) power plant was investigated from an exergoeconomic viewpoint, using the Theory of Exergy Cost methodology. This study was conducted by an implemented model using Aspen Plus. MSWs that fuel the IPGCC power plant are produced in Medellín-Colombia, which are classified according to the sector considering their production rates and moisture contents (MC). Residential (1121 t/day and 57.9% of moisture content), Mixed (1468 t/day, 51.33%), Institutional (75 t/day, 37.92%), Commercial (168 t/day, 32.95%), and Industrial (104 t/day, 26.61%). Regarding the exergy analysis, for all plant cases, the plasma gasifier (PG) and the gas turbine (GT) reached the largest exergy destruction ratio, whose average contribution was 36.2% and 40.3%, respectively. This was ascribed to the exergy destruction by MSW drying into the PG, and by the oxidation reactions in the GT's combustion chamber. Furthermore, as the MC of wastes increased (26.6% to 57.9%), the exergy destruction ratio of PG increased by 23.5%, leading to decrease the energy and exergy efficiencies of the IPGCC plants by 23.7% on average. This behavior was attributed to the adverse effect of high MC of wastes on the syngas quality. The exergy cost of electricity ranged from 11.0 to 14.5 ¢US\$/kWh. Therefore, the plants with a processing capacity from 100 to 1000 t/day require a MSW treatment fee between 86.10 and 50.50 US\$/t to equal the unit exergoeconomic cost of electricity with the hydro-electricity price in the Colombian energy market (6.92 ¢US\$/kWh).

3.1 INTRODUCTION

Electricity is the driving force of the modern economies; thereby, its use is in constant growth for energetic services. Furthermore, electricity demand will increase as a result of the rising household incomes, due to its use for transport and heating, and the growing demand for digitally connected devices. In 2020, the global electricity generation is projected as 28000 TWh, of which ~61% will be produced from fossil fuels (oil, gas, and coal) [100]. In Colombia, the two main energy sources for electricity generation are hydraulic power plants and thermal ones based on fossil fuels (natural gas and coal), with a share participation in the

power mix of ~70% and ~30%, respectively [101]. Important issues have been associated with these two energy resources in the country. The hydraulic power generation is strongly affected by climate phenomena (e.g. “El Niño”) [18] leading to the increase of the electricity price in the national energy market from an average value of 12 ¢US\$/kWh to values up to 30 - 100 ¢US\$/kWh in the dry season where the power is produced by thermal power plants fueled with natural gas or diesel, and coal [102]. On the other hand, the fossil fuels sector has an uncertain future since the reserves-to-production ratios (R/P) for natural gas and oil are 8.3 and 5.6 years, respectively [103]; as well as, the volatility of fossil fuel market could lead risks in the country economy [104].

The high generation rate of municipal solid waste (MSW) and how it is disposed is another important issue for worldwide societies. According to the World Bank’s projections, the global production of MSW will increase up to ~2200 million tons in 2025, reflecting an increase of 60% regarding 2012 [1]. In Colombia, the generation rate of MSW was ~30100 t/day in 2017, while the average annual increase has been ~2% [9]. From the total MSW produced in the country, only 17% is recycled, while the remaining 83% is disposed in landfills and other inappropriate disposal-sites or methods (open dump, waterbody, water streams, burial, and open burning) [10]. Landfilling has been associated with problems such as complex and expensive emissions control, large land use, long-time degradation of waste, and low acceptance by population [13]. Therefore, MSW sector projections indicate that recovery strategies must be implemented in order to reduce landfill disposal, avoiding sanitary emergencies by 2030 [9], [10].

In this scenario, the energy recovery from MSW for power generation could be an important alternative to face the above-described issues, since it reduces the amount of waste disposed in landfills and the conventional sources dependency for power generation (i.e. hydraulic energy and fossil fuels). Furthermore, the power generation from MSW energy recovery contributes to reduce the city’s carbon footprint, since a carbon fraction of MSW is from biogenic origin (~50%) [7], and to develop the circular economy [23]. Power production using MSW can be carried out by means of several technologies [7], [8], [12], [26], [105], known as Waste-to-Energy (WtoE), where the incineration plants coupled to steam turbines are the most widespread technology, whose average efficiency is ~20% [43]. Nevertheless, plasma gasification has recently obtained growing attention because of its high efficiency and flexibility [34]. The plasma gasifier could be coupled to several technologies such as internal combustion engines (ICE) with efficiencies of ~30% [106], gas turbine (~30% of efficiency in combined cycle configuration) [43], [107], or fuel cells (~35-45% of efficiency) [76], [108].

The global installed capacity of WtoE plants was 12912 MW in 2015, this sector is led by developed countries such as United States (2254 MW installed capacity), Germany (1888 MW), and Japan (1501 MW)

[109], where most of the facilities are based on incineration technology. On the other hand, in developing countries (e.g. Colombia) landfill disposal is still the main pathway to manage MSW. Therefore, based on the higher efficiency of the Integrated Plasma Gasification Combined Cycle plants (IPGCC) (~30%) with regard to the conventional incineration plants (20%), as well as its environmental benefits, IPGCC could be an efficient solution alternative to the problems stemmed from the high amount of MSW generated in Colombia, where sanitary emergencies are expected because of the short lifespan (0 - 3 years) of about 40% of those disposal-sites [9].

In order to assess the suitability of power generation by IPGCC plants, the modeling and simulation are valuable tools to develop preliminary feasibility studies from thermodynamic, environmental, and economic viewpoints, since significant results are obtained with relatively low time and investment costs. Several works have focused on modeling and studying the performance of plasma gasification-based systems, analyzing the effect of different operative parameters and feedstock type. Mountouris *et al.* [110], modeled the plasma gasification of sewage sludge for electricity generation with a gas engine. This system is able to process 250 t/day of sewage slug with a moisture content of 68% to produce heat (thermal energy) for drying the feedstock (4.56 MW), and the electricity requirement for the plasma furnace (1.35 MW), and the net electricity power (2.85 MWe), which leads to a net thermal efficiency of ~19%. Minutillo *et al.* [43] and Valmundsson & Janajreh [107] characterized the energy recovery from different solid wastes by modeling an IPGCC technology using Aspen Plus. Both works considered 4000°C and 2500°C as temperatures for plasma and the main gasification reactions, respectively. For the former, the highest efficiency was 31% when refuse derived fuel (RDF) and air were fed to IPGCC plant as feedstock and plasma gas, respectively [43]. Whereas, the use of waste tire as fuel with steam as plasma gas derived an efficiency of 28.5% [107]. Matveev *et al.*, [111] modeled a small scale IPGCC power plant fed with coal. The effect of oxidizer (air, O₂, and steam), the gasifier pressure (1.5 – 10 bar), and the gas turbine (GT) technology (simple cycle or with regeneration) were analyzed. It was highlighted that the use of O₂-water vapor mix as oxidizer, at a pressure level of 7.5 - 8 bar, and with regeneration in the gas turbine leads to reach the highest efficiency of the system, which ranges from 25% - 36.4%. Otherwise, the co-processing of MSW and plastic solid waste (PSW) in an IPGCC was investigated by simulation using Aspen Plus environment. Mixtures of air with O₂ or water steam were considered as plasma gas. The plant's highest efficiency was 38%, which was reached when pure O₂ and a mixture of 70% MSW - 30% PSW were fed to the gasifier; finding a direct relation between the overall plant efficiency and the plasma gasifier efficiency [56].

Pena *et al.* [73] proposed the integration of MSW plasma gasification with intermittent renewable sources for electricity generation. In this system, solar or wind energy were used to produce hydrogen via electrolysis, which is used as plasma gas to be fed to the gasifier, while the syngas is fed to a combined cycle

for power generation. The highest global efficiency was 40%, which indicates that the proposed approach is able to use a low-energy fuel (e.g. MSW) for electricity generation with better performance than that of incineration or conventional gasification. Other previous works have investigated the technical feasibility of coupling MSW plasma gasification with solid oxide fuel technology for power generation, standing out the high efficiency of those systems (27%-45%) [54], [108], [112].

Beyond the techno-economic assessment, WtoE processes have been analyzed from the exergoeconomic viewpoint. This methodology combines exergy analysis and economic principles in order to assess the feasibility of energy conversion systems. The results get from the exergoeconomic analysis provide crucial information about systems' design and operation, which is not possible to obtain through conventional energy and economic analyses [47], [113]. Although several previous works have been focused on assessing WtoE processes from an exergoeconomic viewpoint, no exergoeconomic assessment of an IPGCC plant fed with MSW has been found in the reviewed literature.

A modeled MSW incineration-steam reheat power plant was characterized by means of exergoeconomic calculations. The exergy efficiency of this power plant was 31.36%, and the highest exergy destruction rate and cost of exergy destruction were allocated in the incinerator (2.26 MW and 1626.3 US\$/h, respectively), which is ascribed to the large irreversibility associated with the combustion process. The unit cost of electricity was 55.72 US\$/MWh, which is higher than that of steam power plants fueled by natural gas [114]. Behzadi *et al.* [115] combined the thermo-economic analysis with a multi-objective optimization methodology to investigate and compare gasification and digestion of MSW for electricity generation through a Rankine cycle. The optimal exergy efficiencies were 17.98% and 19.02% for gasification- and digestion-based system, respectively, while the corresponding total product unit cost for the gasification system was 28.31 US\$/GJ, and 27.68 US\$/GJ for the digestion one. The lower performance of the gasifier-based system is ascribed to the moisture content of MSW and the gasification temperature. Meanwhile, Kalinci *et al.* [47] and Nakyai *et al.* [113] analyzed from an exergoeconomic viewpoint the hydrogen production from waste gasification. Kalinci *et al.* [47] used the specific exergy cost method to assess a plasma gasification-hydrogen purification system fed with sewage sludge (~100 t/day) for hydrogen production. The pressure swing adsorption unit was associated with the highest exergy destruction rate (11.66 MW), followed by the plasma gasifier (6.55 MW). Furthermore, the low performance of the system (global efficiency of 2.6%) and high exergy cost of hydrogen (208.6 US\$/GJ) were attributed to the low hydrogen yield in the plasma gasifier (20.23 vol%). Nevertheless, Nakyai *et al.* [113] analyzed the gasification of biomass with methane co-feeding. The results indicated that the addition of methane has a positive effect on hydrogen production. The highest hydrogen yield was 67.31 mol-H₂/kg_{biomass} when air (0.21 kg_{air}/kg_{biomass}) and steam (1.0 kg_{steam}/kg_{biomass}) were used as gasifying agents, and methane was co-fed

with a ratio of $0.36 \text{ kg}_{\text{methane}}/\text{kg}_{\text{biomass}}$. Consequently, at these conditions, the highest exergy efficiency was 71.8%, leading to reach the lowest unit hydrogen cost (2.69 US\$/kg_{H2}) and the lowest unit exergy cost of hydrogen (6.8 ¢US\$/kWh). Casas Ledón *et al.* [116] applied the exergoeconomic analysis on a modeled IPGCC fueled with MSW. The gasifier temperature must range from 850 to 950 °C to produce syngas with enough energy content to fuel the generation island and keep an exergy efficiency of about 49%. The exergy destruction was determined as the major contributor to the exergy cost rate, whilst the gasifier accounted for nearly 60% of the total exergy losses. The thermo-economic cost of the produced electricity was ranged from 7 to 13 ¢US\$/kWh, which could be competitive in the Chilean electricity market (12 ¢US\$/kWh).

Plasma gasification has been recognized as one of the most effective and environmentally friendly methods for MSW treatment and its energy recovery [43]. Likewise, exergoeconomic investigation on IPGCC systems for MSW energy recovery have not been carried out in the Colombian context. Therefore, a comprehensive exergoeconomic assessment of an IPGCC plant using MSW as feedstock is carried out in this chapter, looking for providing relevant technical and economic information for the decision-makers and encourage the implementation of WtoE projects, contributing to mitigate and to avoid the environmental and social issues stemmed from landfill disposal of MSW, as well as, to diversify the national energy mix according to Colombian National Energy Plan projected to 2050 [20], [21].

3.2 METHODOLOGY

The feedstock that fuels the IPGCC power plant is MSW produced in Medellín-Colombia, which can be classified in four waste categories according to the sector from where it comes, as follows: Residential (Res), Commercial (Com), Industrial (Ind), and Institutional (Ins). The generation rate and physical composition of wastes from each sector, as well as the mixture of them (Mixed, Mix), were estimated using data from [64], [65]. Meanwhile, the information from Zhou *et al.* [67], Balcazar *et al.* [68], and Channiwala and Parikh [80] (Eq. 22) was used to estimate the ultimate and proximate analyzes, the moisture contents (MC), and the higher heating value (HHV) of the wastes, respectively. The properties of MSW studied in this work are presented in Table 14. It should be clarified that inert and dangerous wastes have not been considered here.

$$\text{HHV} = 0.3491\text{C} + 1.17833\text{H} + 0.1005\text{S} - 0.1034\text{O} - 0.0151\text{N} - 0.0211\text{A} \quad \text{Eq. 22}$$

The calculation procedure for estimating the above-mentioned properties of wastes was presented in detail by Montiel-Bohórquez and Pérez [19].

Table 14. Generation rate, heating value, and ultimate and proximate analyzes of MSW produced in Medellin.

MSW type (by sector)	Generation rate [t/day] _{wb}	HHV _{wb} [MJ/kg]	Ultimate analysis (wt% dry base)						Proximate analysis (wt% dry base)			MC (wt%)
			C	H	O	N	S	Cl	FC	VM	Ash	
Residential	1121	8.55	53.01	6.91	36.85	2.65	0.34	0.24	12.36	77.53	10.11	57.90
Mixed	1468	10.12	53.64	7.03	36.37	2.38	0.32	0.26	11.90	78.49	9.61	51.33
Institutional	75	13.42	55.04	7.04	36.16	1.41	0.26	0.09	10.92	80.73	8.35	37.92
Commercial	168	15.10	56.05	7.47	34.60	1.47	0.26	0.15	10.19	81.38	8.43	32.95
Industrial	104	16.41	54.98	7.43	34.70	1.87	0.35	0.67	10.82	81.58	7.60	26.61

wb: wet base

3.2.1 IPGCC power plant description

Herein, the IPGCC power plant was roughly divided into three major sections: the plasma gasifier, the syngas treatment system, and the gas turbine combined cycle. The general scheme of the plant layout is shown in Figure 14. Here, each component was conveniently labeled with its corresponding number enclosed by a circle; meanwhile, each stream was labeled by using a square for enclosing its corresponding number. In the plasma gasifier (Component 1), MSW is thermally decomposed by the plasma and transformed into syngas (Stream 4) and non-leachable slag (Stream 5). Since the raw syngas produced in the plasma gasifier contains solid particles (fly ash) and pollutants or impurities (HCl, H₂S, COS), the syngas must be treated to match the quality requirements for the gas turbine (*i.e.* tars \leq 10 mg/Nm³, dust \leq 5 mg/Nm³, alkalis \leq 0.1 ppm-weight basis, and H₂S \leq 20 ppm, volume basis) [34], ensuring the allowable emission levels. Afterward, the treated syngas is compressed and sent to the combined cycle where it is burned to produce power. The plasma gasifier technology considered here is an updraft plasma gasifier (Component 1), which works at atmospheric pressure and uses DC torch as plasma generator for thermal degradation of MSW (Stream 1); the plasma gas used by this reactor is air that is fed as Stream 2. The raw syngas (Stream 4) coming out from the plasma gasifier at high temperature must be cooled down before being fed to the purification units, typically up to 250°C [117], [118]. The heat transferred from the syngas cooling is used to generate steam at high (HP) and intermediate (IP) pressures (Streams 78 and 81, respectively). The cooled syngas (Stream 7) flows through the fabric filter (Component 4) for removing the particulate matter by means of a layer of cloth filtration. Afterward, the syngas flows through a wet scrubber (Component 5) where halogens (*i.e.* HCl), which can cause corrosion and fouling in downstream equipment, are removed by a NaOH aqueous solution (Stream 10) [107], [117]. On the other hand, as the sulfur removal must be carried out at relatively high pressure (4.8 – 24.8 bar), the syngas must be compressed and cooled (Components 6 and 7) before being supplied to the sulfur removal units. First, COS in the gaseous stream is converted into H₂S and CO₂ by means of a COS-hydrolysis unit (Component 8) at temperatures \geq 190 °C [117]. COS must be converted into H₂S since typically sulfur removal methods have been optimized for H₂S

absorption (e.g. methyl-diethanolamine (MDEA) absorption). The syngas that comes out from the COS-hydrolysis unit is cooled up to $\sim 40^{\circ}\text{C}$ in a low-temperature gas cooler (LTGC, Component 9), where low-pressure steam is produced (LP-steam, Stream 75). Forward, the syngas flows through the absorber where an MDEA solution is used as the solvent. The polluted MDEA solution is treated by means of the sour water stripper for sour gases desorption and, subsequently, the treated MDEA solution is recycled and feedback to the absorber. In this work, the MDEA absorber, the sour water stripper, and auxiliary equipment was considered as one component and enclosed by a dashed rectangle (Component 10). Finally, the treated syngas (Stream 20) is preheated by recovering the heat of the compressed syngas (Stream 13), and it is fed to the combustion chamber (Component 12) of the gas turbine, where the syngas (Stream 21) is burned with air (Stream 22) for power generation (Streams 24 and 29). The gas turbine's exhaust gases (Stream 30) flow through a triple pressure heat recovery steam generator (HRSG, Components 16 to 25), where the steam is produced by reclaiming the sensible heat of the exhaust gases. This steam is expanded in the steam turbines (Components 29, 32, and 36) for further power generation (Streams 48, 58, and 67).

3.2.2 IPGCC power plant model description

All units that comprise the IPGCC power plant were modeled using Aspen Plus v10, selecting the suitable thermodynamic methods and operating conditions, which have been adapted from specialized literature. The Peng-Robinson equation of state was used to estimate the physical properties of the plasma gasification process and the syngas streams in downstream units, as well as the properties of gaseous streams in the gas turbine [73], [119], [120]. This equation of state is widely used for estimating physical and chemical properties in processes involving hydrocarbons and light gases [118], [121]. The physical properties of syngas' purification units, where aqueous solutions are used to remove pollutants (e.g. wet scrubber, MDEA absorber/stripper), are based on an activity coefficient model because of the non-ideal behavior of the liquid phase associated with pH change for gas-liquid dissolution, and the presence of electrolytes [118]. Therefore, the ENRTL-RK property method was selected for these purification processes, which uses the Redlich-Kwong equation of state for vapor phase properties and Henry's law for solubility of supercritical gases. This property method was suggested by Aspen Plus for any liquid electrolyte solution containing water. Finally, STEAM-TA was chosen for estimating the properties of water and steam streams involved in the steam power cycle [120]. This fluid package uses 1967 ASME steam table correlations for thermodynamic properties, and the correlations of the International Association for Properties of Steam (IAPS) for transport properties, this method is suitable for pure water at temperature ranges from 273.15 – 1073 K and pressures up to 1000 bar [121].

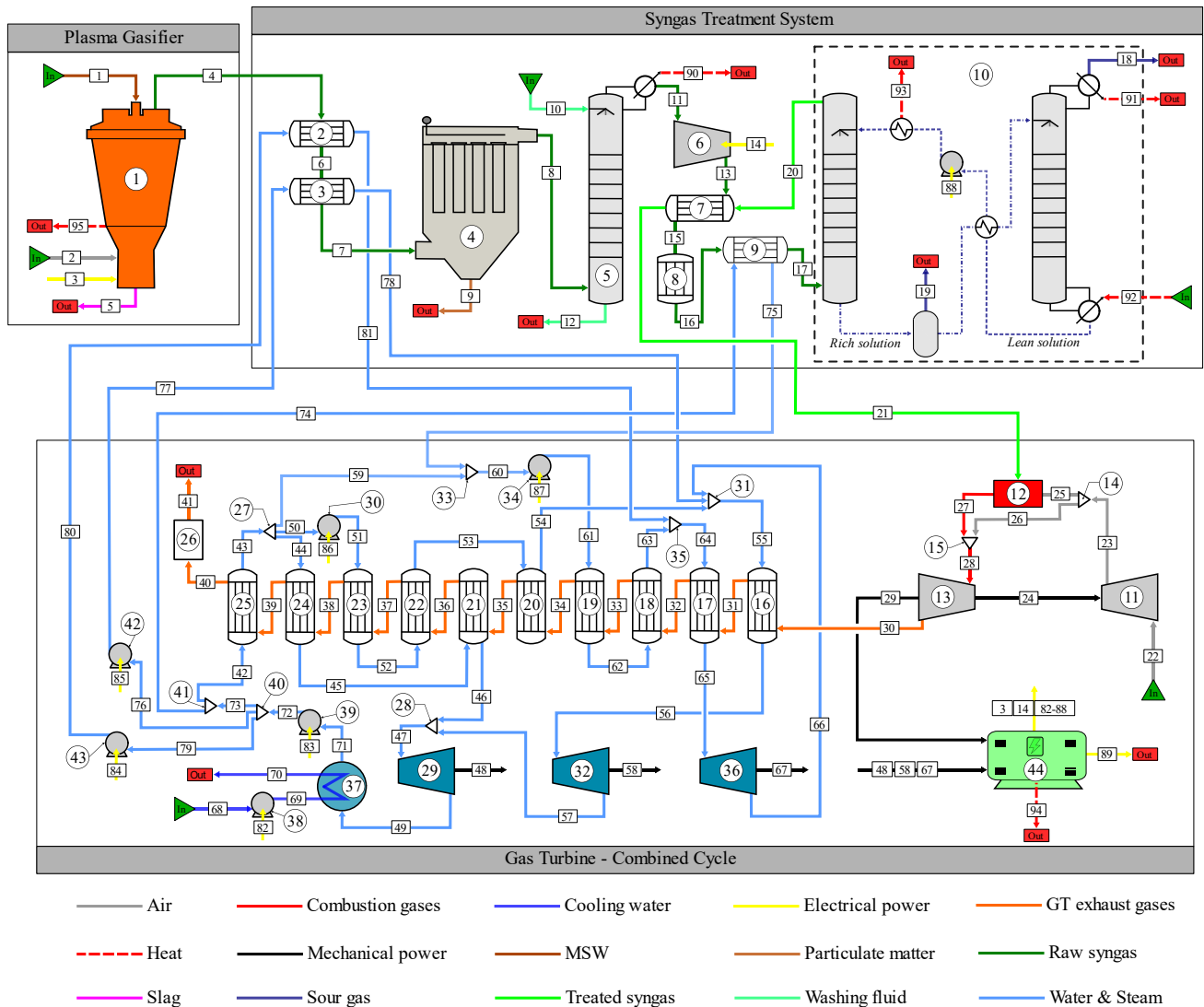


Figure 14. Scheme of layout of the IPGCC power plant. **1:** Plasma Gasifier. **2&3:** Syngas cooling system (SCS). **4:** Fabric filter. **5:** Wet scrubber. **6:** Syngas compressor. **7:** Syngas preheater. **8:** COS-hydrolysis unit. **9:** Low temperature gas cooling (LTGC). **10:** MDEA absorber/stripper system. **11:** Air compressor. **12:** Combustion chamber. **13:** Gas turbine (GT). **14:** Compressed air splitter. **15:** Combustion gases-cooling air mixer. **16:** Reheater. **17:** HP-Superheater. **18:** HP-Evaporator. **19:** HP-Economizer. **20:** IP-Superheater. **21:** LP-Superheater. **22:** IP-Evaporator. **23:** IP-Economizer. **24:** LP-Evaporator. **25:** Feed water (FW) preheater. **26:** Exhaust stack. **27:** Preheated-water splitter. **28:** LP-steam mixer. **29:** LP-steam turbine. **30:** IP-water pump. **31:** IP-steam mixer. **32:** IP-steam turbine. **33:** HP-water mixer. **34:** HP-water pump. **35:** HP-steam mixer. **36:** HP-steam turbine. **37:** Condenser. **38:** Cooling water pump. **39:** FW pump. **40:** Feed water splitter. **41:** LP-water splitter. **42:** IP-SCS water pump. **43:** HP-SCS water pump. **44:** Electric generator.

3.2.2.1 *Plasma Gasification model*

The thermochemical equilibrium model of a moving bed updraft plasma gasifier was developed according to the hypothesis, such as steady-state process, perfect-insulated reactor [55], perfect mixing inside the reactor [74], no tar formation due to the high reaction temperature [43], the gasification reaction reaches the thermochemical equilibrium due to the long residence time of both phases (solid and gas) [53]. The plasma gasification of MSW can be successfully modeled under a thermochemical equilibrium approach because of the relatively high temperature involved in the process, without considering the hydrodynamic phenomenon in the reactor [43], [53], [57], [59], [71]–[73]. The global gasification equation modeled in this work is presented in Eq. 1 [43].

The model encompasses the heat exchange between the hot gaseous phase (syngas) flowing from the bottom to the top, and the solid phase (MSW) which travels from the top to the bottom (see Figure 6 in Section 0). A fraction of the energy absorbed by the solid phase is used for MSW drying at 110 °C; thus, the evaporated moisture mixes with the syngas and exits from the top of the reactor [43], [53], [55]. The remaining absorbed energy increases the temperature of the solid phase until it reaches the high-temperature zone, where it is thermally converted into syngas and slag by the plasma jet. Considering the temperature distribution inside the plasma reactor, the gasifier can be classified into two gasification zones [43], for instance, high temperature (HTZ) and low-temperature zones (LTZ). This approach has been used in previous plasma gasification works [43], [53]–[55], [75]. However, in this work, it is proposed and developed a new model approach. Regarding the previous models presented in the above-mentioned works, some modifications have been implemented looking for a closer representation of the actual process. The contributions implemented to our model are listed, as follows: 1) The energy required to dry MSW has been directly included in the energy balance of the process. This drying energy is composed of the heating process of MSW up to the drying temperature (110 °C) and of evaporating the moisture. 2) The convective heat transfer between the gaseous phase and MSW after the drying process has been considered up to MSW reaches the plasma zone. 3) The inorganic fraction of MSW has been considered for thermochemical equilibrium calculations of the plasma gasification process. The detailed description of the flowsheet and the built-in blocks implemented were presented in section 0, besides the validation results were presented in section 2.3.1.

3.2.2.2 *Syngas treatment system model*

3.2.2.2.1 *Syngas cooling system*

The syngas coming from the plasma gasifier must be cooled until suitable temperatures for downstream conditioning units. The syngas stream is typically cooled up to 250°C before it flows through the particulate

matter removal system (i.e. Fabric Filter) [117], [118]. In this work, the heat from the syngas cooling is used to generate steam at high and intermediate pressures. Thus, two **HeatX** blocks, HP-COOL and IP-COOL, were used for modeling the cooling process at each pressure level (see Figure 15a). In both HeatX blocks had been selected the shortcut and countercurrent modes, and set a minimum temperature approach of 10°C. Furthermore, in these blocks, the syngas streams (streams 4, 6, and 7) were linked to the hot connections, whilst the water (streams 77 and 80) and steam streams (streams 78 and 81) were linked to the cold connections. For HP-COOL block, the cold stream outlet vapor fraction was chosen as specification and set as 1.0; while in the case of IP-COOL block, the specification was the cold stream outlet temperature set at 312°C. For each heat exchanger, the pressure losses of the syngas and steam streams were considered as 1% and 1.5% of corresponding inlet pressure, respectively [122].

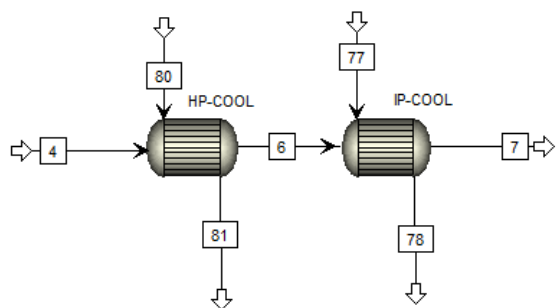
3.2.2.2.2 *Fabric filter*

Although Aspen Plus includes a dedicated built-in block for fabric filter modeling (FabFl), it requires the particle size distribution of solid particles to be removed from the gaseous stream; nevertheless, in this work, the particle size distribution was not considered. Thereby, the fabric filter was modeled by means the built-in block **Sep** (F-Filter), which separates components based on specified flows or split fractions. The Aspen Plus flowsheet for this component is shown in Figure 15b. The syngas coming out from the syngas cooling system (SCS) is fed to the F-FILTER block. Two outlet streams are set for outlet flows, one for cleaned syngas (Stream 8) and another one for solid particles (Stream 9). As outlet stream condition of stream 8, a split fraction equals to 1.0 was set for H₂, CO, CH₄, CO₂, H₂O, HCl, H₂S, and COS; meanwhile, that of C, Cl, and S was set equals to 0.0 in order to computationally remove any unreacted component from the syngas stream. Furthermore, the pressure drop of the syngas stream flowing through the fabric filter was considered as 1.74 kPa [123].

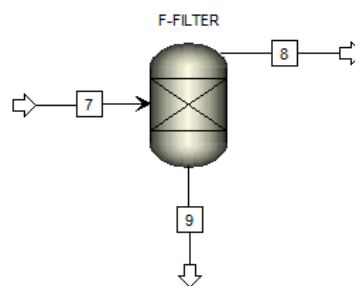
3.2.2.2.3 *Wet scrubber*

After the syngas cooling and solids removal units, HCl from the syngas must be removed. Since this compound causes excessive corrosion and fouling in downstream equipment, the HCl removal must be the first stage in the purification system. To this aim, the syngas (Stream 8) is fed to a wet scrubber where HCl is absorbed by a NaOH aqueous solution (Stream 10). Additionally in this unit, the syngas is further cooled and some of the water vapor in the syngas stream is condensed [107], [110]. The wet scrubber was modeled using a **RadFrac** model (see Figure 15c) [118], which is a rigorous model for simulating all types of multistage vapor-liquid fractionation operations such as ordinary distillation, absorption, stripping, and extractive and azeotropic distillation. In this block, the absorption of HCl was modeled under an equilibrium calculation approach. A partial-vapor condenser type was used to get a syngas temperature of 30°C at the outlet of the wet scrubber (Stream 11); this temperature was obtained by fitting the amount of heat (heat

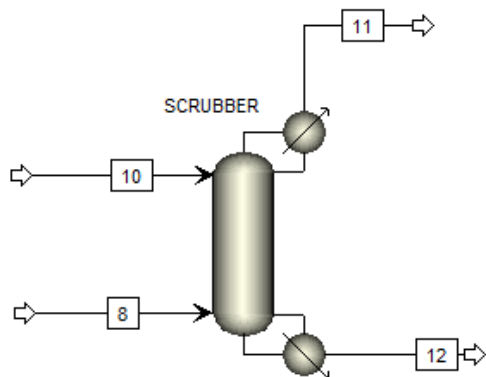
duty) removed from the condenser. The treated syngas leaves at the top of the scrubber, while the polluted NaOH solution (Stream 12) leaves at the bottom. Henry's components were HCl, H₂S, and CO₂, according to the suggestion of Aspen Plus. The considered reaction mechanism that takes place in the system is represented by equations Eq. 23 to Eq. 29 [118], [124]. The operational conditions such as number of stages, pressure drop across the wet scrubber, and mass flow are summarized in Table 15 [118]. As it is shown there, the mass flows of water and NaOH supplied to the wet scrubber as Stream 10 were set as a percentage (0.12% and 9%, respectively) of the syngas that flows through the wet scrubber (Stream 8) [118].



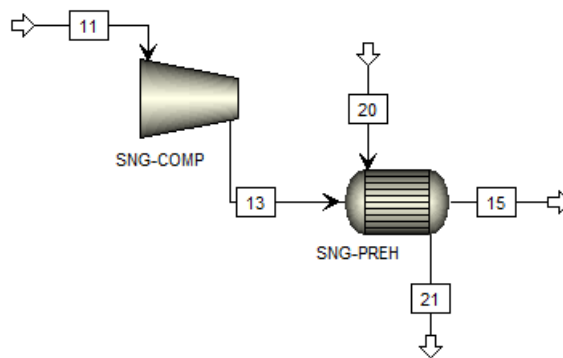
a) Syngas cooling system.



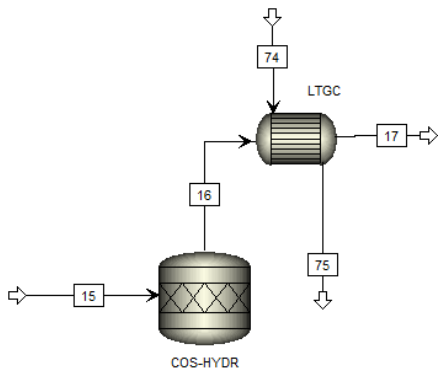
b) Fabric filter as solid separator.



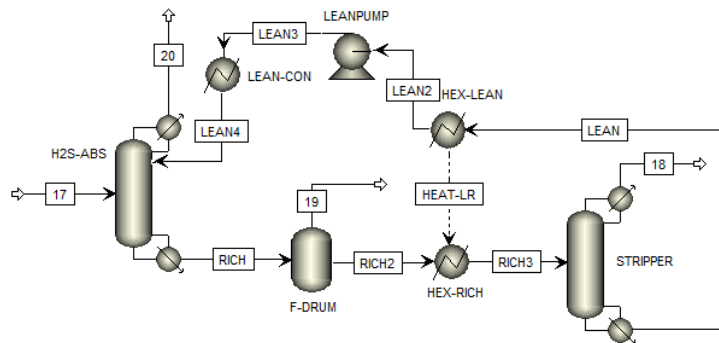
c) Wet Scrubber.



d) Syngas compressor and syngas preheater



e) COS-hydrolysis unit and LTGC.



f) MDEA absorber/sour water stripper system

Figure 15. Aspen Plus model of syngas treatment units.



Table 15. Operative parameters of wet scrubber. Adapted from [118].

Parameter	Unit	Value
Stages	number	10
Pressure drop	%	5
NaOH consumption	mass	0.12% of syngas flow rate
H ₂ O consumption	mass	9% of syngas flow rate

3.2.2.2.4 Syngas compressor and syngas preheater

The syngas must be compressed before it flows through the sulfur abatement units (i.e. COS-hydrolysis unit, MDEA absorber) because the process for sulfur removal have been optimized for high pressures (4.8 – 24.8 bar), as stated earlier. Thereby, a gas compressor was used to increase the pressure of the syngas (Stream 11) up to the pressure working of the gas turbine. The syngas compressor was modeled in Aspen Plus as an isentropic compressor type by using the **Compr** block (SNG-COMP in Figure 15d), the isentropic efficiency was set as 88.4% [107]. Although the inlet pressure of the gas turbine is around 19 bar, the discharge pressure of the syngas compressor must be slightly higher to compensate for pressure losses in the downstream units; thus, the compressor's discharge pressure was set as 21.785 bar.

The exit syngas temperature from the compressor (stream 13) is ~450°C, which is high for COS-hydrolysis process; by that, a heat exchanger (SNG-PREH in Figure 15d) has been implemented for cooling the syngas up to 190°C. The heat is transferred by preheating the syngas that comes from MDEA absorber (Stream 20) before being fueled to the combustion chamber of the gas turbine. A **HeatX** block was implemented, in a similar way of those in SCS, for modeling the syngas preheater. A hot stream outlet temperature equals to 190 °C (Stream 15) was set as the specification for this block, and the pressure losses were considered as 1% of the pressure of input streams of the preheater (13 and 20) [122].

3.2.2.2.5 COS-hydrolysis unit and LTGC

In the COS-hydrolysis unit, COS reacts with water vapor to produce H₂S and CO₂ using alumina as catalyst; typical conversion efficiencies of COS are 99% or higher [124], [125]. The typical sulfur removal technologies have low efficiencies for COS, as they achieve high efficiencies when the sulfur in the syngas stream is H₂S. Thus, the COS hydrolysis operation must be carried out before the H₂S removal. Eq. 30 represents the global reaction modeled in the COS-hydrolysis unit.



COS-hydrolysis unit was modeled by means of a stoichiometric reactor (**RStoic**), which is shown in Figure 15e as COS-HYDR. A pressure loss equivalent to 7% of syngas inlet pressure (Stream 15), and a reactor heat duty equals to 0.0 were set as operating conditions. The reaction represented by Eq. 30 was specified considering a COS fractional conversion of 0.99 [118].

The COS free syngas must be cooled down before it enters the MDEA absorber. Therefore, the syngas (Stream 16) flows through a heat exchanger (LTGC in Figure 15e) where the heat from cooling is exploited for transforming water (Stream 74) into LP-Steam (Stream 75). LTGC unit was modeled by means of a **HeatX** block specifying a cold stream outlet temperature of 141°C (Stream 75), and considering the pressure losses as 1% of syngas inlet pressure and 1.5% of water inlet pressure for the hot and cold side, respectively [122]. The mass flow of water (Stream 74) is adjusted pursuing that the output syngas temperature (Stream 17) is ~40°C.

3.2.2.2.6 MDEA absorption and sour water stripping system

This system encompasses two major processes. First, H₂S absorption by an MDEA aqueous solution, and second, MDEA regeneration by desorption of acid gases from MDEA solution. The flowsheet implemented for modeling the system is presented in Figure 15f. The syngas (Stream 17) is fed to the absorber working at ~20 bar (H₂S-ABS), where the MDEA solution (commonly called as a lean solution) acts as a chemical solvent and absorbs acid gases from the syngas stream, mainly H₂S, where the sulfur compounds are reduced as far as 10 ppm [117], which is lower than the permissible sulfur requirement for the gas turbine of 20 ppm, volume basis [34]. Subsequently, the clean syngas (Stream 20) flows through a heat exchanger to be preheated by the compressed syngas that leaves at high temperature (as stated in section 3.2.2.2.4). Meanwhile, the polluted MDEA solution (rich solution) flows to the flash vessel (F-DRUM) in order to reduce its pressure up to 1.5 bar that is the working pressure for desorption in the stripper (STRIPPER) [118]; furthermore as a secondary process, a fraction of gaseous species contained in the reach solution are

separated from the liquid phase and leave from the flash vessel (F-DRUM) as Stream 19 [126], [127]. Downstream, the rich solution interchanges heat with the hot lean solution that leaves from the stripper (HEX-LEAN and HEX-RICH) seeking to diminish the energy duty in the stripper (STRIPPER) for the desorption operation. The leaving streams associated with the stripper are two, the former is the lean solution (LEAN) that is reconditioned and feedbacked to MDEA absorber, and the second is the acid gas stream that flows to the sulfur recovery plant (Stream 18); which will be considered in a future work.

The columns H2S-ABS and STRIPPER (Figure 15f) have been modeled using the **RadFrac** model under equilibrium and isobaric considerations [118]. Henry's components were H₂S and CO₂ [118], and the equations representing the reaction mechanism in the system are Eq. 31 to Eq. 36. In the case of the STRIPPER block, a condenser and a reboiler are required. The partial-vapor condenser was implemented to adjust the temperature of the acid gas stream (Stream 18) around 105 °C. The reboiler is used to add the heat required for the desorption process, which was adjusted to obtain the desire composition of the lean stream (LEAN) [118].



The flash vessel (F-DRUM) was modeled as a **Flash2** block, which is a two-outlet flash separator working at 1.5 bar and with a heat duty equals to 0.0. The heat exchange between lean and rich solution have been modeled with two isobaric **Heater** blocks (HEX-LEAN and HEX RICH). In the HEX-LEAN block, the outlet temperature (LEAN2) was set ~35°C as a function of the rich solution temperature leaving from the flash vessel (RICH2). In the HEX-RICH block, the temperature condition of the outlet stream (RICH3) was estimated by balancing, considering the heat transferred from the lean solution (HEAT-LR). The pump required to rise the lean solution pressure up to the MDEA absorber working pressure was modeled by means of a **Pump** block, where its discharge pressure is chosen as the specification; the pump efficiency is considered as 75% [117]. Finally, a heat exchanger is used to ensure the proper temperature of the lean

solution (LEAN3) before being supplied to the MDEA absorber. The main operative parameters of the MDEA absorber and stripping system are summarized in Table 16 [118].

Table 16. Main operation parameters of MDEA absorber and stripper system. Adapted from [118].

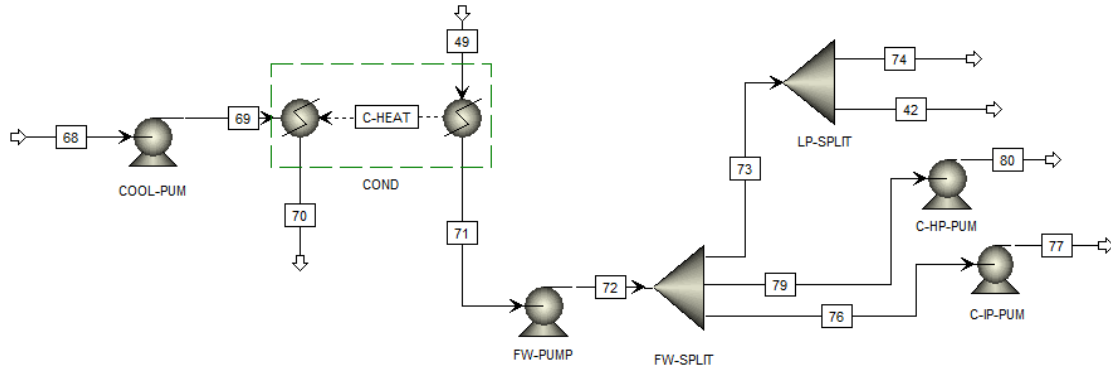
Component	Parameter	Unit	Value
MDEA absorber	Stages	number	5
	Lean solution composition	mass	50%-MDEA
	Lean solution temperature	°C	33
	Pressure*	bar	19.856
Stripper	Stages	number	12
	Pressure	bar	1.5
	Reflux ratio	mass	1.9

* value obtained in this work

3.2.2.3 Combine cycle and power generation model.

3.2.2.3.1 Gas turbine

The gas turbine has been modeled following the approaches proposed by Saddiq et al. [11] and Lan et al. [29] (Figure 16a). In this work, the air from the compressor (Stream 22) is split in two streams, one stream is fed to the combustion chamber to stoichiometrically burn the syngas (Stream 25) [129], while the other stream (remaining air) is used for cooling and controlling the turbine inlet temperature (Stream 26). A **FSplit** splitter block (AIR-SP) was used to split the compressed air stream. The stream 25 is the stoichiometric air mass flow required to burn the syngas (Stream 20) in the combustion chamber, which was calculated as a function of the stoichiometric air/fuel- syngas ratio. Thus, the air mass flow for syngas combustion (Stream 25) was kept constant, in spite of the total air mass flow varies looking for obtaining the desired gas temperature at the turbine inlet (Stream 28). The air compressor has been modeled by means of a **Compr** block (AIR-COMP) selecting the isentropic compressor model and specifying the discharge pressure as 19.657 bar and the isentropic efficiency of 88.4% [107]. The turbine was also modeled using a **Compr** block (GTURBINE) specifying the isentropic turbine model. Isentropic efficiency and discharge pressure of the turbine were set as 91% [107] and 105 kPa, respectively; this value for discharge pressure of hot gases from GTURBINE block (Stream 30) was considered according to the pressure loss in the HRSG (~4 kPa) [130].



d) Condenser

Figure 16. Aspen Plus model of the combine cycle and power generation.

Table 17. Gas turbine model parameters. Adapted from [107].

Parameter	Unit	Value
Pressure ratio	-	19.4
Turbine inlet temperature	°C	1418
Compressor isentropic efficiency	%	88.4
Turbine isentropic efficiency	%	91
Turbine exhaust pressure*	kPa	105

*Value obtained in this work

3.2.2.3.2 HRSG and Steam cycle

The gas turbine's exhaust gases leave at high temperature and flows through HRSG, where its sensible energy is used for steam generation at three pressure levels: high (HP), intermediate (IP), and low pressures (LP). HRSG was modeled here composed by an economizer, an evaporator, and a superheater for each pressure level, as well as a reheater for IP-steam (Figure 16c). These devices were modeled using **HeatX** blocks with the shortcut countercurrent mode. The exhaust gases flow (Stream 30) coming from the gas turbine (Figure 16a) enters to HRSG and exchanges heat with water and steam streams as it flows through the heat exchangers of the HRSG (Streams 30 to 40). **Pump** blocks were used to model the pumps for raising the pressure of the feed water assuming an efficiency of 75% [117]. By **Mixer** blocks was modeled the mixing of water and steam streams coming from the different components. The temperature difference between the saturation temperature and the economizer outlet temperature was set between 3 and 4°C for each pressure level. While the pinch point was set at 10 °C, this point is defined as the temperature difference between the evaporator outlet gas temperature and the saturation temperature of the steam. The total pressure loss of hot gases stream (hot side) in the HRSG was considered as ~4 kPa [130]; this pressure

loss is uniformly distributed among all the heat exchangers of the HRSG. Meanwhile, the pressure loss in the cold side (water and steam streams) was set at 1.5% of the inlet pressure of each device [122]. The feed water (Stream 42) coming from the feedwater pump (see Figure 16d) is fed to the preheater (FW-PREH), where the water temperature is almost increased up to the saturation temperature; thereby, a cold stream outlet temperature equals to 141°C was set as the specification for this block. The feedwater mass flow was set seeking that the flue gas temperature (Stream 40) be about 140°C for avoiding condensates. The preheated water leaving from the FW-PREH block (Stream 43) is split by a **Splitter** block (FW-SEP) into three streams (44, 50, and 59). The mass flow of each stream was set pursuing that the minimum temperature difference between exhaust gases (hot flow) and water/steam (cold flow) passing through each heat exchanger is 10°C [130]. Stream 44 flows to LP evaporator (LP-EVAP) where LP saturated steam is generated by specifying a cold stream outlet vapor fraction equals to 1.0. Stream 50 flows towards the IP-PUMP block for rising its pressure up to IP level (Table 18) and subsequently is fed to the IP-ECON (economizer), whose specification is the cold stream outlet temperature of 229°C. In HP-F-MIX, the Streams 59 and 75 that comes from LTGC are mixed and fed to the HP-PUMP as the Stream 60, where its pressure is increased up to HP level (Table 18) before it flows towards HP-ECON as Stream 61.

The saturated vapor generated in LP-EVAP (Stream 45) flows to the LP-SUPH (superheater) where superheated steam (Stream 46) is generated according to the conditions presented in Table 18. The Stream 52 stemmed from IP-ECON is fed to the IP-EVAP and leaves as saturated IP steam (Stream 53) with a vapor fraction equals to 1.0. Afterward, this saturated steam is superheated in the IP-SUPH up to 312°C. Superheated IP steam (Stream 54) flows towards the IP-MIX where it is combined with the expanded steam from the HP steam turbine (Stream 66) and the IP steam generated in SCS (stream 78, see Figure 15a). The Stream 55 resulting from the IP-MIX feeds the reheater (REHEATER) for further temperature increase up to the inlet temperature of the IP steam turbine (Stream 56, see Figure 16b). In the HP-ECON, the temperature of the Stream 61 is increased up to 322°C resulting in the Stream 62, which flows towards HP-EVAP and it is transformed in saturated steam with a vapor fraction equals to 1.0 (Stream 63). Finally, the Stream 63 is combined with the HP steam generated in the SCS (Stream 81) in HP-MIX resulting the Stream 64. In the HP-SUPH, the Stream 64 is superheated until the inlet temperature of the HP steam turbine (Stream 65).

Steam turbines have been modeled by using the **Compr** model specifying the corresponding discharge pressure and isentropic efficiency (Figure 16b). The superheated steam from HP-SUPH (Stream 65, see Figure 16c) is supplied to the HP steam turbine (HP-ST) and expanded until the IP level. As it was stated above, the Stream 66 is recirculated to the HRSG for reheating. The superheated steam generated in the REHEATER (Stream 56) is expanded by the IP steam turbine (IP-ST) where its pressure decreases up to LP

level. The Stream 57 leaving IP-ST is mixed with the Stream 46 that comes from the LP-SUPH and flows towards the LP steam turbine (LP-ST) as the Stream 47. The LP steam is expanded in LP-ST up to the condenser pressure (Stream 49). The main operative parameters of HRSG and the steam cycle are summarized in Table 18 [107], [117].

As shown in Figure 16d, the condenser was modeled using two **Heater** blocks. In the first Heater block, the steam coming from the LP steam turbine is condensed up to saturated liquid (Stream 71). The heat released in the condensation process (C-HEAT) is connected to the other Heater block where the outlet temperature of the cooling water (Stream 70) is calculated based on energy balance. A **Pump** block (COOL-PUMP), whose efficiency is assumed as 61% [7], was implemented to model the pump for raising the pressure of cooling water (Stream 69). The mass flow of cooling water (Stream 68) was set considering a temperature increase of about 10°C during the condensation process. The water pump required to raise the feedwater pressure (FW-PUMP) has been also modeled by means **Pump** block, considering its efficiency as 61%. The pressure of the Stream 71 increases up to the LP-level (Stream 72) and it is split into several streams to feed several systems, such as: a) SCS (Stream 76 to 77, and Stream 79 to 80, see Figure 15a), b) LTGC (Stream 74, see Figure 15e), and c) HRSG (Stream 42, Figure 16c). The pressure of Streams 76 and 79 increase before flowing toward SCS, such pressure increment is up to their corresponding level (HP or IP), and it is driven by two pumps (C-IP-PUMP and C-HP-PUMP) whose efficiency was considered as 75% [117].

Table 18. Steam cycle model parameters. Adapted from [107], [117].

Component	Parameter	Unit	Value
HP steam turbine	Inlet pressure	bar	120
	Inlet temperature	°C	507
	Isentropic efficiency	%	85.8
IP steam turbine	Inlet pressure	bar	29
	Inlet temperature	°C	510
	Isentropic efficiency	%	90.5
LP steam turbine	Inlet pressure	bar	4.08
	Inlet temperature	°C	255
	Isentropic efficiency	%	84.4
Condenser	Pressure	bar	0.046
Cooling water	Temperature (Stream 68)	°C	15
	Pressure (Stream 69)	bar	10
Stack	Exhaust temperature	°C	144

The mechanical power from gas turbine and steam turbines drives an electrical generator which produces electric power with an efficiency of 98% [117]. A fraction of the generated power is required for self-consumption to drive the water pumps, the syngas compressors, and to provide the power to the torch for

plasma generation (gasification stage). Therefore, the remaining power (net power) is able to be sold and generating incomes for the plant.

3.2.3 Exergoeconomic assessment

The main feature of the exergoeconomic analysis is the integration between thermodynamic and economic analyses to apply the concept of exergy cost. By means of the exergoeconomic analysis is allocated the energy, exergy, and economic cost associated to the losses [133]. The methodology used here for exergy and exergoeconomic analyses is the Theory of Exergy Cost (TEC), which has been developed and presented in detail by Valero and co-workers [133]–[138]. This is a thermoeconomic methodology based on the matrix analysis of thermal conversion processes that allows the generalization and simplification of the assessment to calculate the exergy and economic cost of each flow in complex systems.

3.2.3.1 Exergy analysis.

Here, Aspen Plus software has been used to simulate IPGCC power plant; therefore, all mass and energy (enthalpy) flows are taken from the simulation results. The total exergy of a stream includes physical and chemical exergy (Eq. 8) [47], [79]. In a general way, physical exergy can be calculated using Eq. 9.

$$e_T = e_{ph} + e_{ch} \quad \text{Eq. 37}$$

$$e_{ph} = (h - h_0) - T_0(s - s_0) \quad \text{Eq. 38}$$

Aspen Plus software calculates the physical exergy of conventional streams; thereby, the specific physical exergy of flows was determined from simulations results. However, the slag stream (Stream 5) is a non-conventional substance; thus, its physical exergy was calculated by using Eq. 38, and the correlations proposed by Eisermann *et al.* [139] for enthalpy and entropy estimations. The molar chemical exergy of syngas, which is a mixture of ideal gases, was calculated by Eq. 11.

$$e_{ch,ideal\ gas} = \sum_i y_i e_i^0 + RT_0 \sum_i y_i \ln(y_i) \quad \text{Eq. 39}$$

MSW compositions can be inaccurate due to the variability of wastes, which difficult the chemical exergy calculation [47]. As a consequence, statistical correlations presented by Kotas (Eq. 12) [82] were used to

determine specific chemical exergy (kJ/kg) of MSW. Here, LHV on wet basis (kJ/kg) was calculated from HHV and the moisture and hydrogen content (mass fraction) by Eq. 13 [140]. While φ_{dry} was calculated by Eq. 42 [82], which is suitable for solid fuels with mass ratio $O/C < 0.667$.

$$e_{ch,MSW} = [LHV + 2.442MC]\varphi_{dry} + 9.417S \quad \text{Eq. 40}$$

$$LHV = HHV(1 - MC) - 2440(MC + 9H) \quad \text{Eq. 41}$$

$$\varphi_{dry} = 1.0437 + 0.1882\left(\frac{H}{C}\right) + 0.0610\left(\frac{O}{C}\right) + 0.0404\left(\frac{N}{C}\right) \quad \text{Eq. 42}$$

For the washing fluid (NaOH solution, Streams 10 and 12) used in the wet scrubber (which is a non-ideal solution), the molar chemical exergy (kJ/kmol) was calculated considering the activity coefficient (γ) of the components using Eq. 43 [82]. Exergy of heat and power (mechanical and electrical) were calculated by using Eq. 44 and Eq. 45, respectively.

$$e_{ch} = \sum_i y_i e_i^0 + RT_0 \sum_i y_i \ln(\gamma_i y_i) \quad \text{Eq. 43}$$

$$\dot{E}_{heat} = \left(1 - \frac{T_0}{T}\right) \dot{Q} \quad \text{Eq. 44}$$

$$\dot{E}_{power} = \dot{W} \quad \text{Eq. 45}$$

TEC methodology follows a procedure involving a number of well-defined steps. The application of the methodology starts with the definition of the physical structure for the thermal system. The physical structure represents the relationships between the components and flows (energy or mass) involved in the system, those components and flows are enumerated and labeled, as shown in Figure 14. The incidence matrix ($\mathbf{A}(n \times m)$) defines how the components and flows are linked, where n (rows) corresponds to the number of components, and m (columns) to the number of flows. Every element $\mathbf{A}(i,j)$ can be 1, -1, or 0, if the j flow enters, leaves, or if the j flow is not related to the component i , respectively. Thermodynamic balances in matrix form are performed by using equations from Eq. 46 to Eq. 48. Here, $\dot{\mathbf{m}} (m \times 1)$, $\dot{\mathbf{H}} (m \times 1)$, and $\dot{\mathbf{E}} (m \times 1)$ are vectors that represent the mass flow rate, energy flow rate, and exergy flow rate related to every flow, respectively.

$$\mathbf{A}(n \times m) \times \dot{\mathbf{m}}(m \times 1) = \frac{d\mathbf{m}}{dt}(n \times 1) \quad \text{Eq. 46}$$

$$\mathbf{A}(n \times m) \times \dot{\mathbf{H}}(m \times 1) = \frac{d\mathbf{H}}{dt}(n \times 1) \quad \text{Eq. 47}$$

$$\mathbf{A}(n \times m) \times \dot{\mathbf{E}}(m \times 1) = \left[\frac{d\mathbf{E}}{dt} + \dot{\mathbf{E}}_d \right] (n \times 1) \quad \text{Eq. 48}$$

In actual systems operating at steady state, Eq. 46 and Eq. 47 are equalized to zero vectors; this is ascribed to the unchanging properties with time. On the other hand, Eq. 48 results in a vector containing the exergy destruction rate ($\dot{\mathbf{E}}_d$) of each component.

The products (the purpose, P_k) are the exergy flows resulting from a component- i carrying out its productive purpose. On the other hand, the resources (i.e. fuel, F_k) are the exergy flow required by the component- i to carry out its productive process. The exergy efficiency of a component (or a system) is defined as the ratio between its products (or exergy recovered) and its resources (exergy supplied), see Eq. 49.

$$\eta_k = \frac{P_k}{F_k} \quad \text{Eq. 49}$$

The productive structure is obtained from the definition of the productive purpose of each component. The fuel matrix ($\mathbf{A}_F (n \times m)$) includes information of the resources of every component, in relation to the flows of the system, while the product matrix ($\mathbf{A}_P (n \times m)$) contains information of the products. Product and fuel vectors, that include the products and resources of each component, are obtained by means of Eq. 50 and Eq. 51. Furthermore, as an alternative to Eq. 48, exergy destruction can be estimated with Eq. 52. The productive structure of the IPGCC power plant investigated here is presented in Appendix A (Table A.1).

$$\mathbf{A}_F(n \times m) \times \dot{\mathbf{E}}(m \times 1) = \mathbf{F}(n \times 1) \quad \text{Eq. 50}$$

$$\mathbf{A}_P(n \times m) \times \dot{\mathbf{E}}(m \times 1) = \mathbf{P}(n \times 1) \quad \text{Eq. 51}$$

$$\mathbf{F}(n \times m) - \mathbf{P}(m \times 1) = \dot{\mathbf{E}}_d(n \times 1) \quad \text{Eq. 52}$$

Exergy cost of a flow, \dot{C} (kW), is the amount of exergy that is necessary to spend for producing the given flow. On the other hand, the unit exergy cost, c (kW/kW), is the amount of exergy required to produce a unit of exergy of the given flow. The calculation of \dot{C} and c of every m flow, in the analyzed system, is based on the physical structure (incidence matrix \mathbf{A} and exergy vector $\dot{\mathbf{E}}$) and on the *four propositions* of TEC methodology, which are presented in Table A.2 (Appendix A). The aim is to obtain the matrix structure described by Eq. 53 for \dot{C} calculation; then, c can be calculated by Eq. 54.

$$\mathbf{A} (m \times m) \cdot \dot{\mathbf{C}} (m \times 1) = \mathbf{Y} (m \times 1) \quad \text{Eq. 53}$$

$$c_i = \frac{\dot{C}_i}{\dot{E}_i} \quad i = 1, \dots, m \quad \text{Eq. 54}$$

Where $\dot{\mathbf{C}}$ is the exergy cost vector, \mathbf{A} and \mathbf{Y} are the cost matrix and the exergy amortization vector, which are obtained from Eq. 55 and Eq. 56, respectively.

$$\mathbf{A} (m \times m) = \begin{bmatrix} \mathbf{A} \\ \boldsymbol{\alpha} \end{bmatrix} \quad \text{Eq. 55}$$

$$\mathbf{Y} (m \times 1) = \begin{bmatrix} \mathbf{0} \\ \boldsymbol{\omega} \end{bmatrix} \quad \text{Eq. 56}$$

The vector $\mathbf{0}$ is a zero vector whose order is $(n \times 1)$. The auxiliary matrix $\boldsymbol{\alpha}$ $((m - n) \times m)$ and the auxiliary vector of independent terms $\boldsymbol{\omega}$ $((m - n) \times m)$ result from propositions 1, 3, and 4 (Table A.2). The procedure consists in the arranging of the auxiliary equations from the application of propositions in the matrix $\boldsymbol{\alpha}$, and the independent terms in the vector $\boldsymbol{\omega}$ as it is described by Eq. 57.

$$\boldsymbol{\alpha} \cdot \dot{\mathbf{C}} = \boldsymbol{\omega} \quad \text{Eq. 57}$$

3.2.3.2 Exergoeconomic model

The exergoeconomic cost (\dot{C}^z in \$/h) is the amount of resources assessed in monetary units per unit of time, which is needed to obtain a given flow. Unlike exergy cost, exergoeconomic cost considers thermodynamic costs (fuels), as well as plant installation and operation cost that are known as non-thermodynamic cost \dot{Z} (\$/h). Furthermore, the unit exergoeconomic cost, c^z (\$/kWh), is defined as the amount of resources,

assessed in monetary units per unit of energy, associated to obtain a given flow. The relationship between exergoeconomic cost and unit exergoeconomic cost is given by Eq. 58.

$$c_i^z = \frac{\dot{C}_i^z}{\dot{E}_i} \quad i = 1, \dots, m \quad \text{Eq. 58}$$

Non-thermodynamic costs encompass fixed capital investment (which includes purchased-equipment cost and installation, piping, instrumentation and control, land, civil and architectural work, and service facilities) and other costs such as startup, working capital, licensing, and research & development. The non-thermodynamic costs are distributed among all the components of the system. Thus, the total non-thermodynamic cost associated with the system is the sum of the non-thermodynamic cost of each component (Eq. 59).

$$\dot{Z} = \sum_{k=1}^n \dot{Z}_k \quad \text{Eq. 59}$$

The cost balance states that the exergoeconomic cost of the product from the component k is equal to the exergoeconomic cost of the resources plus the non-thermodynamic cost related to the component. The cost balance is represented in scalar terms by Eq. 60, and in matrix arrangement by Eq. 61.

$$\dot{C}_{P,k}^z = \dot{C}_{F,k}^z + \dot{Z}_k \quad \text{Eq. 60}$$

$$\mathbf{A} (n \times m) \cdot \dot{\mathbf{C}}^z (m \times 1) + \dot{\mathbf{Z}} (n \times 1) = \mathbf{0}_{(n)} \quad \text{Eq. 61}$$

In Eq. 61, $\dot{\mathbf{C}}^z$ is the vector of exergoeconomic costs (US\$/h), and $\dot{\mathbf{Z}}$ is the vector of non-thermodynamic costs (US\$/h). Since $(m - n)$ equations are needed to solve the system represented by Eq. 61, they are obtained from the applying of the *four propositions*, leading to Eq. 62.

$$\boldsymbol{\alpha} \cdot \dot{\mathbf{C}}^z = \mathbf{c}_e^z \cdot \boldsymbol{\omega} \quad \text{Eq. 62}$$

Here, \mathbf{c}_e^z is a vector containing the unit exergoeconomic costs of external resources. By combining Eq. 61 and Eq. 62 the matrix equation represented by Eq. 63 is obtained, which is solved to get the exergoeconomic cost of streams. The vector \dot{Z} is the vector of thermoeconomic amortization and it is acquired by Eq. 64.

$$A (m \times m) \cdot \dot{\mathbf{C}}^z (m \times 1) + \dot{Z} (m \times 1) = \mathbf{0}_{(m)} \quad \text{Eq. 63}$$

$$\dot{Z} = \begin{bmatrix} \dot{Z} \\ -\mathbf{c}_e^z \cdot \boldsymbol{\omega} \end{bmatrix} \quad \text{Eq. 64}$$

The non-thermodynamic costs (\dot{Z}_k) are scarce and hard to obtain from vendors or equipment manufacturers; therefore, a simplified economic model that distributes total plant cost among its components is used. Here, the economic model presented by Silveira and Tuna [141] is used (Eq. 65). The non-thermodynamic cost related to each component is estimated based on the purchased-equipment cost (PEC) of the given component, and by means of some coefficients accounting the costs associated with operating, maintenance, installation, electrical equipment, control system, piping, and local assembly. The economic model and coefficients are represented by equations Eq. 65 to Eq. 67. The assumed values for φ_k , in , ri , a , and b are presented in Table 19.

$$\dot{Z}_k = \frac{\varphi_k \cdot f \cdot PEC_k}{N} \quad \text{Eq. 65}$$

$$f = \left[\frac{q^{(a+b)} - 1}{(q - 1) \cdot q^{(a+b)}} - \frac{q^b - 1}{(q - 1) \cdot q^b} \right]^{-1} \quad \text{Eq. 66}$$

$$q = \left(1 + \frac{in}{100} \right) \left(1 + \frac{ri}{100} \right) \quad \text{Eq. 67}$$

Purchased equipment cost of every component (PEC_k) is estimated by correlations considering operating conditions and constructive characteristics. However, this information is limited to given ranges of operating variables and/or equipment size, as well to specific dates. Thereby, it is used a size correction factor and update PEC_k estimations. For this aim, Eq. 68 is used to correct PEC_k for size and operating conditions. Where, subscript Y corresponds to real capacity of the component and W to the estimation, X is the operating variable used for comparison of components, and β is the scaling exponent.

Table 19. Assumed values for \dot{Z}_k estimations and thermoeconomic analysis.

Parameter	Value	Reference
Effective annual interest rate for debt, in	8 %/year	[61][142]
Annual inflation rate ^a , ri	3.51 %/year	[143]
Annual plant operating time, N	7920 h/year	[95]
Plant lifetime, a	20 years	[61]
Construction time, b	2 years	Assumed
Maintenance factor, φ_k	1.1	[116]
Unit cost of MSW ^b	-10.7 US\$/t	[144]

^a The annual inflation rate is taken as that of 2019 [143].

^b It is assumed that the project receives a MSW disposal fee [95] equals to that of the landfill, which is defined in [144]. The unit cost is calculate considering a market representative rate of 3300 COP/US\$ (December 29th, 2019).

$$PEC_Y = PEC_W \left(\frac{X_Y}{X_W} \right)^B \quad \text{Eq. 68}$$

For PEC_k updating (Eq. 69), the Chemical Engineering Plant Cost Index (CEPCI) is used as an industrial equipment cost index (CI). Subscript 0 corresponds to the year for which PEC is known.

$$PEC = PEC_0 \left(\frac{CI}{CI_0} \right) \quad \text{Eq. 69}$$

The vector containing exergoeconomic costs of resources and products of every component is calculated by means Eq. 70 and Eq. 71, respectively. In addition, the unit exergoeconomic cost of resources and products of every component is calculated using Eq. 72 and Eq. 73, respectively.

$$\dot{C}_F^Z(m \times 1) = \mathbf{A}_F(n \times m) \cdot \dot{C}^Z(m \times 1) \quad \text{Eq. 70}$$

$$\dot{C}_P^Z(m \times 1) = \mathbf{A}_P(n \times m) \cdot \dot{C}^Z(m \times 1) \quad \text{Eq. 71}$$

$$c_{F,k}^Z = \frac{\hat{C}_{F,k}^Z}{F_k} \quad \text{Eq. 72}$$

$$c_{P,k}^Z = \frac{\hat{C}_{P,k}^Z}{P_k} \quad \text{Eq. 73}$$

The relative difference cost (r_k) states the relative increment in the unit exergoeconomic cost of the product from a component, in relation to the unit exergoeconomic cost of the resources of such component (Eq. 74).

$$r_k = \frac{c_{P,k}^z - c_{F,k}^z}{c_{F,k}^z} \quad \text{Eq. 74}$$

The total cost increment, associated with the productive process of a component, encompasses two categories of cost, such as Thermodynamic (concerning the efficiency and irreversibilities) and non-thermodynamic cost (concerning the investment, operation, and maintenance). The relative importance of each cost category is established by the exergoeconomic factor (f_k). A high value of f_k (close to 100%) indicates that the importance of non-thermodynamic cost is higher than that of the thermodynamic cost, conversely, if the value of f_k is lower than 30%, the importance of thermodynamic cost is higher [145]. The exergoeconomic factor was calculated as a percentage by means of Eq. 75. In Eq. 75, \dot{C}_D^z is the exergoeconomic cost of irreversibilities, which is calculated by means of Eq. 76.

$$f_k = \frac{\dot{Z}_k}{\dot{Z}_k + \dot{C}_{D,k}^z} \times 100 \quad \text{Eq. 75}$$

$$\dot{C}_{D,k}^z = c_{F,k}^z \dot{E}_{d,k} \quad \text{Eq. 76}$$

3.3 RESULTS AND DISCUSSION

The thermodynamic performance of the IPGCC power plant was investigated by means of exergy analysis using the TEC methodology (see section 3.2.3.1). According to the different waste types generated in Medellín city, and their generation rates presented in Table 14, five plant cases have been considered as shown in Table 20.

3.3.1 Plasma gasification operative parameters

As the wastes from the different sectors have different compositions (moisture content and heating value, see Table 2), the operative conditions of the plasma gasifier must be set seeking to get the best gasifier performance for each waste type. From the sensitivity analysis presented in sections 2.2.5 and 2.3.3, the operative parameters (air to waste mass ratio -AWR- and plasma temperature) that allows reaching the best performance (first -CGE- and second -ExE- law efficiencies) were determined. In that analysis, AWR and plasma temperature were varied from 0.1 to 1.5 $\text{kg}_{\text{air}}/\text{kg}_{\text{MSW}}$ and from 1500 to 4500°C, respectively.

Results of the best CGE and the gasifier’s operational conditions are summarized in Table 20. The syngas produced, under those operational and behavior conditions, is used to fuel the power combined cycle.

Table 20. Plan capacity and operative conditions of plasma gasifier as function of waste type.

Waste type (Sector)	Plant capacity (t/day)	AWR ($\text{kg}_{\text{air}}/\text{kg}_{\text{MSW}}$)	T_{plasma} (°C)	W_{torch} ($\text{MJ}/\text{kg}_{\text{MSW}}$)	HHV _{syngas} (kJ/kg)	CGE (%)	ExE (%)
Institutional	75	0.4	4300	2.64	9860	82.76	80.04
Industrial	100	0.5	4100	3.14	11210	82.84	81.18
Commercial	150	0.4	4500	2.77	11100	83.46	81.38
Mixed	1000	0.3	4500	2.08	8060	82.77	79.47
Residential	1000	0.5	2800	2.09	5780	79.22	75.12

3.3.2 Exergy analysis

The mass, energy, and exergy flow rates of each stream involved in each plant case (see Figure 14) are presented in Appendix B (Table B.1 to Table B.5). The rate of exergy destruction for each component has been calculated through Eq. 48. Figure 17 shows the rate of exergy destruction for each component of the IPGCC power plant fed with industrial wastes. Component 1 (plasma gasifier), component 12 (combustion chamber), and component 15 (combustion gases-cooling air mixer) were the three subsystems with the highest rate of exergy destruction, which account 34%, 27%, and 9% of the total rate of exergy destruction in the power plant, respectively. In the plasma gasifier, the highest rate of exergy destruction (4385.8 kW) was attributed to the irreversibilities associated with MSW drying and the chemical reactions taking place for transforming the waste to syngas and slag [116], [145]. Furthermore, a fraction of high-quality energy (HHV_{MSW} and electricity) that enter to the gasifier is converted into thermal energy (sensible energy of syngas and slag) that is a low-quality energy and leads to destroy exergy in this component. The high exergy destruction in the combustion chamber (3475.2 kW) was ascribed to the irreversibilities of the oxidation reactions of the syngas to produce thermal energy and the significative temperature difference between the reactants and the reaction zone (flame) [115], [146]. Regarding the component 15, its rate of exergy destruction (1151.4 kW) referred to the mixing process between the hot gases and the cooling air, where the cooling process destroys the exergy of the hot gases stream in the mixer. Similar results and trends for the rate of exergy destruction were obtained for the other four plant cases (wastes types by sector), and they are presented in Figure C.1 of Appendix C.

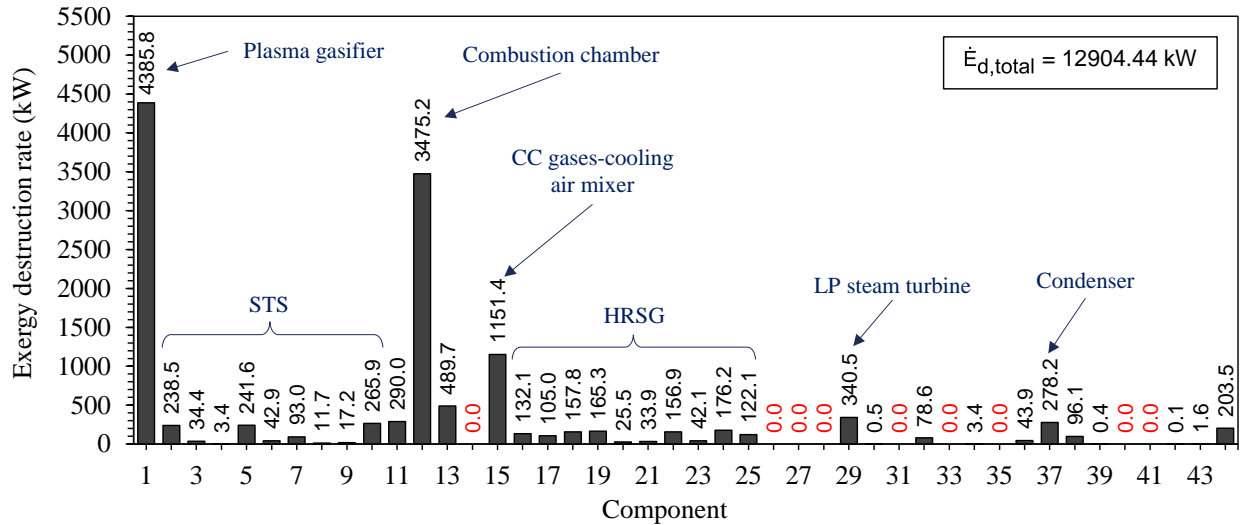


Figure 17. Exergy destruction rate in each component of IPGCC plant processing industrial waste. Capacity: 100 t/day. Red numbers are related with fictitious components.

The exergy destruction ratio (δ_D) of a component is defined as the ratio between its rate of exergy destruction and the total rate of exergy destruction of the plant. Therefore, this parameter reflects the share of every component to the total irreversibility of the system. Here, the exergy destruction ratio was calculated for five different subsystems, in which the components of the IPGCC power plant have been grouped. The considered subsystems were Plasma gasifier (PG), Syngas treatment system (STS), Gas turbine (GT), Steam Cycle (SC), and Electric generator (EG). STS encompasses the devices used for cleaning and conditioning the syngas (components 2 to 11), GT includes components of the gas turbine (components 11 to 15), and SC covers the steam turbines, HRSG, stack, condenser, and water-pumps (components 16 to 43). In Figure 18, the exergy destruction ratios of the five subsystems for each plant case (waste type) are depicted. For all plant cases, PG and GT reached the two larger values for the exergy destruction ratio. The average contributions of PG and GT to the total rate of exergy destruction in the five plants were 36.2% and 40.3%, respectively. This is mainly related to the high rates of exergy destruction associated with the plasma gasifier, the combustion chamber, and the combustion gases-cooling air mixer, as stated earlier. Furthermore, it is highlighted a relationship found between the exergy destruction ratio in PG and the moisture content of wastes supplied to PG. The exergy destruction ratio of PG increased by 23.5% as the moisture content of wastes increased from 26.6 to 57.9% (see Table 2). The highest exergy destruction ratio of PG was ~42% when the reactor was fed with residential waste. The highest moisture content of residential waste (57.9%) produces a syngas with high water (steam) content, which adversely affects the syngas exergy content (see Eq. 9 and Eq. 11). The average exergy destruction ratio of SC was 14.5%. In this subsystem, the exergy destruction was mainly allocated in the HRSG, the LP steam turbine, and the condenser, as shown in Figure 17. In the case of HRSG, the exergy destruction was attributed to the heat

exchange between the gas turbine's exhaust gases and the water/steam [147]; for the LP steam turbine, the exergy destruction was due to the irreversibilities associated with the expansion of steam, these irreversibilities are related to the isentropic efficiency of the steam turbine [148]. From Table 18, it can be seen that the isentropic efficiency of the LP steam turbine (84.4%) is lower than that of IP and HP steam turbines (90.5 and 85.4%, respectively). On the other hand, the destroyed exergy in the condenser was associated with the heat transfer between the expanded steam and the cooling water at low temperatures (15 – 25 °C), where the reclaimed heat from the steam was not used in the process; whereby this heat is considered as wasted energy (destroyed exergy) [147]. Furthermore, in these components (HRSG, LP steam turbine, and condenser), the high rates of exergy destruction are also favored by the high mass flows of their respective working fluids flowing through them.

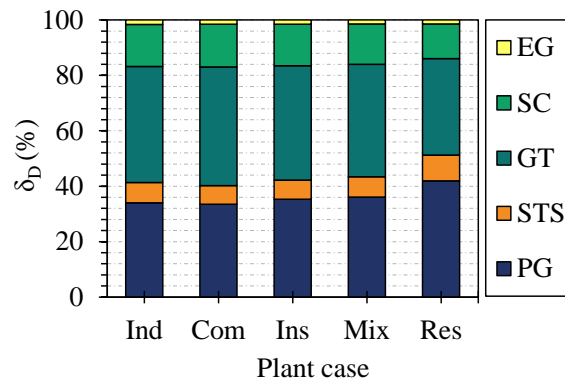


Figure 18. Exergy destruction ratio for the five subsystems in each plant case. Plasma gasifier (PG): component 1; Syngas treatment system (STS): components 2 to 11, Gas turbine (GT): components 11 to 15; Steam cycle (SC): components 16 to 43, Electric generator (EG): component 44.

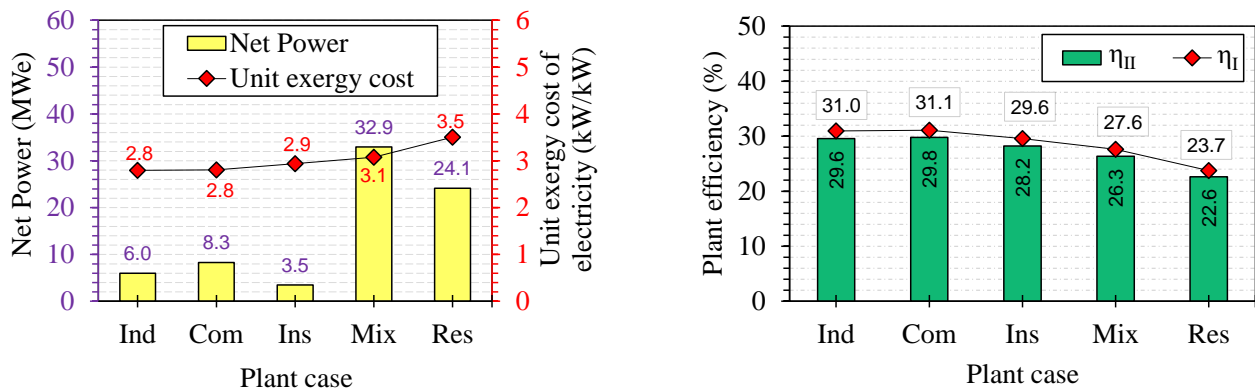
In the STS subsystem, its average contribution to the total exergy destruction in the five IPGGC plants was 7.51% (Figure 18). The largest rates of exergy destruction in this subsystem are allocated in component 2 (HP syngas cooler), component 5 (wet scrubber), and component 10 (MDEA absorber/stripper system), see Figure 17 and Figure C.1. The high rate of exergy destruction in the HP syngas cooler stems from the relatively large temperature difference between the syngas at the plasma gasifier outlet (727.7 – 468 C) and the cooling fluid (33 °C), streams 4 and 80, respectively [116]. With regard to wet scrubber, two main drivers for exergy destruction were identified. First, the physical exergy destruction due to the syngas cooling (from 250°C to 30°C), whose cooling on average account ~70% of the total exergy destruction in the wet scrubber; and second, the chemical exergy destruction associated with the irreversible nature of exothermic reactions between the NaOH solution (stream 10) and the acid gases in the syngas (mainly HCl). The total exergy destruction in sweetening gas systems, for instance component 10 (MDEA absorber/stripper system), is mainly attributed to the chemical exergy destruction. Moreover, significant

exergy destruction rates are allocated in the flash drum (expansion process) and gas cooling devices (e.g. the stripper condenser) [126]. Finally, the exergy destruction ratio of EG (electric generator, component 44) was on average 1.5%, which is quite low regarding that of the other subsystems. In this component (electric machine), the exergy destruction was mainly attributed to the heat losses (stream 94) to the environment.

The net electrical power of IPGCC plant generated by each analyzed case (waste type) is shown in Figure 19a. The significant difference of the produced power as a function of the analyzed cases was ascribed to the waste processing capacity, which varied from 75 up to 1000 t/day (Table 20). Therefore, according to the mass conservation, it was worth note that the syngas mass flow increased with the waste processing capacity of the IPGCC plants, which led to increase the produced power. The IPGCC power plant fed with wastes from Institutional sector, that has the lowest processing capacity of 75 t/day, generated the lowest power (3.5 MWe), followed by Industrial (100 t/day) and Commercial (150 t/day) cases with 6.0 and 8.3 MWe, respectively. On the other hand, Mixed and Residential plants, both with capacities of 1000 t/day, generated 32.9 MWe and 24.1 MWe, respectively. Despite these plants have the same capacity, the electric power generated by Residential plant is 26.7% lower than that of Mixed plant; this result is mainly related to the operation conditions of plasma gasifier and to the higher moisture content of residential waste, 57.9% for residential against 51.33% for the mixture. Moreover, the higher AWR for residential wastes ($0.5 \text{ kg}_{\text{air}}/\text{kg}_{\text{MSW}}$) than that of mixed ($0.3 \text{ kg}_{\text{air}}/\text{kg}_{\text{MSW}}$) in the plasma gasifier (see Table 20) led to increase the syngas mass flow of the former (16.8 kg/s against 14.5 kg/s); whereby for residential wastes, the power consumed by the syngas compressor increased at the expense of the net power output. Furthermore, the high moisture content of residential wastes favored a reduction of the syngas' HHV (Table 20), exergy per unit mass of syngas, as well as the stoichiometric air/syngas ratio, which adversely affected the thermal power and exergy available in the gas turbine and in the steam cycle for power generation. A syngas with a low stoichiometric air/syngas ratio requires less air to be burned, leading to reduce the combustion gases mass flow that drive the gas turbine and produce the steam in the HRSG.

In spite of the plants (waste types) with high capacity produced high electric power, as commented above, it was found that the energy and exergy efficiencies of the IPGCC plants decreased by 23.5% - 23.8%, if the moisture content of wastes increased from 26.6% to 57.9% (Figure 19b). This behavior was mainly attributed to the adverse effect of high moisture content of wastes on the syngas quality as fuel for powering the combined cycle. The energy and exergy content per unit mass of syngas produced in the plasma gasifier diminished by ~50% as the moisture content of wastes increases, this low syngas' quality was due to the high amount of water (steam) in the syngas stream.

The unit exergy costs of electricity produced by each plant case is presented in Figure 19a. According to the trends of efficiencies, the unit exergy cost of generated electricity increased (from 2.8 up to 3.5 kW/kW) as the moisture content of wastes increased (from 26.6% to 57.9%). Here, it is highlighted the significant effect of the moisture content of the wastes on the energy and exergy behavior of IPGCC power plant. As the moisture content of wastes increased (26.61% to 57.9%), the following aspect contribute to increase the unit exergy cost of electricity. First, the syngas' quality diminished, which is evaluated by HHV_{syngas} that decreased from 11210 kJ/kg to 5780 kJ/kg, and by the exergy per unit mass that decreased from 11160 kJ/kg to 5563 kJ/kg; and second, the required energy for drying the waste increased, as well as self-power consumption in IPGCC plant. The high moisture content contributed to the exergy destruction, which led to waste exergy in the drying process into the gasifier. Therefore, the first and second law efficiencies decreased, whilst the exergy unit cost increased, indicating that a higher supplied exergy is required to recover a unit of exergy (electric power). The unit exergy costs and exergy costs for all streams of each IPGCC plant case are presented from Table C.1 to Table C.5 of Appendix C.



a) Net electrical power generated and its unit exergy cost in each plant case.

b) Thermal and exergy efficiency for each plant case.

Figure 19. Net electrical power generated, unit exergy cost, and thermal and exergy efficiencies of each plant case. Thermal efficiency was calculated based on the wet basis HHV of MSW.

3.3.3 Exergoeconomic analysis.

According to the method described in section 2.3.4.1, the PEC of plasma gasifier (component 1) was estimated using the information presented by Clark and Rogoff, but considering only the cost of furnace and plasma-arc equipment [61]. The PEC of the Fabric Filter (component 4) was estimated by means of the information presented by Turner et al. [123] for the Pulse Jet (Common housing) type. The Gas-to-Cloth

ratio of the filter was defined using the similar application method, assuming fly ash as the particulate matter to be removed from the gaseous stream (syngas). The estimation encompasses cost of baghouse, bags, insulation, and auxiliary equipment. The PEC of syngas purification units, such as wet scrubber (component 5) and MDEA absorber/stripper system (component 10), was estimated by means of the Aspen Process Economic Analyzer module, using the results from IPGCC simulations as input. This methodology for equipment cost estimating has been successfully implemented in previous works [149], [150]. Since it was not possible to obtain the information for estimating PEC of the COS-hydrolysis unit (component 8), this component was not considered for the economical calculations. Nevertheless, the cost of the COS-hydrolysis unit is a small fraction of the total cost of the power plant; thereby, this limitation is not a significant issue [151]. The PEC of the remaining components was calculated using cost correlations reported in literature. The total purchased equipment (PEC) and non-thermodynamic (\dot{Z}) costs estimated for IPGCC plants processing each waste type are presented in Table 21. All values have been updated to 2020 price. The used cost correlations, and the estimated PEC and the non-thermodynamic costs for every component are presented in Appendix D (Table D.1 and Table D.2). The significant difference between the overall PEC for each analyzed case (Table 21), from 27.25 to US\$ 207.7 million, was attributed to the waste processing capacity (from 75 t/day to 1000 t/day), since a plant with a high processing capacity requires high size of equipment. Meanwhile, although the Mixed and Residential plants have the same capacity, the higher PEC of the former was ascribed to the better quality of its produced syngas, which led to increase the thermal power in the combined cycle. Thus, the size of the components of the combined cycle should be slightly larger in the Mixed plant than that of the Residential one.

Table 21. Purchased equipment and non-thermodynamic cost estimated for the IPGCC plant processing each waste type.

Waste type	PEC (US\$)	\dot{Z} (US\$/h)
Institutional	27,255,351	625.1
Industrial	36,367,298	834.0
Commercial	49,129,683	1,126.7
Mixed	207,700,772	4,763.3
Residential	204,631,669	4,692.9

Figure 20 depicts the contribution of the five subsystems to the overall non-thermodynamic cost (\dot{Z}) in each considered case for the IPGCC power plant, according to the processed waste (Industrial, Commercial, Institutional, Mixed, and Residential). As well as, in Table 22, the non-thermodynamic cost of each subsystem is presented. For all plant cases, the PG has the highest contribution, accounting between 70%

and 80% of the overall \dot{Z} of each plant case. This was ascribed to the high PEC of the plasma gasification technology (see Table D.2) that requires to use plasma torch, very high-temperature-resistant materials, and the technology is not commercially mature enough [22], [61], [85]. GT and SC have average contributions to the overall \dot{Z} of 9.0% and 13.0%, respectively. In these subsystems, the gas turbine and steam turbines were the component with highest PEC. Whilst, the contributions of STS and EG were 3.1% and 1.6% on average, respectively. The low contribution found for GT, SC, STS, and EG on the non-thermodynamic costs is attributed to these technologies are currently developed and are commercially available [92].

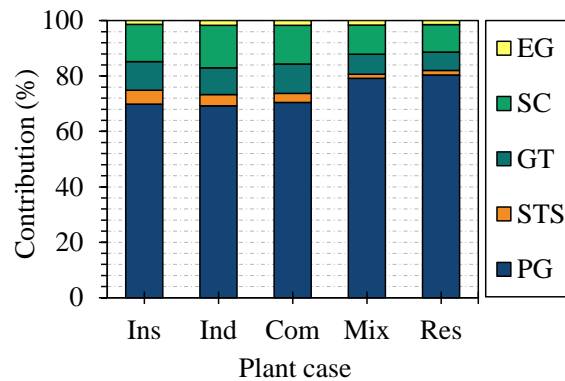


Figure 20. Contribution of the five subsystems to the overall \dot{Z} in each plant case. Plasma gasifier (PG): component 1; Syngas treatment system (STS): components 2 to 11, Gas turbine (GT): components 11 to 15; Steam cycle (SC): components 16 to 43, Electric generator (EG): component 44.

The exergoeconomic cost of irreversibilities (\dot{C}_D^Z , US\$/h) of the five subsystems of each plant case is presented in Table 22. The global value of \dot{C}_D^Z ranged between 557 US\$/h for Institutional plant (75 t/day) to 5198.8 US\$/h for Residential plant (1000 t/day). For all plant cases, the two highest values of \dot{C}_D^Z were allocated in GT and SC, which on average account 51.8% and 26.2% of the global value of \dot{C}_D^Z found for each plant case, respectively. This result was mainly ascribed to the high rate of exergy destruction of the components included in GT and SC, such as the combustion chamber (component 12), gas turbine (component 13), combustion gases-cooling air mixer (component 15), HRSG (components 16 to 25), LP steam turbine (component 29), and condenser (component 37), see Figure 17 and Figure C.1. Although the plasma gasifier (component 1) was the component with the highest rate of exergy destruction in all plant cases, the value of \dot{C}_D^Z for PG was lower than that of GT and SC, on average representing 10.9% of the overall \dot{C}_D^Z . According to Eq. 76, the low value of \dot{C}_D^Z reached for PG stemmed from the reduction on the exergoeconomic cost of the resources of PG, whose reduction is sponsored by the MSW disposal fee received by the plants (Table 19).

The exergoeconomic factors (f_k) of the five subsystems in each plant case, which was calculated using the Eq. 75, are shown in Table 22. A value of f_k higher than 70% indicates a dominant impact of non-thermodynamic cost on the total cost increment ($\dot{Z}_k + \dot{C}_{D,k}^z$). Conversely, when the value of f_k is lower than 30%, the cost of irreversibilities has the main impact on the total cost increment [116]. PG and GT accounted the highest and lowest values of f_k , respectively. According to the high PEC of plasma gasifier (component 1, see Table D.2), the average value of f_k for PG was 88.0%, reflecting the dominant impact of the non-thermodynamic cost in the total cost increment on this component. On the other hand, the value of f_k ranged from 11.1% to 19.3% associated to GT was attributed to the high rates of exergy destruction of the components (12, 13, and 15), which led to increase the cost of irreversibilities in GT, resulting in a dominant effect of this cost category on the total cost increment. The costs of irreversibilities and exergoeconomic factors of every component in the IPGCC power plant processing the different waste types are presented in Table D.3 of Appendix D.

Table 22. Non-thermodynamic cost (\dot{Z} , US\$/h), exergoeconomic cost of irreversibilities (\dot{C}_D^z , US\$/h), and exergoeconomic factor (f_k , %) for the five subsystems in each plant case. Plasma gasifier (PG): component 1; Syngas treatment system (STS): components 2 to 11; Gas turbine (GT): components 11 to 15; Steam cycle (SC): components 16 to 43; Electric generator (EG): component 44.

	Institutional			Industrial			Commercial			Mixed			Residential		
	\dot{Z}_k	$\dot{C}_{D,k}^z$	f_k	\dot{Z}_k	$\dot{C}_{D,k}^z$	f_k	\dot{Z}_k	$\dot{C}_{D,k}^z$	f_k	\dot{Z}_k	$\dot{C}_{D,k}^z$	f_k	\dot{Z}_k	$\dot{C}_{D,k}^z$	f_k
PG	436.7	59.3	88.0	577.5	68.8	89.4	794.1	86.4	90.2	3770.6	452.5	89.3	3770.6	760.0	83.2
STS	31.3	39.3	44.3	33.8	51.8	39.5	37.2	63.0	37.1	68.3	342.9	16.6	76.5	549.7	12.2
GT	64.2	292.8	18.0	80.3	365.6	18.0	118.8	497.8	19.3	344.8	2296.3	13.1	314.9	2515.5	11.1
SC	84.0	149.3	36.0	128.3	187.2	40.7	157.9	255.0	38.2	503.1	1166.2	30.1	462.5	1222.3	27.5
EG	8.71	17.2	33.6	14.1	22.3	38.7	18.8	29.4	39.0	76.6	129.0	37.3	68.4	151.3	31.1

The relative cost differences (r_k) for each component of the IPGCC power plant processing industrial wastes are shown in Figure 21. The plasma gasifier (component 1) presented the highest value of r_k of 2.18, which indicated that the unit exergoeconomic cost of the products from the plasma gasifier was increased by 218% in relation to the unit exergoeconomic cost of the resources of that component. As can be seen in Figure 21 (dashed line-circle graph), the high value of r_k in the plasma gasifier stemmed from the high increment of the total cost, which according to f_k (see Table 22 and Table D.3) for the plasma gasifier, was mainly due to the high non-thermodynamic costs of the component. Therefore, based on the values of r_k and f_k , the results suggested that alternative strategies must be investigated to reduce the non-thermodynamic cost of the plasma gasifier looking for enhancing the overall exergoeconomic performance of the plasma gasifier and the IPGCC power plant. Besides the plasma gasifier, the components 25 (FW preheater) and 21 (LP superheater) presented values of r_k relatively high of 1.51 and 1.06, respectively. These results were attributed to the nature of their respective productive process, where the sensible heat of hot gases stream at high temperatures (400 and 200°C) is exploited to produce preheated water (component 25) and

superheated LP steam (component 21), whose temperature is significantly lower (256 and 141 °C), which leads to reach exergy efficiencies of 50% and 61.25% for components 25 and 21, respectively. As a consequence, the unit exergoeconomic costs of products from these components were significantly higher than that of resources, resulting in high values of r_k according to Eq. 74. Similar values for r_k to those presented in Figure 21 were obtained for the components in the remaining plant cases (Institutional, Commercial, Mixed, and Residential), which are presented in Table D.3.

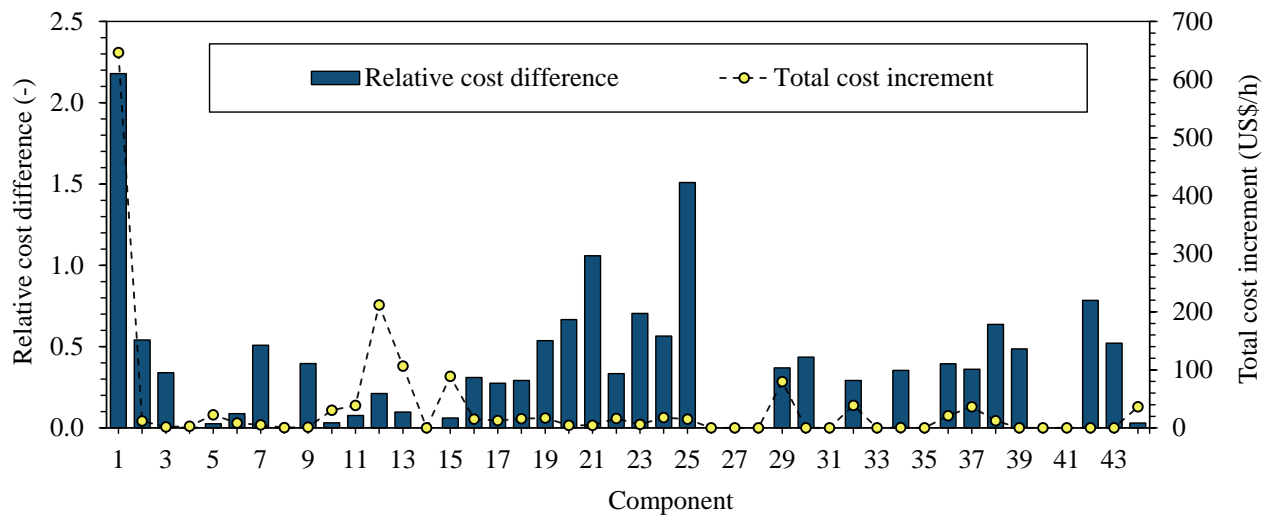


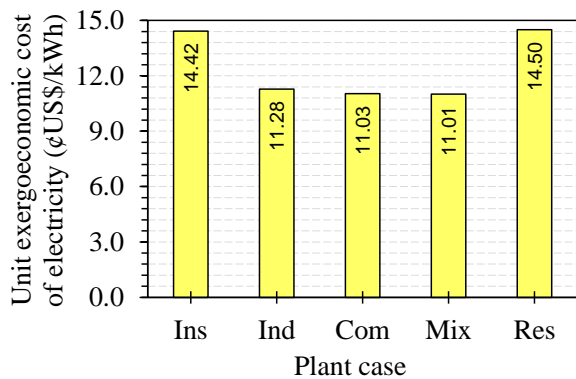
Figure 21. Relative cost difference and the total cost increment in each component of the IPGCC plant processing industrial waste (100 t/day).

The unit exergoeconomic costs of the available electricity for selling in each plant case are presented in Figure 22a. The values of this parameter ranged from 11.01 to 14.50 ¢US\$/kWh, which are higher than the average price of the hydro-electricity in the energy market from Colombia (~6.92 ¢US\$/kWh for 2019) [152]. The results presented in Figure 22a are analyzed by classifying the plant cases into two groups according to their processing capacity, as follows, Group 1: Institutional, Industrial, and Commercial plants, and Group 2: Mixed and Residential plants. In Group 1, the Institutional plant presented a high unit exergoeconomic cost of electricity of 14.42 ¢US\$/kWh, in relation to that of Industrial (11.28 ¢US\$/kW-h) and Commercial plant (11.03 ¢US\$/kWh). The high unit exergoeconomic cost of electricity in the Institutional plant related to two issues. First, the economy of scale since the processing capacity of the Institutional plant is 25% and 50% lower than that of Industrial and Commercial plants, respectively; and second, the high moisture content of the institutional wastes, which adversely affects the electricity generation in the IPGCC power plant, as described in section 3.3.2. In Group 2, a significant difference between the unit exergoeconomic cost of the electricity of Mixed and Residential plants was found. In the

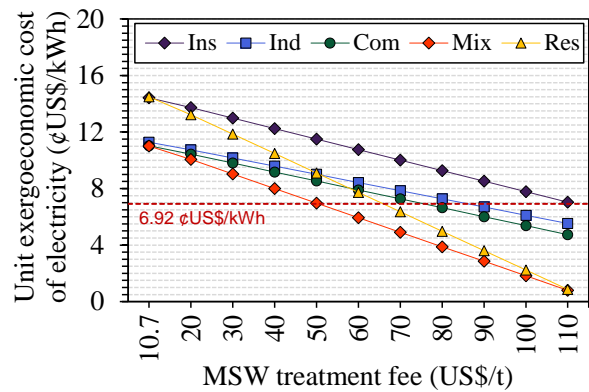
case of the Residential plant, this parameter was 14.5 ¢US\$/kWh, which is 32% higher than that of the Mixed plant (11.01 ¢US\$/kWh). This difference was attributed to the low electricity generation of the Residential plant because of the operative conditions of the plasma gasifier (see section 3.3.2). For all analyzed plants, the lowest unit exergoeconomic cost of electricity was obtained by the Mixed plant despite the high moisture content of the mixed waste. Therefore, the positive effect of the economy of scale on the electricity price generated via waste processing in the IPGCC power plant investigated is highlighted in this work. Nevertheless, by comparing the Industrial, Commercial, and Mixture cases, it is worth note the mild difference between their unit exergoeconomic costs of the available electricity, with a variation lower than 2.4%. In spite of the processing capacity of these three plants is quite different, 100, 150, and 1000 t/day, respectively, it was expected a markable effect of economic of scale. However, this tight difference regarding the unit exergoeconomic cost of electricity is attributed to low moisture content of Industrial (26.61%) and Commercial (32.95%) wastes that led to decrease the destroyed exergy in PG by MSW drying. Whereas for the Mixture case, despite its high moisture content (51.33%) that favored the exergy destruction, the processing capacity of this plant case produce the highest power leading to diminish its unit exergoeconomic cost of electricity. Therefore, it is highlighted that the country could assess IPGCC projects feed with mass flow rate of MSW between 100 to 150 t/day with a moisture content lower than 33 wt%.

The MSW treatment fee paid to WtoE plants in countries with a well-established MSW treatment system contributes to reducing exergoeconomic costs of electricity up to competitive prices [22], [95]. Here, a sensitivity analysis assessing the MSW treatment fee on the unit exergoeconomic cost of the electricity was carried out. The MSW treatment fee was ranged between 10.7 US\$/t, which is the current charge for final disposal of MSW in Medellín-Colombia (Figure 22a), and 110 US\$/t [95]. The results obtained from the sensitivity analysis are shown in Figure 22b. For the plant case processing institutional wastes, when the MSW treatment fee was 110 US\$/t, the unit exergoeconomic cost of the electricity decreased up to 7.04 ¢US\$/kWh, which is still higher than the average price of electricity in the Colombian energy market (6.92 ¢US\$/kWh). In the case of industrial and commercial plants, the unit exergoeconomic cost of the electricity was reduced up to 5.53 and 4.74 ¢US\$/kWh, respectively, meanwhile, for plant cases processing mixed and residential wastes, it fell to 0.80 and 0.86 ¢US\$/kWh, respectively. The significant difference of the unit exergoeconomic cost of the electricity, between the plants processing mixed and residential wastes and the plants processing the remaining waste types, was explained by the difference between plant capacities according to the economy of scale. Furthermore, the effect of the economy of scale was also reflected in the required MSW treatment fee seeking to equalize the unit exergoeconomic cost of the electricity generated in each plant case with the Colombian energy price (6.92 ¢US\$/kWh). The values of MSW treatment fee were >110, 86.10, 75.60, 50.50, and 65.90 US\$/t for the IPGCC plants fed with institutional, industrial,

commercial, mixed, and residential wastes, respectively. Therefore, according to the unit exergoeconomic cost of electricity found in this work, the IPGCC power plant fed with mixed wastes (processing 1000 t/day) was found as the most feasible project because of its unit exergoeconomic cost of electricity as well as its required MSW treatment fee are the lowest. However, the MSW treatment fee required to match the electricity price in the Colombian market (50.5 US\$/t) is higher than the current MSW treatment fee (~10.7 US\$/t) paid to the sanitary landfill, where the MSW from Medellín are disposed. This result suggests that new public policies are needed to encourage the energy recovery from MSW seeking for the sustainability of cities.



a) Unit exergoeconomic cost of the electricity generated in each plant case.



b) Unit exergoeconomic cost of the electricity vs MSW treatment fee.

Figure 22. Unit exergoeconomic cost of electricity available for selling for each plant case (waste type).

In Table 23, the costs of electricity generation obtained for the IPGCC power plants are compared with the cost of electricity generation obtained in previous works, that were based on other WtoE technologies such as incineration and autothermal gasification. The costs of electricity generation gotten for our five IPGCC power plants (11.01 – 14.50) is similar to those obtained for incineration and autothermal gasification, which suggests that the plasma gasification could be an alternative for the energy recovery from the MSW. However, it is worth note that the results presented in Table 23 were acquired from several studies under different conditions for the investigated systems (e.g. processing capacity, MSW treatment fee, and MSW composition).

Table 23. Comparison between some results obtained for the IPGCC power plant and other technologies investigated in selected previous works.

Parameter	This work	Medina Jimenez <i>et al.</i> [31]	Jack and Oko [114]	Casas <i>et al.</i> [116]	Nordi <i>et al.</i> [51]	
Technology	PG + CC	I + SC	AG + SC	I + SC	AG + CC	I + SC
Capacity (t/day)	75 - 1000	806	806	2500	36	491
Capital investment (Million US\$)	27.2 – 207.8	189.5	136.4	326.46	-	100.1
Net power (MW)	3.5 – 32.9	21.65	16.61	117.00	0.37 – 0.43	12.41
Thermal efficiency (%)	23.7 – 31.0	25.1	19.3	36.9	34.0 – 67.0	25.0
Cost of electricity (¢US\$/kWh)	11.01 – 14.50	11.30	13.90	5.60	7.00 – 13.00	9.43

I: Incineration, AG: Autothermal gasification, PG: Plasma gasification, SC: Steam cycle, CC: Combined cycle.

3.4 CONCLUSIONS

The energy recovery of MSW through an IPGCC plant for power generation has been investigated from an exergoeconomic point of view. The wastes from four sectors (Industrial, Commercial, Institutional, and Residential), as well as the mixture between them (Mixed), generated in Medellin-Colombia were considered as fuels. According to the generation rate of the MSW types, five IPGCC plant cases with different processing capacities have been modeled and simulated using Aspen Plus. The Theory of Exergy Cost (TEC) methodology has been applied to assess the exergoeconomic performance of the five plant cases.

The plasma gasifier and the gas turbine were found as the components with the highest rates of exergy destruction, which was associated with the irreversibility nature of the chemical reaction of gasification and combustion, as well as the large temperature difference between the combustion gases and the cooling air in the gas turbine. Furthermore, an adverse effect of the wastes' moisture content on the exergy performance of the plasma gasifier was found. The exergy destruction ratio of the plasma gasifier increased from 34% to 42% when the moisture content of the wastes increased from 26.6% to 57.9%. Regarding the processing capacity of power plants (75, 100, 150, and 1000 t/day), the net power output of the five plants ranged between 3.5 and 32.9 MW. As a function of the moisture content of the wastes, the efficiencies decreased as follows, energy efficiency diminished from 31.1% to 23.7%, whilst exergy yield decreased from 29.8% to 22.6%.

From the exergoeconomic analysis, the overall PEC for the five plant cases was estimated at US\$ 27.25, US\$ 36.37, US\$ 49.13 US\$ 207.7, and US\$ 204.6 million for the plants fueled with Institutional, Industrial, Commercial, Mixed and Residential wastes, respectively. By far, the component with the highest PEC was the plasma gasifier, whose contribution to the non-thermodynamic cost in the five plant cases was between 70% and 80%. The unit exergoeconomic costs of the electricity generated in the five plant cases varied from 11.01 to 14.5 ¢US\$/kWh, which are still higher than the average price of the electricity in the Colombian

energy market (~6.92 ¢US\$/kWh in 2019). The IPGCC power plant fueled with the mixed wastes presented the lowest unit exergoeconomic cost of the electricity (11.01 ¢US\$/kWh), which was attributed to the syngas quality produced in the plasma gasifier and the high processing capacity (1000 t/day) according to the economy of scale.

Assessing the effect of the MSW treatment fee (from 10.7 to 110 US\$/t) on the unit exergoeconomic cost of the plants fueled with institutional, industrial, commercial, mixed, and residential wastes, it was found that the lowest unit exergoeconomic costs of the electricity were 7.04, 5.53, 4.74, 0.8, and 0.86 ¢US\$/kWh, respectively. Furthermore, the MSW treatment fee received by each plant for matching the unit exergoeconomic cost to the price of the electricity in the Colombian energy market must be 86.10, 75.60, 50.50, and 65.90 US\$/t, respectively. Therefore, the more feasible alternative for energy recovery, from the MSW produced in Medellín through the proposed IPGCC plant for power generation, is to use the mixed wastes as fuel that reach a unit exergoeconomic cost of electricity of 11.01 ¢US\$/kWh. The exergoeconomic performance of the plant with mixed wastes is favored because it requires the lowest MSW treatment fee (50.50 US\$/t), which is ascribed to its processing capacity (1000 t/day), and thus, to its power produced (32.9 MWe). Therefore, further energy policies are required pursuing the feasibility of WtoE projects by IPGCC power plants in Colombia.

Nomenclature

Abbreviations

AWR	Air to waste ratio, kg/kg
CC	Combustion chamber
CGE	Cold gas efficiency, %
CI	Cost index
EG	Electric generator
ExE	Exergy efficiency, %
F	Fuel
FC	Fixed carbon
FW	Feed water
GT	Gas turbine
HHV	Higher heating value, MJ/kg
HP	High pressure
IP	Intermediate pressure
IPGCC	Integrated plasma gasification combined cycle
LHV	Lower heating value, kJ/kg
LP	Low pressure
LTGC	Low temperature gas cooling
MC	Moisture content, wt%
MDEA	Methyl-diethanolamine
MSW	Municipal solid waste
P	Product
PEC	Purchased equipment cost, US\$
SC	Steam cycle
SCS	Syngas cooling system
STS	Syngas treatment system
TEC	Theory of exergy cost
VM	Volatile matter
wt%	Weight percentage, %
TEC	Theory of exergy cost

Symbols

A	Incidence matrix
A _F	Fuels matrix
A _P	Products matrix
Δ	Cost matrix
a	Plant lifetime, year
b	Construction time, year
c	Unit exergy cost, kW/kW
\dot{C}	Exergy cost, kW
c ^z	Unit exergoeconomic cost, US\$/kWh
\dot{C}^z	Exergoeconomic cost, US\$/h
\dot{C}_D^z	Exergoeconomic cost of irreversibilities, US\$/h

e	Specific exergy, kJ/kg
e ₀	Standard chemical exergy, kJ/kmol
\dot{E}	Exergy flow rate, kW
\dot{E}_d	Rate of exergy destruction, kW
f	Annuity factor, dimensionless
f _k	Exergoeconomic factor, %
h	Enthalpy, kJ/kg
\dot{H}	Enthalpy flow rate, kW
in	Effective annual interest rate, %/year
\dot{m}	Mass flow rate, kg/s
N	Annual plant operating time, h/year
P	Pressure, bar
\dot{Q}	Heat flow rate, kW
R	Universal gas constant, kJ/kmol-K
r _i	Annual inflation rate, %/year
r _k	Relative cost difference, dimensionless
s	Entropy, kJ/kg-K
T	Temperature, °C
US\$	United states dollar
\dot{W}	Power, kW
y	Molar fraction, dimensionless
Y	Exergy amortization vector
Z	Non-thermodynamic cost, US\$/h
Z	Vector of thermoeconomic amortization

Subscripts

0	Dead state
ch	chemical
e	External resources
F	Fuel
P	Product
ph	Physical
T	Total
0	Dead state

Greeks

α	Auxiliary matrix
γ	Activity coefficient, dimensionless
δ _D	Exergy destruction ratio, %
η	Efficiency, %
φ _{drv}	Chemical exergy to net calorific value, dimensionless
φ _k	Maintenance factor, dimensionless
ω	Vector of independent terms

Appendix A. Productive structure of the IPGCC power plant and the *four propositions* of TEC methodology.

In this appendix are presented two tables. Table A.1 contains the equations to calculate the fuels and products for each component involved in the IPGCC power plant. In Table A.2, the description and equations for the *four propositions* of the TEC methodology are presented.

Table A.1. Productive structure of IPGCC power plant.

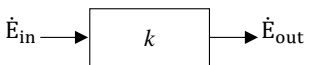
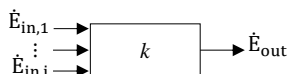
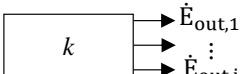
Components		Fuel	Product
1	Plasma gasifier	$\dot{E}_1 + \dot{E}_2 + \dot{E}_3$	$\dot{E}_4 + \dot{E}_5 + \dot{E}_{95}$
2	HP syngas cooler	$\dot{E}_4 - \dot{E}_6$	$\dot{E}_{81} - \dot{E}_{80}$
3	IP syngas cooler	$\dot{E}_6 - \dot{E}_7$	$\dot{E}_{78} - \dot{E}_{77}$
4	Fabric filter	\dot{E}_7	$\dot{E}_8 + \dot{E}_9$
5	Wet scrubber	$\dot{E}_8 + \dot{E}_{10}$	$\dot{E}_{11} + \dot{E}_{12} + \dot{E}_{90}$
6	Syngas compressor	\dot{E}_{14}	$\dot{E}_{13} - \dot{E}_{11}$
7	Syngas preheater	$\dot{E}_{13} - \dot{E}_{15}$	$\dot{E}_{21} - \dot{E}_{20}$
8	COS-hydrolysis unit	\dot{E}_{15}	\dot{E}_{16}
9	LTGC	$\dot{E}_{16} - \dot{E}_{17}$	$\dot{E}_{75} - \dot{E}_{74}$
10	MDEA absorber/stripper system	$\dot{E}_{17} + \dot{E}_{88} + \dot{E}_{92}$	$\dot{E}_{18} + \dot{E}_{19} + \dot{E}_{20} + \dot{E}_{91} + \dot{E}_{93}$
11	Air compressor	\dot{E}_{24}	$\dot{E}_{23} + \dot{E}_{22}$
12	Combustion chamber	$\dot{E}_{21} + \dot{E}_{25}$	\dot{E}_{27}
13	Gas turbine	$\dot{E}_{28} - \dot{E}_{30}$	$\dot{E}_{24} + \dot{E}_{29}$
14	Compressed air splitter	\dot{E}_{23}	$\dot{E}_{26} + \dot{E}_{25}$
15	Combustion gas-cooling air mixer	$\dot{E}_{26} + \dot{E}_{27}$	\dot{E}_{28}
16	IP Reheater	$\dot{E}_{30} - \dot{E}_{31}$	$\dot{E}_{56} - \dot{E}_{55}$
17	HP Superheater	$\dot{E}_{31} - \dot{E}_{32}$	$\dot{E}_{65} - \dot{E}_{64}$
18	HP Evaporator	$\dot{E}_{32} - \dot{E}_{33}$	$\dot{E}_{63} - \dot{E}_{62}$
19	HP Economizer	$\dot{E}_{33} - \dot{E}_{34}$	$\dot{E}_{62} - \dot{E}_{61}$
20	IP Superheater	$\dot{E}_{34} - \dot{E}_{35}$	$\dot{E}_{54} - \dot{E}_{53}$
21	LP Superheater	$\dot{E}_{35} - \dot{E}_{36}$	$\dot{E}_{46} - \dot{E}_{45}$
22	IP Evaporator	$\dot{E}_{36} - \dot{E}_{37}$	$\dot{E}_{53} - \dot{E}_{52}$
23	IP Economizer	$\dot{E}_{37} - \dot{E}_{38}$	$\dot{E}_{52} - \dot{E}_{51}$
24	LP Evaporator	$\dot{E}_{38} - \dot{E}_{39}$	$\dot{E}_{45} - \dot{E}_{44}$
25	Feedwater preheater	$\dot{E}_{39} - \dot{E}_{40}$	$\dot{E}_{43} - \dot{E}_{42}$
26	Exhaust stack	\dot{E}_{40}	\dot{E}_{41}
27	Preheated feedwater splitter	\dot{E}_{43}	$\dot{E}_{44} + \dot{E}_{50} + \dot{E}_{59}$
28	LP steam mixer	$\dot{E}_{46} + \dot{E}_{57}$	\dot{E}_{47}
29	LP steam turbine	$\dot{E}_{47} - \dot{E}_{49}$	\dot{E}_{48}
30	IP water pump	\dot{E}_{86}	$\dot{E}_{51} - \dot{E}_{50}$
31	IP steam mixer	$\dot{E}_{54} + \dot{E}_{66} + \dot{E}_{78}$	\dot{E}_{55}
32	IP steam turbine	$\dot{E}_{56} - \dot{E}_{57}$	\dot{E}_{58}
33	HP water mixer	$\dot{E}_{59} + \dot{E}_{75}$	\dot{E}_{60}
34	HP water pump	\dot{E}_{87}	$\dot{E}_{60} - \dot{E}_{61}$
35	HP steam mixer	$\dot{E}_{63} + \dot{E}_{81}$	\dot{E}_{64}

Continued in the next page...

Table A.1. Productive structure of IPGCC power plant.

	Components	Fuel	Product
36	HP steam turbine	$\dot{E}_{65} - \dot{E}_{66}$	\dot{E}_{67}
37	Condenser	$\dot{E}_{49} - \dot{E}_{71}$	$\dot{E}_{70} - \dot{E}_{69}$
38	Cooling water pump	\dot{E}_{82}	$\dot{E}_{69} - \dot{E}_{68}$
39	Feedwater pump	\dot{E}_{83}	$\dot{E}_{72} - \dot{E}_{71}$
40	Feedwater splitter	\dot{E}_{72}	$\dot{E}_{73} + \dot{E}_{76} + \dot{E}_{79}$
41	LP water splitter	\dot{E}_{73}	$\dot{E}_{42} + \dot{E}_{74}$
42	IP-SCS water pump	\dot{E}_{85}	$\dot{E}_{77} - \dot{E}_{76}$
43	HP-SCS water pump	\dot{E}_{84}	$\dot{E}_{80} - \dot{E}_{79}$
44	Electric generator	$\dot{E}_{29} + \dot{E}_{48} + \dot{E}_{58} + \dot{E}_{67}$	$\dot{E}_3 + \dot{E}_{14} + (\dot{E}_{82} + \dots + \dot{E}_{89}) + \dot{E}_{94}$

Table A.2. Propositions of TEC methodology, adapted from [133]–[138].

Proposition	Description	Formula
P1: External resources	In the absence of external considerations (origin of resources) the exergy cost of the resources entering to the system are equal to their exergy. Thus, the unit exergy cost of external resource is equal to 1.	$c_e = \frac{\dot{C}_e}{\dot{E}_e} = 1$
P2: Conservation of exergy cost	Exergy cost is a conservative property. Thus, for every component (k) of a system, the sum of the exergy costs of inlet flows is equal to the sum of those of outlet flows.	$\left(\sum \dot{C}_{in}\right)_k = \left(\sum \dot{C}_{out}\right)_k \quad k = 1, \dots, n$ $\mathbf{A}(n \times m) \cdot \dot{\mathbf{C}}(m \times 1) = \mathbf{0}(n \times 1)$
P3: Exergy cost of fuel in <i>doublet</i> or <i>multiplet</i>	If a component has a fuel in <i>doublet</i> , the exergy cost of the outlet flow will be the same as that of the inlet flow.  $F_k = \dot{E}_{in} - \dot{E}_{out}$	$c_{out} = \frac{\dot{C}_{out}}{\dot{E}_{out}} = c_{in} = \frac{\dot{C}_{in}}{\dot{E}_{in}}$
	If a component has a fuel in <i>multiplet</i> , the unit exergy cost of the outlet flow can be taken as the average unit exergy cost of the corresponding inlet flows.  $F_k = (\dot{E}_{in,1} + \dots + \dot{E}_{in,i}) - \dot{E}_{out}$	$c_{out} = \frac{\dot{C}_{out}}{\dot{E}_{out}} = c_{in} = \frac{\sum \dot{C}_{in}}{\sum \dot{E}_{in}}$
P4: Multiple products from one component	All products from one component have the same unit exergy cost since they are formed simultaneously in the same productive process.  $P_k = \dot{E}_{out,1} + \dots + \dot{E}_{out,i}$	$c_{out,1} = \frac{\dot{C}_{out,1}}{\dot{E}_{out,1}} = \dots = c_{out,i} = \frac{\dot{C}_{out,i}}{\dot{E}_{out,i}}$

Appendix B. Properties of streams in the IPGCC power plants.

Here, the properties of the streams (mass flow, temperature, pressure, enthalpy, and exergy) are presented for each plant cases according to the processed waste.

Table B.1. Properties of streams in the IPGCC plant processing institutional waste.

Stream	\dot{m} (kg/s)	P (bar)	T (°C)	\dot{H} (kW)	\dot{E} (kW)	Stream	\dot{m} (kg/s)	P (bar)	T (°C)	\dot{H} (kW)	\dot{E} (kW)
1	0.868	1.013	25.0	-7641.8	12082.2	49	1.789	0.046	31.4	-24371.0	84.1
2	0.347	1.013	25.0	-0.1	1.5	50	0.536	4.200	141.0	-8249.3	41.0
3	-	-	-	2293.3	2293.3	51	0.536	30.800	141.5	-8247.2	42.7
4	1.170	1.013	468.0	-5872.1	11334.0	52	0.536	30.340	229.0	-8039.1	115.2
5	0.045	1.013	1691.1	58.0	66.1	53	0.536	29.890	233.7	-7065.3	516.1
6	1.170	1.003	354.2	-6097.6	11205.5	54	0.536	29.440	312.0	-6944.8	569.4
7	1.170	0.993	249.9	-6295.9	11108.8	55	1.360	29.440	312.8	-17614.8	1445.8
8	1.170	0.976	249.9	-6295.9	11106.4	56	1.360	29.000	510.0	-17002.2	1786.4
9	0.000	0.976	249.9	0.0	0.0	57	1.360	4.080	254.7	-17689.8	1054.5
10	0.107	1.013	25.0	-1688.7	18.2	58	-	-	-	687.6	687.6
11	0.871	0.927	30.0	-2697.5	10761.2	59	0.107	4.200	141.0	-1649.9	8.2
12	0.406	0.927	74.8	-6329.0	107.4	60	0.666	4.200	141.0	-10253.9	51.0
13	0.871	21.785	454.3	-2156.4	11276.1	61	0.666	125.560	143.3	-10242.2	60.6
14	-	-	-	541.1	541.1	62	0.666	123.680	322.0	-9667.9	296.3
15	0.871	21.567	190.0	-2506.8	11102.5	63	0.666	121.830	325.8	-8860.2	701.8
16	0.871	20.057	190.0	-2506.8	11095.3	64	0.755	121.830	325.8	-10042.0	795.4
17	0.871	19.856	40.0	-2764.6	11042.4	65	0.755	120.000	507.0	-9526.3	1080.3
18	0.031	1.500	110.1	-398.2	87.9	66	0.755	29.440	313.4	-9781.3	803.5
19	0.003	1.500	30.5	-12.6	95.6	67	-	-	-	254.9	254.9
20	0.837	19.856	40.1	-2275.2	10885.3	68	97.222	1.013	15.0	-	69.8
21	0.837	19.657	333.5	-1925.4	11000.7	69	97.222	10.000	15.1	-	161.3
22	8.125	1.013	25.0	-2.3	36.0	70	97.222	10.000	25.2	-	87.9
23	8.125	19.657	456.6	3663.5	3522.1	71	1.789	0.046	31.4	-28352.1	0.2
24	-	-	-	3665.8	3665.8	72	1.789	4.260	31.5	-28350.8	1.2
25	3.194	19.657	456.6	1440.2	1384.6	73	1.631	4.260	31.5	-25854.7	1.1
26	4.931	19.657	456.6	2223.3	2137.4	74	0.559	4.260	31.5	-8861.8	0.4
27	4.031	19.067	2381.6	-485.1	10234.4	75	0.559	4.200	141.0	-8604.0	42.8
28	8.962	19.067	1418	1738.1	11653.5	76	0.069	4.260	31.5	-1087.4	0.0
29	-	-	-	4586.2	4586.2	77	0.069	29.890	31.8	-1087.1	0.2
30	8.962	1.050	672.9	-6513.8	3098.6	78	0.069	29.440	312.0	-888.8	72.9
31	8.962	1.046	615.2	-7126.4	2682.5	79	0.089	4.260	31.5	-1408.7	0.1
32	8.962	1.043	566.1	-7642.1	2342.1	80	0.089	123.680	32.8	-1407.3	1.1
33	8.962	1.039	488.1	-8449.8	1832.9	81	0.089	121.830	325.8	-1181.8	93.6
34	8.962	1.035	431.7	-9024.2	1489.5	82	-	-	-	143.3	143.3
35	8.962	1.032	419.7	-9144.7	1417.7	83	-	-	-	1.2	1.2
36	8.962	1.028	409.6	-9246.5	1357.3	84	-	-	-	1.4	1.4
37	8.962	1.024	311.6	-10220.3	839.7	85	-	-	-	0.2	0.2
38	8.962	1.021	290.3	-10428.5	736.9	86	-	-	-	2.1	2.1
39	8.962	1.017	195.0	-11348.6	347.3	87	-	-	-	11.7	11.7
40	8.962	1.013	142.9	-11842.9	183.9	88	-	-	-	0.1	0.1
41	8.962	1.013	142.9	-11842.9	183.9	89	-	-	-	3505.3	3505.3
42	1.072	4.260	31.5	-16992.9	0.7	90	-	-	-	1041.8	17.2
43	1.072	4.200	141.0	-16498.6	82.0	91	-	-	-	133.0	29.5
44	0.429	4.200	141.0	-6599.4	32.8	92	-	-	-	211.6	211.6
45	0.429	4.140	144.9	-5679.3	296.6	93	-	-	-	0.0	0.0
46	0.429	4.080	256.0	-5577.5	333.0	94	-	-	-	132.6	10.3
47	1.789	4.080	255.0	-23267.3	1387.5	95	-	-	-	465.5	107.9
48	-	-	-	1103.7	1103.7						

Table B.2. Properties of streams in the IPGCC plant processing industrial waste.

Stream	\dot{m} (kg/s)	P (bar)	T (°C)	\dot{H} (kW)	\dot{E} (kW)	Stream	\dot{m} (kg/s)	P (bar)	T (°C)	\dot{H} (kW)	\dot{E} (kW)
1	1.157	1.013	25.0	-8646.9	19668.2	49	3.050	0.046	31.4	-41551.9	143.5
2	0.579	1.013	25.0	-0.2	2.6	50	0.800	4.200	141.0	-12307.7	61.2
3	-	-	-	3633.6	3633.6	51	0.800	30.800	141.5	-12304.6	63.7
4	1.672	1.013	727.7	-5832.3	18653.8	52	0.800	30.340	229.0	-11994.0	171.9
5	0.065	1.013	1680.7	82.1	93.8	53	0.800	29.890	233.7	-10541.2	770.0
6	1.672	1.003	356.4	-6910.4	17973.2	54	0.800	29.440	312.0	-10361.4	849.6
7	1.672	0.993	250.4	-7191.4	17835.8	55	2.414	29.440	312.9	-31271.5	2567.1
8	1.672	0.976	250.4	-7191.4	17832.4	56	2.414	29.000	510.0	-30184.5	3171.4
9	0.000	0.976	250.4	0.0	0.0	57	2.414	4.080	254.7	-31405.1	1872.1
10	0.153	1.013	25.0	-2416.4	25.9	58	-	-	-	1220.7	1220.7
11	1.409	0.927	30.0	-4292.2	17480.6	59	0.176	4.200	141.0	-2703.5	13.4
12	0.415	0.927	68.9	-6432.9	117.7	60	1.092	4.200	141.0	-16808.4	83.5
13	1.409	21.785	454.5	-3406.7	18323.3	61	1.092	125.560	143.3	-16789.3	99.3
14	-	-	-	885.6	885.6	62	1.092	123.680	322.0	-15847.8	485.7
15	1.409	21.567	190.0	-3980.2	18039.1	63	1.092	121.830	325.8	-14523.8	1150.4
16	1.409	20.057	190.0	-3980.2	18027.4	64	1.517	121.830	325.8	-20174.5	1597.9
17	1.409	19.856	39.7	-4402.8	17940.7	65	1.517	120.000	507.0	-19138.5	2170.3
18	0.053	1.500	109.1	-649.2	216.7	66	1.517	29.440	313.4	-19650.7	1614.2
19	0.007	1.500	29.3	-26.1	201.4	67	-	-	-	512.2	512.2
20	1.350	19.856	42.4	-3593.8	17567.2	68	180.556	1.013	15.0	-2874001.5	129.6
21	1.350	19.657	336.6	-3021.16	17758.3	69	180.556	10.000	15.1	-2873735.3	299.6
22	13.111	1.013	25.0	-3.7	58.1	70	180.556	10.000	24.4	-2866947.8	164.6
23	13.111	19.657	456.6	5911.7	5683.5	71	3.050	0.046	31.4	-48339.4	0.3
24	-	-	-	5915.4	5915.4	72	3.050	4.260	31.5	-48337.3	2.0
25	5.194	19.657	456.6	2342.1	2251.7	73	2.528	4.260	31.5	-40061.0	1.7
26	7.917	19.657	456.6	3569.6	3431.8	74	0.917	4.260	31.5	-14527.6	0.60
27	6.544	19.067	2369.7	-679.0	16534.9	75	0.917	4.200	141.0	-14105.0	70.1
28	14.461	19.067	1418.0	2890.5	18815.3	76	0.097	4.260	31.5	-1540.8	0.1
29	-	-	-	7411.9	7411.9	77	0.097	29.890	31.8	-1540.5	0.3
30	14.461	1.050	672.2	-10436.7	4998.3	78	0.097	29.440	312.0	-1259.4	103.3
31	14.461	1.046	608.8	-11523.7	4261.8	79	0.425	4.260	31.5	-6735.5	0.3
32	14.461	1.043	547.5	-12559.7	3584.4	80	0.425	123.680	32.8	-6728.7	5.4
33	14.461	1.039	468.0	-13883.7	2761.9	81	0.425	121.830	325.8	-5650.7	447.6
34	14.461	1.035	410.4	-14825.2	2210.3	82	-	-	-	266.2	266.2
35	14.461	1.0316	399.4	-15005.0	2105.2	83	-	-	-	2.1	2.1
36	14.461	1.028	390.0	-15155.9	2017.2	84	-	-	-	6.8	6.8
37	14.461	1.024	299.1	-16608.7	1262.3	85	-	-	-	0.3	0.3
38	14.461	1.021	279.4	-16919.31	1111.9	86	-	-	-	3.1	3.1
39	14.461	1.017	191.8	-18282.8	544.8	87	-	-	-	19.1	19.1
40	14.461	1.013	143.3	-19025.6	300.6	88	-	-	-	0.2	0.2
41	14.461	1.013	143.3	-19025.6	300.6	89	-	-	-	5988.9	5988.9
42	1.611	4.260	31.5	-25533.3	1.1	90	-	-	-	1117.3	18.4
43	1.611	4.200	141.0	-24790.6	123.2	91	-	-	-	226.6	49.8
44	0.636	4.200	141.0	-9779.5	48.6	92	-	-	-	360.1	360.1
45	0.636	4.140	144.9	-8416.0	439.5	93	-	-	-	0.0	0.0
46	0.636	4.080	256.0	-8265.1	493.5	94	-	-	-	220.5	17.1
47	3.050	4.080	255.0	-39670.2	2365.6	95	-	-	-	736.7	170.8
48	-	-	-	1881.7	1881.7						

Table B.3. Properties of streams in the IPGCC plant processing commercial waste.

Stream	\dot{m} (kg/s)	P (bar)	T (°C)	\dot{H} (kW)	\dot{E} (kW)	Stream	\dot{m} (kg/s)	P (bar)	T (°C)	\dot{H} (kW)	\dot{E} (kW)
1	1.736	1.013	25.0	-14198.9	27127.6	49	4.074	0.046	31.4	-55497.0	191.6
2	0.694	1.013	25.0	-0.2	3.1	50	1.208	4.200	141.0	-18592.9	92.4
3	-	-	-	4813.2	4813.2	51	1.208	30.800	141.5	-18588.3	96.3
4	2.332	1.013	578.8	-10508.6	25609.2	52	1.208	30.340	229.0	-18119.1	259.7
5	0.098	1.013	1785.7	143.0	158.2	53	1.208	29.890	233.7	-15924.3	1163.2
6	2.332	1.003	342.7	-11459.8	25044.1	54	1.208	29.440	312.0	-15652.7	1283.4
7	2.332	0.993	249.9	-11809.1	24875.3	55	3.107	29.440	312.8	-40241.2	3303.0
8	2.332	0.976	249.9	-11809.1	24870.7	56	3.107	29.000	510.0	-38841.9	4081.0
9	0.000	0.976	249.9	0.0	0.0	57	3.107	4.080	254.7	-40412.6	2409.0
10	0.213	1.013	25.0	-3366.6	36.2	58	-	-	-	1570.7	1570.7
11	1.823	0.927	30.0	-5778.1	24264.4	59	0.242	4.200	141.0	-3718.6	18.5
12	0.723	0.927	73.0	-11278.8	189.0	60	1.403	4.200	141.0	-21584.9	107.3
13	1.823	21.785	442.5	-4674.8	25313.3	61	1.403	125.560	143.3	-21560.4	127.5
14	-	-	-	1103.3	1103.3	62	1.403	123.680	322.0	-20351.3	623.7
15	1.823	21.567	190.0	-5380.7	24966.8	63	1.403	121.830	325.8	-18651.0	1477.3
16	1.823	20.057	190.0	-5380.7	24952.0	64	1.778	121.830	325.8	-23637.0	1872.2
17	1.823	19.856	40.1	-5916.0	24841.8	65	1.778	120.000	507.0	-22423.1	2542.8
18	0.065	1.500	109.6	-815.2	220.9	66	1.778	29.440	313.4	-23023.2	1891.3
19	0.009	1.500	28.9	-35.2	276.2	67	-	-	-	600.0	600.0
20	1.749	19.856	41.3	-4901.9	24387.8	68	222.222	1.013	15.0	-3537232.6	159.4
21	1.749	19.657	323.9	-4197.2	24617.0	69	222.222	10.000	15.1	-3536905.0	368.8
22	18.236	1.013	25.0	-5.1	80.8	70	222.222	10.000	25.1	-3527839.4	201.0
23	18.236	19.657	456.6	8222.5	7905.1	71	4.074	0.046	31.4	-64562.6	0.4
24	-	-	-	8227.6	8227.6	72	4.074	4.260	31.5	-64559.8	2.7
25	7.299	19.657	456.6	3291.0	3164.0	73	3.578	4.260	31.5	-56701.7	2.3
26	10.937	19.657	456.6	4931.5	4741.1	74	1.161	4.260	31.5	-18401.6	0.8
27	9.048	19.067	2370.0	-906.2	22845.9	75	1.161	4.200	141.0	-17866.3	88.8
28	19.985	19.067	1418	4025.2	25997.0	76	0.121	4.260	31.5	-1915.0	0.1
29	-	-	-	10186.7	10186.7	77	0.121	29.890	31.8	-1914.6	0.4
30	19.985	1.050	672.3	-14389.0	6906.1	78	0.121	29.440	312.0	-1565.3	128.3
31	19.985	1.046	613.2	-15788.4	5956.4	79	0.375	4.260	31.5	-5943.1	0.2
32	19.985	1.043	561.4	-17002.2	5157.3	80	0.375	123.680	32.8	-5937.1	4.8
33	19.985	1.039	487.7	-18702.4	4086.9	81	0.375	121.830	325.8	-4985.9	394.9
34	19.985	1.035	434.5	-19911.5	3362.9	82	-	-	-	327.6	327.6
35	19.985	1.032	422.5	-20183.1	3200.6	83	-	-	-	2.8	2.8
36	19.985	1.028	412.3	-20412.6	3064.1	84	-	-	-	6.0	6.0
37	19.985	1.024	313.3	-22607.4	1894.0	85	-	-	-	0.4	0.4
38	19.985	1.021	291.8	-23076.6	1661.7	86	-	-	-	4.6	4.6
39	19.985	1.017	195.6	-25150.4	781.1	87	-	-	-	24.5	24.5
40	19.985	1.013	143.0	-26264.5	412.4	88	-	-	-	0.2	0.2
41	19.985	1.013	143.0	-26264.5	412.4	89	-	-	-	8290.7	8290.7
42	2.417	4.260	31.5	-38300.0	1.6	90	-	-	-	1881.1	31.0
43	2.417	4.200	141.0	-37185.9	184.8	91	-	-	-	277.2	61.9
44	0.967	4.200	141.0	-14874.3	73.9	92	-	-	-	440.6	440.6
45	0.967	4.140	144.9	-12800.5	668.4	93	-	-	-	0.0	0.0
46	0.967	4.080	256.0	-12571.0	750.6	94	-	-	-	297.4	23.0
47	4.074	4.080	255.0	-52983.6	3159.7	95	-	-	-	979.6	227.1
48	-	-	-	2513.3	2513.3						

Table B.4. Properties of streams in the IPGCC plant processing mixed waste.

Stream	\dot{m} (kg/s)	P (bar)	T (°C)	\dot{H} (kW)	\dot{E} (kW)	Stream	\dot{m} (kg/s)	P (bar)	T (°C)	\dot{H} (kW)	\dot{E} (kW)
1	11.574	1.013	25.0	-119134.8	121619.74	49	16.889	0.046	31.4	-230085.6	794.37
2	3.472	1.013	25.0	-1.0	15.38	50	5.583	4.200	141.0	-85912.2	426.90
3	-	-	-	24065.9	24065.91	51	5.583	30.800	141.5	-85890.8	444.76
4	d.a	d.a	d.a	d.a	d.a	52	5.583	30.340	229.0	-83722.8	1200.07
5	0.541	1.013	1666.5	675.1	775.66	53	5.583	29.890	233.7	-73581.3	5374.97
6	d.a	d.a	d.a	d.a	d.a	54	5.583	29.440	312.0	-72326.4	5930.34
7	14.505	1.013	120.0	-100658.0	113877.90	55	12.422	29.440	312.8	-160893.7	13205.80
8	14.505	0.996	120.0	-100657.7	113847.36	56	12.422	29.000	510.0	-155298.0	16316.69
9	0.000	0.996	120.0	0.0	0.00	57	12.422	4.080	254.7	-161578.1	9631.87
10	1.323	1.013	25.0	-20930.1	225.11	58	-	-	-	6280.2	6280.17
11	8.867	0.946	30.0	-27257.9	108842.89	59	1.117	4.200	141.0	-17182.4	85.38
12	6.961	0.946	78.9	-108644.4	1579.51	60	6.839	4.200	141.0	-105231.7	522.90
13	8.867	21.785	454.9	-21680.5	114150.01	61	6.839	125.560	143.3	-105112.1	621.52
14	-	-	-	5577.3	5577.31	62	6.839	123.680	322.0	-99217.5	3040.50
15	8.867	21.567	190.0	-25287.8	112362.65	63	6.839	121.830	325.8	-90928.4	7202.05
16	8.867	20.057	190.0	-25287.8	112288.50	64	6.839	121.830	325.8	-90928.4	7202.05
17	8.867	19.856	40.4	-27925.9	111745.60	65	6.839	120.000	507.0	-86259.0	9781.73
18	0.325	1.500	109.3	-4010.4	1242.85	66	6.839	29.440	313.4	-88567.3	7275.47
19	0.039	1.500	31.3	-149.7	1125.82	67	-	-	-	2308.3	2308.32
20	8.503	19.856	42.3	-22950.3	109664.21	68	888.889	1.013	15.0	-	637.76
21	8.503	19.657	335.8	-19348.3	110863.75	69	888.889	10.000	15.1	-	1475.11
22	81.972	1.013	25.0	-23.1	363.14	70	888.889	10.000	25.3	-	856.94
23	81.972	19.657	456.6	36960.5	35533.75	71	16.889	0.046	31.4	-267671.8	1.74
24	-	-	-	36983.7	36983.65	72	16.889	4.260	31.5	-267660.0	11.09
25	32.109	19.657	456.6	14477.5	13918.61	73	16.889	4.260	31.5	-267660.0	11.09
26	49.864	19.657	456.6	22483.0	21615.14	74	5.722	4.260	31.5	-90687.4	3.76
27	40.612	19.067	2383.3	-4870.8	103321.54	75	5.722	4.200	141.0	-88049.3	437.52
28	90.475	19.067	1418	17612.2	117666.03	76	d.a	d.a	d.a	d.a	d.a
29	-	-	-	46344.9	46344.92	77	d.a	d.a	d.a	d.a	d.a
30	90.475	1.050	672.6	-65716.4	31276.54	78	d.a	d.a	d.a	d.a	d.a
31	90.475	1.046	620.4	-71312.1	27468.31	79	d.a	d.a	d.a	d.a	d.a
32	90.475	1.043	576.5	-75981.5	24369.33	80	d.a	d.a	d.a	d.a	d.a
33	90.475	1.039	497.4	-84270.5	19105.84	81	d.a	d.a	d.a	d.a	d.a
34	90.475	1.035	440.2	-90165.2	15553.66	82	-	-	-	1310.6	1310.57
35	90.475	1.032	427.9	-91420.0	14800.41	83	-	-	-	11.7	11.72
36	90.475	1.028	417.5	-92480.4	14166.84	84	d.a	d.a	d.a	d.a	d.a
37	90.475	1.024	316.6	-102622.0	8729.15	85	d.a	d.a	d.a	d.a	d.a
38	90.475	1.021	294.7	-104789.9	7650.41	86	-	-	-	21.4	21.41
39	90.475	1.017	196.4	-114372.4	3562.94	87	-	-	-	119.6	119.63
40	90.475	1.013	142.7	-119520.5	1857.79	88	-	-	-	1.1	1.13
41	90.475	1.013	142.7	-119520.5	1857.79	89	-	-	-	32939.2	32939.18
42	11.167	4.260	31.5	-176972.5	7.33	90	-	-	-	14314.5	236.10
43	11.167	4.200	141.0	-171824.3	853.81	91	-	-	-	1387.9	305.87
44	4.467	4.200	141.0	-68729.7	341.52	92	-	-	-	2202.3	2202.33
45	4.467	4.140	144.9	-59147.3	3088.68	93	-	-	-	0.0	0.00
46	4.467	4.080	256.0	-58086.9	3468.50	94	-	-	-	1307.1	101.12
47	16.889	4.080	255.0	-219665.1	13100.37	95	-	-	-	4913.0	1139.18
48	-	-	-	10420.5	10420.53						

Note: since in Mixed plant the temperature of the syngas coming from the gasifier is low (< 250°C), the SCS is not required. Thus, some changes are made in the physical and productive structure, such as: the stream 7 comes from the gasifier and streams 4 and 6 are deleted, streams from 76 to 81 are deleted, as well as streams 84 and 85. In this table, the properties of such streams are shown as "d.a" (does not apply).

Table B.5. Properties of streams in the IPGCC plant processing residential waste.

Stream	\dot{m} (kg/s)	P (bar)	T (°C)	\dot{H} (kW)	\dot{E} (kW)	Stream	\dot{m} (kg/s)	P (bar)	T (°C)	\dot{H} (kW)	\dot{E} (kW)
1	11.574	1.013	25.0	-127806.8	102880.7	49	14.361	0.046	31.4	-195649.9	675.5
2	5.787	1.013	25.0	-1.6	25.6	50	3.639	4.200	141.0	-55992.5	278.2
3	-	-	-	24135.7	24135.7	51	3.639	30.800	141.5	-55978.6	289.9
4	d.a	d.a	d.a	d.a	d.a	52	3.639	30.340	229.0	-54565.6	782.1
5	0.493	1.013	1286.8	311.5	454.7	53	3.639	29.890	233.7	-47955.9	3503.1
6	d.a	d.a	d.a	d.a	d.a	54	3.639	29.440	312.0	-47138.1	3865.0
7	16.868	1.013	109.3	-108896.6	93843.8	55	11.450	29.440	312.9	-148296.2	12174.
8	16.868	0.996	109.3	-108896.3	93807.0	56	11.450	29.000	510.0	-143143.6	15039.
9	0.000	0.996	109.3	0.0	0.0	57	11.450	4.080	254.7	-148932.3	8878.0
10	1.538	1.013	25.0	-24340.6	261.8	58	-	-	-	5788.7	5788.7
11	10.565	0.946	30.1	-26649.9	88472.3	59	0.728	4.200	141.0	-11198.5	55.6
12	7.842	0.946	77.1	-122462.0	1671.2	60	7.811	4.200	141.0	-120191.5	597.2
13	10.565	21.785	500.8	-19294.3	95492.1	61	7.811	125.560	143.3	-120054.9	709.9
14	-	-	-	7355.5	7355.5	62	7.811	123.680	322.0	-113322.3	3472.7
15	10.565	21.567	190.0	-24240.3	92963.6	63	7.811	121.830	325.8	-103854.9	8225.9
16	10.565	20.057	190.0	-24240.3	92869.9	64	7.811	121.830	325.8	-103854.9	8225.9
17	10.565	19.856	40.2	-27505.9	92202.5	65	7.811	120.000	507.0	-98521.7	11172.
18	0.402	1.500	110.7	-5183.1	757.1	66	7.811	29.440	313.4	-101158.1	8309.8
19	0.020	1.500	34.8	-53.5	227.4	67	-	-	-	2636.5	2636.5
20	10.143	19.856	39.4	-21252.7	91649.5	68	750.000	1.013	15.0	-11938160.1	538.1
21	10.143	19.657	374.7	-16312.0	93385.2	69	750.000	10.000	15.1	-11937054.3	1244.6
22	66.842	1.013	25.0	-18.9	296.1	70	750.000	10.000	25.3	-11905095.2	723.0
23	66.842	19.657	456.6	30138.3	28974.9	71	14.361	0.046	31.4	-227609.0	1.5
24	-	-	-	30157.2	30157.2	72	14.361	4.260	31.5	-227599.1	9.4
25	24.254	19.657	456.6	10936.1	10513.9	73	14.361	4.260	31.5	-227599.1	9.4
26	42.587	19.657	456.6	19202.2	18460.9	74	7.083	4.260	31.5	-112258.7	4.7
27	34.398	19.067	2387.9	-5375.9	87948.0	75	7.083	4.200	141.0	-108993.0	541.6
28	76.985	19.067	1418	13826.3	100186.3	76	d.a	d.a	d.a	d.a	d.a
29	-	-	-	40770.2	40770.2	77	d.a	d.a	d.a	d.a	d.a
30	76.985	1.050	672.9	-57101.1	26654.4	78	d.a	d.a	d.a	d.a	d.a
31	76.985	1.046	616.5	-62253.7	23153.0	79	d.a	d.a	d.a	d.a	d.a
32	76.985	1.043	557.4	-67586.9	19646.2	80	d.a	d.a	d.a	d.a	d.a
33	76.985	1.039	450.4	-77054.3	13792.9	81	d.a	d.a	d.a	d.a	d.a
34	76.985	1.035	372.6	-83786.9	9971.6	82	-	-	-	1105.8	1105.8
35	76.985	1.032	363.0	-84604.8	9510.9	83	-	-	-	10.0	10.0
36	76.985	1.028	354.9	-85295.9	9122.3	84	d.a	d.a	d.a	d.a	d.a
37	76.985	1.024	276.7	-91905.5	5839.5	85	d.a	d.a	d.a	d.a	d.a
38	76.985	1.021	259.7	-93318.5	5181.1	86	-	-	-	14.0	14.0
39	76.985	1.017	184.1	-99563.8	2679.7	87	-	-	-	136.6	136.6
40	76.985	1.013	142.9	-102923.6	1591.7	88	-	-	-	1.0	1.0
41	76.985	1.013	142.9	-102923.6	1591.7	89	-	-	-	24135.7	24135.
42	7.278	4.260	31.5	-115340.3	4.8	90	-	-	-	15875.0	261.8
43	7.278	4.200	141.0	-111985.0	556.5	91	-	-	-	1712.0	382.4
44	2.911	4.200	141.0	-44794.0	222.6	92	-	-	-	2731.1	2731.1
45	2.911	4.140	144.9	-38548.7	2013.0	93	-	-	-	3.3	0.1
46	2.911	4.080	256.0	-37857.6	2260.6	94	-	-	-	1161.1	89.8
47	14.361	4.080	255.0	-186789.9	11139.6	95	-	-	-	4912.4	1139.0
48	-	-	-	8860.0	8860.0						

Note: since in Residential plant the temperature of the syngas coming from the gasifier is low (< 250°C), the SCS is not required. Thus, some changes are made in the physical and productive structure, such as: the stream 7 comes from the gasifier and streams 4 and 6 are deleted, streams from 76 to 81 are deleted, as well as streams 84 and 85. In this table, the properties of such streams are shown as "d.a" (does not apply).

Appendix C. Rate of exergy destruction, exergy cost and unit exergy cost in the IPGCC power plants.

Here, the rates of exergy destruction in each component of the five cases are presented in Figure C.1. In addition, the exergy and unit exergy costs of each stream are presented from Table C.1 to Table C.5.

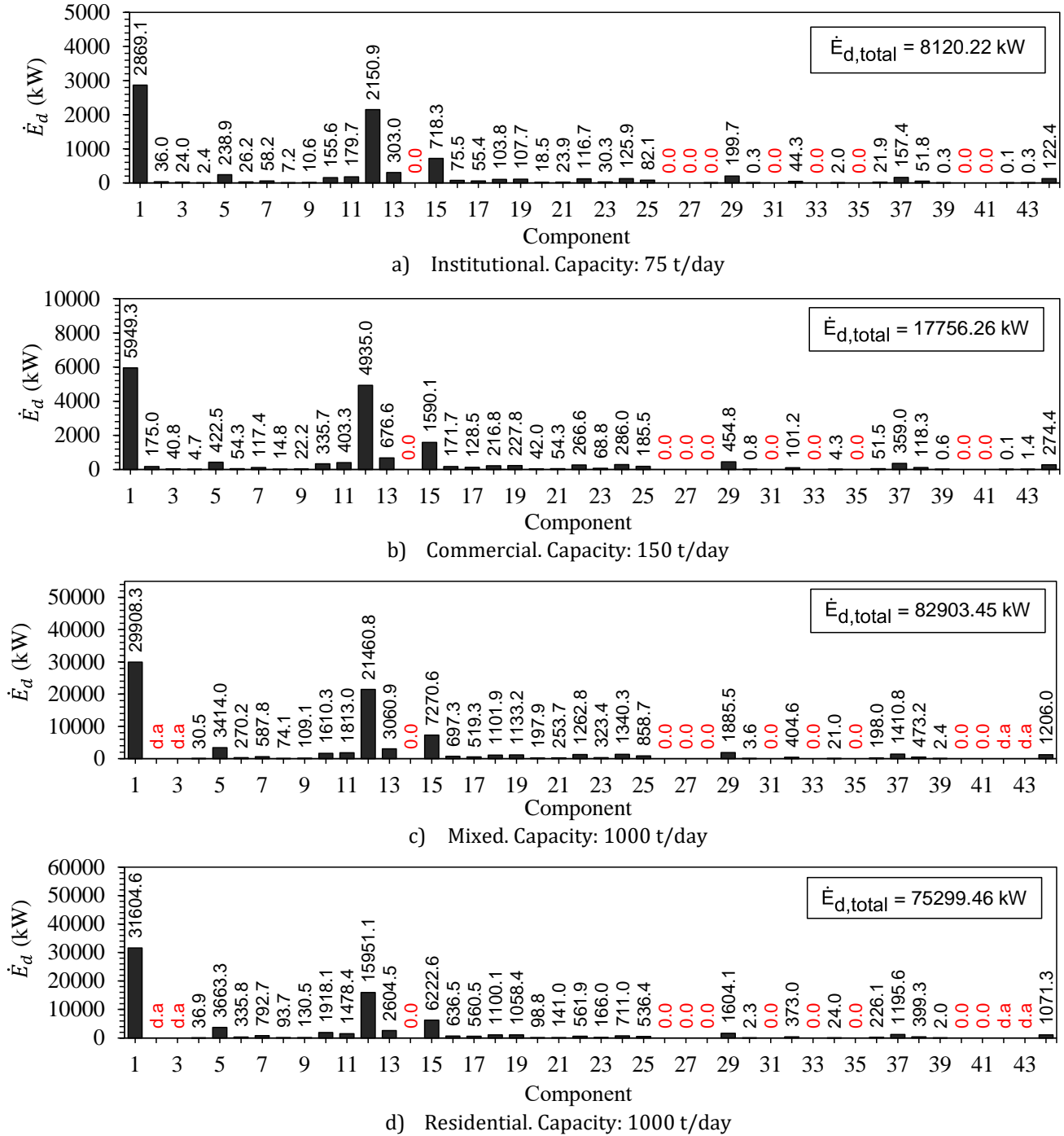


Table C.1. Exergy cost and unit exergy cost of streams in the IPGCC plant processing industrial wastes.

Stream	\dot{C} (kW)	c (kW/kW)	Stream	\dot{C} (kW)	c (kW/kW)
1	19668.2	1.00	49	438.3	3.06
2	2.6	1.00	50	287.8	4.71
3	10167.6	2.80	51	296.4	4.65
4	29420.9	1.58	52	650.9	3.79
5	148.0	1.58	53	2431.4	3.16
6	28347.4	1.58	54	2679.2	3.15
7	28130.8	1.58	55	7504.3	2.92
8	28130.8	1.58	56	9241.1	2.91
9	0.0	1.58	57	5455.1	2.91
10	25.9	1.00	58	3786.0	3.10
11	27939.0	1.60	59	63.2	4.71
12	188.2	1.60	60	209.2	2.51
13	30417.0	1.66	61	262.7	2.65
14	2478.0	2.80	62	1563.7	3.22
15	29945.3	1.66	63	3503.4	3.05
16	29945.3	1.66	64	4596.9	2.88
17	29801.4	1.66	65	6194.4	2.85
18	362.4	1.67	66	4607.3	2.85
19	336.8	1.67	67	1587.1	3.10
20	29379.4	1.67	68	129.5	1.00
21	29851.1	1.68	69	874.5	2.92
22	58.1	1.00	70	1311.8	7.97
23	14521.0	2.55	71	1.0	3.06
24	14462.9	2.44	72	6.9	3.44
25	5753.0	2.55	73	5.7	3.44
26	8767.9	2.55	74	2.1	3.44
27	35604.1	2.15	75	146.0	2.08
28	44372.0	2.36	76	0.2	3.44
29	18121.7	2.44	77	1.2	3.59
30	11787.4	2.36	78	217.7	2.11
31	10050.6	2.36	79	1.0	3.44
32	8453.1	2.36	80	20.0	3.67
33	6513.4	2.36	81	1093.5	2.44
34	5212.4	2.36	82	744.9	2.80
35	4964.6	2.36	83	5.9	2.80
36	4757.2	2.36	84	19.0	2.80
37	2976.8	2.36	85	0.9	2.80
38	2622.2	2.36	86	8.6	2.80
39	1284.9	2.36	87	53.5	2.80
40	708.8	2.36	88	0.5	2.80
41	708.8	2.36	89	16758.3	2.80
42	3.6	3.44	90	29.5	1.60
43	579.7	4.71	91	83.3	1.67
44	228.7	4.71	92	360.1	1.00
45	1566.0	3.56	93	0.0	0.00
46	1773.4	3.59	94	47.7	2.80
47	7228.5	3.06	95	269.4	1.58
48	6790.1	3.61			

Table C.2. Exergy cost and unit exergy cost of streams in the IPGCC plant processing commercial wastes.

Stream	\dot{C} (kW)	c (kW/kW)	Stream	\dot{C} (kW)	c (kW/kW)
1	27127.6	1.00	49	598.9	3.13
2	3.1	1.00	50	436.3	4.72
3	13502.7	2.81	51	449.3	4.67
4	40031.0	1.56	52	995.6	3.83
5	247.2	1.56	53	3747.6	3.22
6	39147.7	1.56	54	4129.2	3.22
7	38883.9	1.56	55	9854.3	2.98
8	38883.9	1.56	56	12087.7	2.96
9	0.0	1.56	57	7135.5	2.96
10	36.2	1.00	58	4952.3	3.15
11	38570.3	1.59	59	87.3	4.72
12	300.5	1.59	60	271.4	2.53
13	41665.4	1.65	61	340.2	2.67
14	3095.1	2.81	62	2042.9	3.28
15	41094.9	1.65	63	4560.3	3.09
16	41094.9	1.65	64	5461.3	2.92
17	40913.4	1.65	65	7340.7	2.89
18	366.2	1.66	66	5459.9	2.89
19	457.8	1.66	67	1880.8	3.13
20	40427.8	1.66	68	159.4	1.00
21	40998.3	1.67	69	1078.6	2.92
22	80.8	1.00	70	1676.2	8.34
23	20141.6	2.55	71	1.3	3.13
24	20060.8	2.44	72	9.2	3.46
25	8061.5	2.55	73	8.1	3.46
26	12080.0	2.55	74	2.6	3.46
27	49059.8	2.15	75	184.1	2.07
28	61139.8	2.35	76	0.3	3.46
29	24837.3	2.44	77	1.4	3.60
30	16241.7	2.35	78	265.3	2.07
31	14008.3	2.35	79	0.9	3.46
32	12128.9	2.35	80	17.7	3.68
33	9611.5	2.35	81	901.0	2.28
34	7908.8	2.35	82	919.1	2.81
35	7527.2	2.35	83	7.9	2.81
36	7206.2	2.35	84	16.8	2.81
37	4454.2	2.35	85	1.2	2.81
38	3907.9	2.35	86	13.0	2.81
39	1836.9	2.35	87	68.8	2.81
40	969.9	2.35	88	0.5	2.81
41	969.9	2.35	89	23258.3	2.81
42	5.5	3.46	90	49.3	1.59
43	872.5	4.72	91	102.7	1.66
44	349.0	4.72	92	440.6	1.00
45	2420.0	3.62	93	0.0	0.00
46	2741.0	3.65	94	64.5	2.81
47	9876.5	3.13	95	355.1	1.56
48	9277.5	3.69			

Table C.3. Exergy cost and unit exergy cost of streams in the IPGCC plant processing institutional wastes.

Stream	\dot{C} (kW)	c (kW/kW)	Stream	\dot{C} (kW)	c (kW/kW)
1	12082.2	1.00	49	276.5	3.29
2	1.5	1.00	50	202.6	4.94
3	6741.2	2.94	51	208.6	4.89
4	18540.3	1.64	52	462.0	4.01
5	108.1	1.64	53	1737.8	3.37
6	18330.2	1.64	54	1914.8	3.36
7	18172.0	1.64	55	4545.3	3.14
8	18172.0	1.64	56	5570.8	3.12
9	0.0	1.64	57	3288.5	3.12
10	18.2	1.00	58	2282.3	3.32
11	17982.0	1.67	59	40.5	4.94
12	179.4	1.67	60	133.8	2.63
13	19572.6	1.74	61	168.1	2.78
14	1590.6	2.94	62	1014.4	3.42
15	19271.3	1.74	63	2269.6	3.23
16	19271.3	1.74	64	2484.1	3.12
17	19179.4	1.74	65	3322.9	3.08
18	153.6	1.75	66	2471.5	3.08
19	167.1	1.75	67	851.4	3.34
20	19018.9	1.75	68	69.8	1.00
21	19320.1	1.76	69	491.1	3.04
22	36.0	1.00	70	767.0	8.72
23	9403.1	2.67	71	0.6	3.29
24	9367.1	2.56	72	4.3	3.62
25	3696.6	2.67	73	3.9	3.62
26	5706.4	2.67	74	1.3	3.62
27	23016.7	2.25	75	93.3	2.18
28	28723.2	2.46	76	0.2	3.62
29	11718.9	2.56	77	0.9	3.78
30	7637.2	2.46	78	159.0	2.18
31	6611.7	2.46	79	0.2	3.62
32	5772.8	2.46	80	4.4	3.86
33	4517.6	2.46	81	214.5	2.29
34	3671.3	2.46	82	421.4	2.94
35	3494.3	2.46	83	3.6	2.94
36	3345.4	2.46	84	4.2	2.94
37	2069.6	2.46	85	0.7	2.94
38	1816.3	2.46	86	6.0	2.94
39	855.9	2.46	87	34.3	2.94
40	453.3	2.46	88	0.2	2.94
41	453.3	2.46	89	10303.7	2.94
42	2.6	3.62	90	28.7	1.67
43	405.2	4.94	91	51.6	1.75
44	162.1	4.94	92	211.6	1.00
45	1122.4	3.78	93	0.0	0.00
46	1271.3	3.82	94	30.2	2.94
47	4559.9	3.29	95	176.6	1.64
48	4283.3	3.88			

Table C4. Exergy cost and unit exergy cost of streams in the IPGCC plant processing mixed wastes.

Stream	\dot{C} (kW)	c (kW/kW)	Stream	\dot{C} (kW)	c (kW/kW)
1	121619.7	1.00	49	2798.9	3.52
2	15.4	1.00	50	2199.2	5.15
3	73986.2	3.07	51	2265.0	5.09
4	d.a	d.a	52	5029.9	4.19
5	1310.4	1.69	53	18967.1	3.53
6	d.a	d.a	54	20897.7	3.52
7	192386.4	1.69	55	44954.0	3.40
8	192386.4	1.69	56	54714.7	3.35
9	0.0	1.69	57	32298.5	3.35
10	225.1	1.00	58	22416.2	3.57
11	189451.2	1.74	59	439.8	5.15
12	2749.3	1.74	60	1437.4	2.75
13	206597.6	1.81	61	1805.1	2.90
14	17146.4	3.07	62	10909.6	3.59
15	203362.7	1.81	63	24400.3	3.39
16	203362.7	1.81	64	24400.3	3.39
17	202379.5	1.81	65	32343.2	3.31
18	2263.4	1.82	66	24056.3	3.31
19	2050.3	1.82	67	8287.0	3.59
20	199714.6	1.82	68	637.8	1.00
21	202949.5	1.83	69	4666.9	3.16
22	363.1	1.00	70	7459.6	8.70
23	98636.8	2.78	71	6.1	3.52
24	98273.7	2.66	72	42.2	3.80
25	38636.2	2.78	73	42.2	3.80
26	60000.7	2.78	74	14.3	3.80
27	241585.7	2.34	75	997.5	2.28
28	301586.3	2.56	76	d.a	d.a
29	123148.7	2.66	77	d.a	d.a
30	80164.0	2.56	78	d.a	d.a
31	70403.2	2.56	79	d.a	d.a
32	62460.3	2.56	80	d.a	d.a
33	48969.6	2.56	81	d.a	d.a
34	39865.1	2.56	82	4029.1	3.07
35	37934.5	2.56	83	36.0	3.07
36	36310.6	2.56	84	d.a	d.a
37	22373.4	2.56	85	d.a	d.a
38	19608.5	2.56	86	65.8	3.07
39	9132.1	2.56	87	367.8	3.07
40	4761.7	2.56	88	3.5	3.07
41	4761.7	2.56	89	101265.4	3.07
42	27.9	3.80	90	410.9	1.74
43	4398.3	5.15	91	557.0	1.82
44	1759.3	5.15	92	2202.3	1.00
45	12235.8	3.96	93	0.0	0.00
46	13859.7	4.00	94	310.9	3.07
47	46158.2	3.52	95	1924.5	1.69
48	43359.3	4.16			

Note: Since in Mixed plant the temperature of the syngas coming from the gasifier is low (< 250°C), the SCS is not required. Thus, some changes are made in the physical and productive structure, such as: the stream 7 comes from the gasifier and streams 4 and 6 are deleted, streams from 76 to 81 are deleted, as well as streams 84 and 85. In this table, the properties of such streams are shown as “d.a” (does not apply).

Table C.5. Exergy cost and unit exergy cost of streams in the IPGCC plant processing residential wastes.

Stream	\dot{C} (kW)	c (kW/kW)	Stream	\dot{C} (kW)	c (kW/kW)
1	102880.7	1.00	49	2607.2	3.86
2	25.6	1.00	50	1629.2	5.86
3	84613.1	3.51	51	1678.1	5.79
4	d.a	d.a	52	3637.2	4.65
5	893.3	1.96	53	13406.5	3.83
6	d.a	d.a	54	14777.6	3.82
7	184388.1	1.96	55	45641.3	3.75
8	184388.1	1.97	56	56060.8	3.73
9	0.0	1.97	57	33093.2	3.73
10	261.8	1.00	58	22967.7	3.97
11	180701.7	2.04	59	325.8	5.86
12	3413.5	2.04	60	1790.6	3.00
13	206488.1	2.16	61	2269.6	3.20
14	25786.5	3.51	62	13641.3	3.93
15	201020.8	2.16	63	31059.7	3.78
16	201020.8	2.16	64	31059.7	3.78
17	199576.0	2.16	65	41495.6	3.71
18	1646.8	2.17	66	30863.6	3.71
19	494.7	2.17	67	10632.0	4.03
20	199337.4	2.17	68	538.1	1.00
21	204804.8	2.19	69	4414.7	3.55
22	296.1	1.00	70	7016.2	9.70
23	93334.7	3.22	71	5.7	3.86
24	93038.6	3.09	72	40.7	4.31
25	33867.8	3.22	73	40.7	4.31
26	59466.9	3.22	74	20.1	4.31
27	238672.6	2.71	75	1464.8	2.70
28	298139.5	2.98	76	d.a	d.a
29	125781.3	3.09	77	d.a	d.a
30	79319.6	2.98	78	d.a	d.a
31	68900.0	2.98	79	d.a	d.a
32	58464.1	2.98	80	d.a	d.a
33	41045.8	2.98	81	d.a	d.a
34	29674.1	2.98	82	3876.6	3.51
35	28303.0	2.98	83	34.9	3.51
36	27146.7	2.98	84	d.a	d.a
37	17377.4	2.98	85	d.a	d.a
38	15418.3	2.98	86	48.9	3.51
39	7974.5	2.98	87	479.0	3.51
40	4736.7	2.98	88	3.6	3.51
41	4736.7	2.98	89	84612.8	3.51
42	20.6	4.31	90	534.8	2.04
43	3258.4	5.86	91	831.6	2.17
44	1303.4	5.86	92	2731.1	1.00
45	8747.2	4.35	93	0.2	2.17
46	9903.4	4.38	94	314.9	3.51
47	42996.6	3.86	95	2238.0	1.96
48	40389.4	4.56			

Note: since in Residential plant the temperature of the syngas coming from the gasifier is low (< 250°C), the SCS is not required. Thus, some changes are made in the physical and productive structure, such as: the stream 7 comes from the gasifier and streams 4 and 6 are deleted, streams from 76 to 81 are deleted, as well as streams 84 and 85. In this table, the properties of such streams are shown as “d.a” (does not apply).

Appendix D. Cost equations and results from exergoeconomic analysis.

In this appendix the cost equations used for PEC estimations are presented in Table D.1, meanwhile, Table D.2 contains the PEC and non-thermodynamic costs estimated for each component of the five plant cases. Finally, in Table D.3 the exergoeconomic cost of irreversibilities, the exergoeconomic factor, and the relative cost difference of each component are presented.

Table D.1. Cost equations used for PEC estimation.

Component		Cost equation	Parameter	Unit	Source			
Syngas cooler	2, 3	$1066(A_h)^{0.075}$	A_h (m ²) < 9	2009 US\$	[116]			
Compressor	6, 11	$91562 \left(\frac{\dot{W}_{comp}}{445} \right)^{0.67}$	\dot{W}_{comp} (kW)	2008 US\$	[153]			
Syngas preheater	7	$2290(A_h)^{0.6}$	A_h (m ²)	1994 US\$	[154]			
LTGC	9	$1632(A_h)^{0.6375}$	$9 < A_h$ (m ²) < 500	2009 US\$	[116]			
Combustion chamber	12	$\left(\frac{48.64\dot{m}_{air}}{0.995 - \frac{P_{out}}{P_{in}}} \right) (1 + e^{(0.018T_{out}-26.4)})$	\dot{m}_{air} (kg/s)	2003 US\$	[141]			
			T_{out} (°C)					
Gas turbine	13	$(-98.328 \ln(\dot{W}_{GT}) + 1318.5)\dot{W}_{GT}$	\dot{W}_{GT} (kW)	2008 US\$	[153]			
HRSG components	16 – 25	$1000 \left[a \left(\frac{\dot{Q}}{\Delta T_{ml}} \right)^{0.8} + b\dot{m}_s + c\dot{m}_g^{1.2} \right]$	\dot{Q} (kW)	1999 US\$	[155]			
			<i>Subcomponent</i>			<i>a</i>	<i>b</i>	<i>c</i>
			Evaporator			6.5	21.276	1.184
		Economizer, Superheater, and Reheater	13	21.276	1.184			
Steam turbine	29, 32, 36	$6000(\dot{W}_{ST})^{0.7}$	\dot{W}_{ST} (kW)	2003 US\$	[141]			
Water pump	30, 34, 38, 39, 42, 43	$705.48(\dot{W}_P)^{0.71} \left(1 + \frac{0.2}{1 - \eta_P} \right)$	\dot{W}_P (kW) $0.6 < \eta_P < 0.9$	2014 US\$	[116]			
Condenser	37	$3000 \left(\frac{\dot{Q}_{cond}}{10} \right)^{0.55}$	\dot{Q}_{cond} (kW)	1987 US\$	[156]			
Electric generator	44	$60(\dot{W}_{elec.})^{0.95}$	$\dot{W}_{elec.}$ (kW)	2003 US\$	[141]			

Table D.2. Purchased equipment and non-thermodynamic costs for each component of the IPGCC power plants.

Component	PEC _k (US\$)					Z _k (US\$/h)				
	Inst.	Ind.	Com.	Mix.	Res.	Inst.	Ind.	Com.	Mix.	Res.
1 Plasma gasifier	19,043,559	25,181,566	34,624,653	164,414,639	164,414,639	436.7	577.5	794.1	3,770.6	3,770.6
2 HP syngas cooler	1,259	1,363	1,377	d.a	d.a	0.0	0.0	0.0	d.a	d.a
3 IP syngas cooler	1,339	1,373	1,407	d.a	d.a	0.0	0.0	0.0	d.a	d.a
4 Fabric filter	88,265	119,730	161,578	561,379	659,030	2.0	2.7	3.7	12.9	15.1
5 Wet scrubber	451,300	463,600	522,300	900,800	1,009,100	10.3	10.6	12.0	20.7	23.1
6 Syngas compressor	110,204	153,293	177,618	526,011	633,173	2.5	3.5	4.1	12.1	14.5
7 Syngas preheater	7,391	10,048	11,337	30,198	35,679	0.2	0.2	0.3	0.7	0.8
8 COS-hydrolysis unit	0	0	0	0	0	0.0	0.0	0.0	0.0	0.0
9 LTGC	17,730	24,695	27,578	76,418	93,422	0.4	0.6	0.6	1.8	2.1
10 MDEA absorber/stripper	688,400	699,000	716,900	881,300	904,000	15.8	16.0	16.4	20.2	20.7
11 Air compressor	397,474	547,704	683,206	1,870,181	1,631,206	9.1	12.6	15.7	42.9	37.4
12 Combustion chamber	33,817	54,570	75,901	341,180	278,206	0.8	1.3	1.7	7.8	6.4
13 Gas turbine	2,370,252	2,900,776	4,420,790	12,823,529	11,823,464	54.4	66.5	101.4	294.1	271.2
14 Compressed air splitter	0	0	0	0	0	0.0	0.0	0.0	0.0	0.0
15 CC gas-cooling air mixer	0	0	0	0	0	0.0	0.0	0.0	0.0	0.0
16 IP Reheater	115,522	197,264	257,264	1,083,403	963,553	2.6	4.5	5.9	24.8	22.1
17 HP Superheater	100,754	188,506	226,891	918,735	925,807	2.3	4.3	5.2	21.1	21.2
18 HP Evaporator	78,400	131,190	169,745	827,261	842,689	1.8	3.0	3.9	19.0	19.3
19 HP Economizer	90,940	151,251	191,696	906,582	972,985	2.1	3.5	4.4	20.8	22.3
20 IP Superheater	60,257	98,250	138,912	700,553	575,845	1.4	2.3	3.2	16.1	13.2
21 LP Superheater	51,106	83,300	120,452	629,587	501,894	1.2	1.9	2.8	14.4	11.5
22 IP Evaporator	96,094	153,061	206,643	925,310	807,951	2.2	3.5	4.7	21.2	18.5
23 IP Economizer	76,416	121,889	169,602	803,449	664,232	1.8	2.8	3.9	18.4	15.2
24 LP Evaporator	103,432	158,744	219,885	963,607	788,589	2.4	3.6	5.0	22.1	18.1
25 Feedwater preheater	148,525	222,282	313,828	1,344,885	1,016,212	3.4	5.1	7.2	30.8	23.3
26 Exhaust stack	0	0	0	0	0	0.0	0.0	0.0	0.0	0.0
27 Preheated feedwater splitter	0	0	0	0	0	0.0	0.0	0.0	0.0	0.0
28 LP steam mixer	0	0	0	0	0	0.0	0.0	0.0	0.0	0.0
29 LP steam turbine	1,223,124	1,776,876	2,175,938	5,888,359	5,256,254	28.1	40.8	49.9	135.0	120.5
30 IP water pump	2,234	2,969	3,979	11,795	8,704	0.1	0.1	0.1	0.3	0.2
31 IP steam mixer	0	0	0	0	0	0.0	0.0	0.0	0.0	0.0
32 IP steam turbine	878,192	1,312,454	1,565,833	4,130,965	3,901,898	20.1	30.1	35.9	94.7	89.5
33 HP water mixer	0	0	0	0	0	0.0	0.0	0.0	0.0	0.0
34 HP water pump	7,661	10,881	12,996	40,020	43,981	0.2	0.2	0.3	0.9	1.0

Continued in the next page...

Table D.2. Purchased equipment and non-thermodynamic costs for each component of the IPGCC power plants.

Component	PEC _k (US\$)					\dot{Z}_k (US\$/h)				
	Inst.	Ind.	Com.	Mix.	Res.	Inst.	Ind.	Com.	Mix.	Res.
35 HP steam mixer	0	0	0	0	0	0.0	0.0	0.0	0.0	0.0
36 HP steam turbine	438,493	714,580	798,367	2,050,116	2,250,025	10.1	16.4	18.3	47.0	51.6
37 Condenser	151,493	203,156	238,210	520,782	476,341	3.5	4.7	5.5	11.9	10.9
38 Cooling water pump	38,242	59,351	68,778	184,040	163,127	0.9	1.4	1.6	4.2	3.7
39 Feedwater pump	1,313	1,918	2,355	6,464	5,761	0.0	0.0	0.1	0.1	0.1
40 Feedwater splitter	0	0	0	0	0	0.0	0.0	0.0	0.0	0.0
41 LP water splitter	0	0	0	0	0	0.0	0.0	0.0	0.0	0.0
42 IP-SCS water pump	480	615	717	d.a	d.a	0.0	0.0	0.0	d.a	d.a
43 HP-SCS water pump	1,720	5,224	4,780	d.a	d.a	0.0	0.1	0.1	d.a	d.a
44 Electric generator	379,961	615,819	818,169	3,339,222	2,983,902	8.7	14.1	18.8	76.6	68.4
Total	27,255,351	36,367,298	49,129,683	207,700,772	204,631,669	625	834	1,127	4,763	4,693

Note: In Mixed and Residential plant, the SCS and the respective pumps are not required. These components are labelled as d.a (does not apply).

Table D.3. Exergoeconomic cost of irreversibilities (\dot{C}_D^z , US\$/h), exergoeconomic factor (f_k , %), and relative cost difference (r_k , -) of every component in each plant case.

Component	Institutional			Industrial			Commercial			Mixed			Residential		
	\dot{C}_D^z	f_k	r_k	\dot{C}_D^z	f_k	r_k	\dot{C}_D^z	f_k	r_k	\dot{C}_D^z	f_k	r_k	\dot{C}_D^z	f_k	r_k
1 Plasma gasifier	59.32	88.04	2.08	68.78	89.36	2.18	86.39	90.19	2.33	452.52	89.28	2.41	759.96	83.23	1.97
2 HP syngas cooler	2.29	1.24	0.39	11.89	0.26	0.54	8.47	0.37	0.45	d.a	d.a	d.a	d.a	d.a	d.a
3 IP syngas cooler	1.53	1.96	0.34	1.71	1.80	0.34	1.98	1.61	0.32	d.a	d.a	d.a	d.a	d.a	d.a
4 Fabric filter	0.15	92.95	0.00	0.17	94.21	0.00	0.23	94.23	0.00	1.58	89.10	0.00	2.64	85.15	0.00
5 Wet scrubber	15.33	40.30	0.04	12.13	46.70	0.03	20.60	36.77	0.03	177.53	10.42	0.03	263.89	8.06	0.04
6 Syngas compressor	3.78	40.10	0.08	4.84	42.11	0.09	5.99	40.47	0.09	29.76	28.84	0.07	48.70	22.97	0.06
7 Syngas preheater	4.11	3.96	0.53	5.10	4.33	0.51	6.22	4.01	0.53	33.38	2.03	0.50	64.22	1.26	0.46
8 COS-hydrolysis unit	0.51	0.00	0.00	0.64	0.00	0.00	0.78	0.00	0.00	4.21	0.00	0.00	7.59	0.00	0.00
9 LTGC	0.75	35.28	0.38	0.94	37.55	0.40	1.18	34.99	0.39	6.20	22.04	0.32	10.58	16.84	0.29
10 MDEA absorber/stripper	10.85	59.28	0.03	14.39	52.70	0.03	17.59	48.32	0.03	90.28	18.29	0.02	152.04	12.00	0.02
11 Air compressor	20.90	30.37	0.07	26.09	32.50	0.08	35.55	30.59	0.07	161.35	21.00	0.07	179.10	17.28	0.06
12 Combustion chamber	168.18	0.46	0.21	210.45	0.59	0.21	288.87	0.60	0.22	1318.09	0.59	0.21	1378.61	0.46	0.18
13 Gas turbine	32.07	62.89	0.10	40.13	62.37	0.10	53.93	65.28	0.11	252.33	53.82	0.08	294.73	47.92	0.07
14 Compressed air splitter	0.00	0.00	0.00	0.00	0.00	0.00	0.00	0.00	0.00	0.00	0.00	0.00	0.00	0.00	0.00
15 CC gas-cooling air mixer	71.61	0.00	0.06	88.92	0.00	0.06	119.44	0.00	0.06	564.48	0.00	0.06	663.01	0.00	0.06
16 IP Reheater	7.99	24.89	0.30	10.83	29.47	0.31	13.69	30.12	0.32	57.49	30.18	0.32	72.03	23.48	0.29
17 HP Superheater	5.87	28.25	0.27	8.61	33.43	0.28	10.24	33.68	0.29	42.81	32.98	0.30	63.42	25.08	0.25

Continued in the next page...

Table D.3. Exergoeconomic cost of irreversibilities (\dot{C}_D^z , US\$/h), exergoeconomic factor (f_k , %), and relative cost difference (r_k , -) of every component in each plant case.

Component		Institutional			Industrial			Commercial			Mixed			Residential		
		\dot{C}_D^z	f_k	r_k	\dot{C}_D^z	f_k	r_k	\dot{C}_D^z	f_k	r_k	\dot{C}_D^z	f_k	r_k	\dot{C}_D^z	f_k	r_k
18	HP Evaporator	10.98	14.07	0.30	12.93	18.88	0.29	17.28	18.38	0.31	90.84	17.28	0.32	124.49	13.44	0.27
19	HP Economizer	11.39	15.47	0.54	13.55	20.39	0.54	18.16	19.49	0.57	93.42	18.20	0.57	119.78	15.70	0.45
20	IP Superheater	1.96	41.41	0.59	2.09	51.84	0.67	3.35	48.73	0.68	16.31	49.62	0.71	11.18	54.15	0.60
21	LP Superheater	2.53	31.63	0.96	2.78	40.76	1.06	4.33	38.97	1.08	20.92	40.84	1.13	15.96	41.90	0.98
22	IP Evaporator	12.36	15.13	0.34	12.86	21.45	0.33	21.25	18.23	0.36	104.10	16.93	0.36	63.59	22.56	0.27
23	IP Economizer	3.20	35.36	0.65	3.45	44.73	0.70	5.49	41.48	0.72	26.66	40.87	0.72	18.79	44.77	0.61
24	LP Evaporator	13.32	15.11	0.56	14.44	20.14	0.56	22.80	18.11	0.59	110.49	16.67	0.59	80.46	18.35	0.49
25	Feedwater preheater	8.69	28.17	1.41	10.01	33.74	1.51	14.78	32.74	1.51	70.79	30.35	1.46	60.70	27.74	1.35
26	Exhaust stack	0.00	0.00	0.00	0.00	0.00	0.00	0.00	0.00	0.00	0.00	0.00	0.00	0.00	0.00	0.00
27	Preheated feedwater splitter	0.00	0.00	0.00	0.00	0.00	0.00	0.00	0.00	0.00	0.00	0.00	0.00	0.00	0.00	0.00
28	LP steam mixer	0.00	0.00	0.00	0.00	0.00	0.00	0.00	0.00	0.00	0.00	0.00	0.00	0.00	0.00	0.00
29	LP steam turbine	30.08	48.26	0.35	39.10	51.03	0.37	52.30	48.83	0.35	233.17	36.67	0.29	252.34	32.33	0.27
30	IP water pump	0.05	51.01	0.41	0.06	54.23	0.43	0.08	51.83	0.41	0.39	40.87	0.34	0.34	37.27	0.32
31	IP steam mixer	0.00	0.00	0.00	0.00	0.00	0.00	0.00	0.00	0.00	0.00	0.00	0.00	0.00	0.00	0.00
32	IP steam turbine	6.28	76.23	0.27	8.51	77.96	0.29	10.91	76.69	0.28	47.28	66.71	0.19	56.16	61.44	0.17
33	HP water mixer	0.00	0.00	0.00	0.00	0.00	0.00	0.00	0.00	0.00	0.00	0.00	0.00	0.00	0.00	0.00
34	HP water pump	0.30	37.31	0.34	0.38	39.72	0.35	0.48	38.54	0.35	2.31	28.40	0.30	3.48	22.47	0.27
35	HP steam mixer	0.00	0.00	0.00	0.00	0.00	0.00	0.00	0.00	0.00	0.00	0.00	0.00	0.00	0.00	0.00
36	HP steam turbine	3.02	76.92	0.37	4.54	78.30	0.40	5.30	77.57	0.38	22.41	67.72	0.27	33.34	60.75	0.22
37	Condenser	23.70	12.78	0.46	31.95	12.73	0.36	41.29	11.68	0.42	174.47	6.41	0.44	188.08	5.49	0.43
38	Cooling water pump	7.46	10.52	0.63	10.85	11.15	0.64	13.04	10.79	0.63	52.11	7.49	0.61	57.91	6.07	0.60
39	Feedwater pump	0.04	45.32	0.47	0.05	47.57	0.49	0.06	46.05	0.47	0.26	36.14	0.40	0.29	31.05	0.37
40	Feedwater splitter	0.00	0.00	0.00	0.00	0.00	0.00	0.00	0.00	0.00	0.00	0.00	0.00	0.00	0.00	0.00
41	LP water splitter	0.00	0.00	0.00	0.00	0.00	0.00	0.00	0.00	0.00	0.00	0.00	0.00	0.00	0.00	0.00
42	IP-SCS water pump	0.01	58.53	0.72	0.01	61.98	0.78	0.01	61.03	0.76	d.a	d.a	d.a	d.a	d.a	d.a
43	HP-SCS water pump	0.05	44.46	0.57	0.18	39.39	0.52	0.16	40.82	0.53	d.a	d.a	d.a	d.a	d.a	d.a
44	Electric generator	17.16	33.68	0.03	22.28	38.80	0.03	29.35	39.00	0.03	128.95	37.26	0.03	151.25	31.15	0.03

Note: In Mixed and Residential plant, the SCS (components 2 and 3) and the respective pumps (components 42 and 43) are not required. These components are labelled as “d.a” (does not apply).

References

- [1] D. Hoornweg and P. Bhada-Tata, "What a waste: A global review of solid waste management," 2012.
- [2] L. Larochele, M. Turner, and M. LaGiglia, "Evaluation of NAMA opportunities in Colombia's solid waste sector," p. 162, 2012.
- [3] A. Kumar and S. R. Samadder, "An empirical model for prediction of household solid waste generation rate – A case study of Dhanbad, India," *Waste Manag.*, vol. 68, pp. 3–15, 2017.
- [4] O. K. M. Ouda, S. A. Raza, A. S. Nizami, M. Rehan, R. Al-Waked, and N. E. Korres, "Waste to energy potential: A case study of Saudi Arabia," *Renew. Sustain. Energy Rev.*, vol. 61, pp. 328–340, 2016.
- [5] A. Fazeli, F. Bakhtvar, L. Jahanshaloo, N. A. Che Sidik, and A. E. Bayat, "Malaysia's stand on municipal solid waste conversion to energy: A review," *Renew. Sustain. Energy Rev.*, vol. 58, pp. 1007–1016, 2016.
- [6] J. A. M. Sepúlveda, "Outlook of Municipal Solid Waste in Bogota (Colombia)," *Am. J. Eng. Appl. Sci.*, vol. 9, no. 3, pp. 477–483, 2016.
- [7] L. Lombardi, E. Carnevale, and A. Corti, "A review of technologies and performances of thermal treatment systems for energy recovery from waste," *Waste Manag.*, vol. 37, pp. 26–44, 2015.
- [8] N. AlQattan, M. Acheampong, F. M. Jaward, F. C. Ertem, N. Vijayakumar, and T. Bello, "Reviewing the potential of Waste-to-Energy (WTE) technologies for Sustainable Development Goal (SDG) numbers seven and eleven," *Renew. Energy Focus*, vol. 27, pp. 97–110, 2018.
- [9] Superintendencia de Servicios Públicos Domiciliarios, "Informe de Disposición Final de Residuos Sólidos – 2017," Bogotá D.C., Colombia, 2017.
- [10] Consejo Nacional de Política Económica y Social, "Documento Conpes 3874 : Política Nacional para la Gestión Integral de Residuos Sólidos," Bogotá Colombia, 2016.
- [11] K. M. Noguera and J. T. Olivero, "Los rellenos sanitarios en Latinoamérica: caso colombiano," *Rev. Acad. Colomb. Cienc.*, vol. 34, pp. 347–356, 2010.
- [12] A. Kumar and S. R. R. Samadder, "A review on technological options of waste to energy for effective management of municipal solid waste," *Waste Manag.*, vol. 69, pp. 407–422, 2017.
- [13] A. U. Zaman, "Comparative study of municipal solid waste treatment technologies using life cycle assessment method," *Int. J. Environ. Sci. Technol.*, vol. 7, no. 2, pp. 225–234, 2010.

- [14] J. M. González Díaz, "Una propuesta de localización óptima para un nuevo sitio de disposición final de residuos sólidos no peligrosos para Bogotá, D.C.," *Perspect. Geográfica*, vol. 20, no. 1, p. 155, 2017.
- [15] S. M. Gascón, L. M. Jiménez, and H. Pérez, "Óptima ubicación de un relleno sanitario para el Área Metropolitana del Valle de Aburrá empleando Sistemas de Información Geográfica," *Ing. USBmed*, vol. 6, no. 1, p. 38, 2016.
- [16] J. Zuo, Y. Yan, G. Chen, P. Yin, Y. Wang, and B. Yan, "Effectiveness of waste-to-energy approaches in China: from the perspective of greenhouse gas emission reduction," *J. Clean. Prod.*, vol. 163, pp. 99–105, 2015.
- [17] F. Cucchiella, I. D'Adamo, and M. Gastaldi, "Sustainable waste management: Waste to energy plant as an alternative to landfill," *Energy Convers. Manag.*, vol. 131, pp. 18–31, 2017.
- [18] S. Alzate-Arias, Á. Jaramillo-Duque, F. Villada, and B. Restrepo-Cuestas, "Assessment of government incentives for energy from waste in Colombia," *Sustain.*, vol. 10, no. 4, pp. 1–16, 2018.
- [19] N. D. Montiel-Bohórquez and J. F. Pérez, "Generación de Energía a partir de Residuos Sólidos Urbanos. Estrategias Termodinámicas para Optimizar el Desempeño de Centrales Térmicas," *Inf. tecnológica*, vol. 30, no. 1, pp. 273–284, 2019.
- [20] Unidad de Planeación Minero-energética (UPME), "Plan energético nacional de Colombia: Ideario energético 2050," 2015. .
- [21] Congreso de la República, "Ley 1715 de 2014: Por la cual se regula la integración de energías renovables no convencionales al Sistema Energético Nacional," May-2014. .
- [22] C. Ducharme, "Technical and economic analysis of Plasma-assisted Waste-to-Energy processes," Columbia University, 2010.
- [23] J. Malinauskaite *et al.*, "Municipal solid waste management and waste-to-energy in the context of a circular economy and energy recycling in Europe," *Energy*, vol. 141, pp. 2013–2044, 2017.
- [24] C. J. Sprenger, J. Agnew, and A. Harrison, "Pelletization of Refuse-Derived Fuel Fluff to Produce High Quality Feedstock," vol. 140, pp. 1–10, 2018.
- [25] T. V Ramachandra, H. A. Bharath, G. Kulkarni, and S. S. Han, "Municipal solid waste generation, composition and GHG emissions in Bangalore, India," *Renew. Sustain. Energy Rev.*, vol. 82, pp. 1122–1136, 2018.
- [26] H. D. Beyene, A. A. Werkneh, and T. G. Ambaye, "Current updates on waste to energy - WtE - technologies: A review," *Renew. Energy Focus*, vol. 24, pp. 1–11, 2018.

- [27] F. J. G. Ortiz, A. Kruse, F. Ramos, and P. Ollero, "Integral energy valorization of municipal solid waste reject fraction to biofuels," *Energy Convers. Manag.*, vol. 180, pp. 1167–1184, 2019.
- [28] R. Sarc and K. E. Lorber, "Production , quality and quality assurance of Refuse Derived Fuels (RDFs)," *Waste Manag.*, vol. 33, pp. 1825–1834, 2013.
- [29] L. Zhao *et al.*, "Characterization of Singapore RDF resources and analysis of their heating value," *Sustain. Environ. Res.*, vol. 26, no. 1, pp. 51–54, 2016.
- [30] M. Castaldi *et al.*, "Progress and prospects in the field of biomass and waste to energy and added-value materials," *Waste and Biomass Valorization*, vol. 8, no. 6, pp. 1875–1884, 2017.
- [31] A. C. Medina Jimenez, G. H. Nordi, M. C. Palacios Bereche, R. P. Bereche, A. G. Gallego, and S. A. Nebra, "Evaluation of two different alternatives of energy recovery from municipal solid waste in Brazil," *Waste Manag. Res.*, vol. 35, no. 11, pp. 1137–1148, 2017.
- [32] P. O. Kaplan, J. DeCarolis, and S. Thorneloe, "Is It Better To Burn or Bury Waste for Clean Electricity Generation?," *Environ. Sci. Technol.*, vol. 43, no. 6, pp. 1711–1717, Mar. 2009.
- [33] H. A. Arafat and K. Jijakli, "Modeling and comparative assessment of municipal solid waste gasification for energy production," *Waste Manag.*, vol. 33, no. 8, pp. 1704–1713, 2013.
- [34] U. Arena, "Process and technological aspects of municipal solid waste gasification. A review," *Waste Manag.*, vol. 32, no. 4, pp. 625–639, 2012.
- [35] J. D. Murphy and E. McKeogh, "Technical, economic and environmental analysis of energy production from municipal solid waste," *Renew. Energy*, vol. 29, no. 7, pp. 1043–1057, 2004.
- [36] F. C. Luz *et al.*, "Techno-economic analysis of municipal solid waste gasification for electricity generation in Brazil," *Energy Convers. Manag.*, vol. 103, pp. 321–337, 2015.
- [37] S. Thakare and S. Nandi, "Study on potential of gasification technology for municipal solid waste (MSW) in Pune City," *Energy Procedia*, vol. 90, pp. 509–517, 2015.
- [38] M. Hrabovsky, M. Konrad, V. Kopecky, M. Hlina, T. Kavka, and O. Chumak, "Plasma aided gasification of biomass and plastics using CO₂ as oxidizer," in *International symposium on non-thermal/thermal plasma pollution control technology and sustainable energy*, 2010.
- [39] A. Mountouris, E. Voutsas, and D. Tassios, "Solid waste plasma gasification : Equilibrium model development and exergy analysis," *Energy Convers. Manag.*, vol. 47, no. 13–14, pp. 1723–1737, 2006.
- [40] B. K. Verma, E. Rajeshkannan, T. Renganathan, and S. Pushpavanam, "A hybrid thermo-kinetic model for high temperature plasma gasification," *AIChE J.*, vol. 64, no. 7, pp. 2592–2602, 2018.

- [41] O. Chumak *et al.*, "Plasma gasification of refuse derived fuel in a single-stage system using different gasifying agents," vol. 47, pp. 246–255, 2016.
- [42] L. Tang, H. Huang, H. Hao, and K. Zhao, "Development of plasma pyrolysis/gasification systems for energy efficient and environmentally sound waste disposal," *J. Electrostat.*, vol. 71, no. 5, pp. 839–847, 2013.
- [43] M. Minutillo, A. Perna, and D. Di Bona, "Modelling and performance analysis of an integrated plasma gasification combined cycle (IPGCC) power plant," *Energy Convers. Manag.*, vol. 50, no. 11, pp. 2837–2842, 2009.
- [44] A. Sanlisoy and M. O. Carpinlioglu, "A review on plasma gasification for solid waste disposal," *Int. J. Hydrogen Energy*, vol. 42, no. 2, pp. 1361–1365, 2017.
- [45] C. Tendero, C. Tixier, P. Tristant, J. Desmaison, and P. Leprince, "Atmospheric pressure plasmas : A review," *Spectrochim. Acta Part B At. Spectrosc.*, vol. 61, no. 1, pp. 2–30, 2006.
- [46] A. Fridman, *Plasma Chemistry*. New York: Cambridge University Press, 2008.
- [47] Y. Kalinci, A. Hepbasli, and I. Dincer, "Exergoeconomic analysis of hydrogen production from plasma gasification of sewage sludge using specific exergy cost method," *Int. J. Hydrogen Energy*, vol. 36, no. 17, pp. 11408–11417, 2011.
- [48] B. Ruj and S. Ghosh, "Technological aspects for thermal plasma treatment of municipal solid waste — A review," vol. 126, pp. 298–308, 2014.
- [49] S. Samal, "Thermal plasma technology : The prospective future in material processing," *J. Clean. Prod.*, vol. 142, pp. 3131–3150, 2017.
- [50] N. D. Couto, V. B. Silva, and A. Rouboa, "Thermodynamic Evaluation of Portuguese municipal solid waste gasification," *J. Clean. Prod.*, vol. 139, pp. 622–635, 2016.
- [51] G. H. Nordi, R. Palacios-Bereche, A. G. Gallego, and S. A. Nebra, "Electricity production from municipal solid waste in Brazil," *Waste Manag. Res.*, vol. 35, no. 7, pp. 1–12, 2017.
- [52] O. Chumak *et al.*, "Plasma gasification of refuse derived fuel in a single-stage system using different gasifying agents," *Waste Manag.*, vol. 47, pp. 246–255, 2016.
- [53] N. Indrawan, S. Mohammad, A. Kumar, and R. L. Huhnke, "Modeling low temperature plasma gasification of municipal solid waste," *Environ. Technol. Innov.*, vol. 15, pp. 1–12, 2019.
- [54] G. Galeno, M. Minutillo, and A. Perna, "From waste to electricity through integrated plasma gasification/fuel cell (IPGFC) system," *Int. J. Hydrogen Energy*, vol. 36, no. 2, pp. 1692–1701, 2011.

- [55] I. Janajreh, S. S. Raza, and A. S. Valmundsson, "Plasma gasification process: Modeling, simulation and comparison with conventional air gasification," *Energy Convers. Manag.*, vol. 65, pp. 801–809, 2013.
- [56] L. Mazzoni and I. Janajreh, "Plasma gasification of municipal solid waste with variable content of plastic solid waste for enhanced energy recovery," *Int. J. Hydrogen Energy*, vol. 42, no. 30, pp. 19446–19457, 2017.
- [57] A. Khuriati, W. S. Budi, M. Nur, I. Istadi, and G. Suwoto, "Modeling of Heating Value of Municipal Solid Waste Based on Ultimate Analysis Using Multiple Stepwise Regresion Linear in Semarang," *ARNP J. Eng. Appl. Sci.*, vol. 12, no. 9, pp. 2870–2876, 2017.
- [58] Q. Zhang, Y. Wu, L. Dor, W. Yang, and W. Blasiak, "A thermodynamic analysis of solid waste gasification in the Plasma Gasification Melting process," *Appl. Energy*, vol. 112, pp. 405–413, 2013.
- [59] J. Favas, E. Monteiro, and A. Rouboa, "Hydrogen production using plasma gasification with steam injection," *Int. J. Hydrogen Energy*, vol. 42, no. 16, pp. 10997–11005, 2017.
- [60] V. Galvita, V. E. Messerle, and A. B. Ustimenko, "Hydrogen production by coal plasma gasification for fuel cell technology," vol. 32, pp. 3899–3906, 2007.
- [61] B. J. Clark and M. J. Rogoff, "Economic feasibility of a plasma arc gasification plant, city of Marion,Iowa," in *18th Annual Noth American Waste-to-Energy Conference*, 2010.
- [62] Y. Byun *et al.*, "Hydrogen recovery from the thermal plasma gasification of solid waste," *J. Hazard. Mater.*, vol. 190, no. 1–3, pp. 317–323, 2011.
- [63] G. Zang, J. Jia, Y. Shi, T. Sharma, and A. Ratner, "Modeling and economic analysis of waste tire gasification in fluidized and fixed bed gasifiers," *Waste Manag.*, vol. 89, no. 1, pp. 201–211, 2019.
- [64] Secretaria de gestión y control territorial and Universidad de Medellín, "Plan de gestión integral de residuos sólidos del municipio de Medellín. Documento de actualización - parte 1," Medellín, 2015.
- [65] S. L. P. Velez and N. E. Mora, "System dynamics model for the municipal solid waste management system in the metropolitan area of Medellín, Colombia," *Int. J. Environ. Waste Manag.*, vol. 18, no. 2, p. 161, 2016.
- [66] A. M. Lozano *et al.*, "Refuse Derived Fuel (RDF) production and gasification in a pilot plant integrated with an otto cycle ICE through Aspen Plus™ modelling: Thermodynamic and economic viability," *Waste Manag.*, vol. 69, pp. 187–201, 2017.
- [67] H. Zhou, A. Meng, Y. Long, Q. Li, and Y. Zhang, "Classification and comparison of municipal solid waste based on thermochemical characteristics," *J. Air Waste Manag. Assoc.*, vol. 64, no. 5, pp. 597–616,

2014.

- [68] J. G. C. Balcazar, R. A. Dias, and J. A. P. Balestieri, "Analysis of hybrid waste-to-energy for medium-sized cities," *Energy*, vol. 55, pp. 728–741, 2013.
- [69] U. de M. Grupo de Extensión GEAR, "Estudio de producción y caracterización de residuos sólidos generados en el sector residencia y por estrato socioeconómico de la ciudad de Medellín y sus cinco corregimientos," Medellín, 2011.
- [70] U. de M. Grupo de Extensión GEAR, "Estudio de producción y caracterización de residuos sólidos generados en el sector no residencial de la ciudad de Medellín y sus cinco corregimientos," Medellín, 2012.
- [71] R. Barrera, C. Salazar, and J. F. Pérez, "Thermochemical Equilibrium Model of Synthetic Natural Gas Production from Coal Gasification Using Aspen Plus," *Int. J. Chem. Eng.*, vol. 2014, pp. 1–18, 2014.
- [72] R. Tavares, A. Ramos, and A. Rouboa, "A theoretical study on municipal solid waste plasma gasification," *Waste Manag.*, vol. 90, pp. 37–45, 2019.
- [73] A. Perna, M. Minutillo, and E. Jannelli, "Hydrogen from intermittent renewable energy sources as gasification medium in integrated waste gasification combined cycle power plants: A performance comparison," *Energy*, vol. 94, pp. 457–465, 2016.
- [74] A. Gagliano, F. Nocera, M. Bruno, and G. Cardillo, "Development of an Equilibrium-based Model of Gasification of Biomass by Aspen Plus," *Energy Procedia*, vol. 111, pp. 1010–1019, 2017.
- [75] L. Mazzoni, R. Ahmed, and I. Janajreh, "Plasma gasification of two waste streams: Municipal solid waste and hazardous waste from the oil and gas industry," *Energy Procedia*, vol. 105, pp. 4159–4166, 2017.
- [76] A. Perna, M. Minutillo, A. Lubrano, and E. Jannelli, "Combining plasma gasification and solid oxide cell technologies in advanced power plants for waste to energy and electric energy storage applications," *Waste Manag.*, vol. 73, pp. 424–438, 2018.
- [77] Aspen Technology Inc., "Aspen plus model for moving bed coal gasifier." Bedford, USA, 2010.
- [78] Y. A. Çengel, *Thermodynamics : an engineering approach*. Sixth edition. Boston : McGraw-Hill Higher Education, [2008] ©2008.
- [79] M. Ozdinc Carpinlioglu and A. Sanlisoy, "Performance assessment of plasma gasification for waste to energy conversion: A methodology for thermodynamic analysis," *Int. J. Hydrogen Energy*, vol. 43, no. 25, pp. 11493–11504, 2018.

- [80] S. A. Channiwala and P. P. Parikh, "A unified correlation for estimating HHV of solid, liquid and gaseous fuels," *Fuel*, vol. 81, no. 8, pp. 1051–1063, 2002.
- [81] Westinghouse Plasma Corporation, "Westinghouse plasma torch." .
- [82] T. J. Kotas, "The Exergy Method of Thermal Plant Analysis," T. J. Kotas, Ed. Butterworth-Heinemann, 1985, pp. 29–56, 267–269.
- [83] Solena Fuels Corporation, "One stage atmospheric pressure thermo-catalytic plasma gasification and vitrification of organic material such as biomass for the production of the renewable energy," WO 2014/126895 A2, 2014.
- [84] C. A. Estrada, A. Melgar, and J. F. Pérez, "Performance prediction of a decentralized power plant (120 kWe) using a multi-particle model of a downdraft biomass gasification process," *Energy Convers. Manag.*, vol. 181, no. September 2018, pp. 258–271, 2019.
- [85] K. P. Willis, S. Osada, and K. L. Willerton, "Plasma gasification: Lessons learned at ecovalley WTE facility," in *18th Annual North American Waste-to-Energy Conference, NAWTEC18*, 2010, pp. 133–140.
- [86] M. Bruck, P. Sandborn, and N. Goudarzi, "A Levelized Cost of Energy (LCOE) model for wind farms that include Power Purchase Agreements (PPAs)," *Renew. Energy*, vol. 122, pp. 131–139, 2018.
- [87] A. Castillo-Ramírez, D. Mejía-Giraldo, and J. D. Giraldo-Ocampo, "Geospatial levelized cost of energy in Colombia: GeoLCOE," *2015 IEEE PES Innov. Smart Grid Technol. Lat. Am. ISGT LATAM 2015*, pp. 298–303, 2016.
- [88] J. D. Saldarriaga-Loaiza, F. Villada, and J. F. Pérez, "Análisis de Costos Nivelados de Electricidad de Plantas de Cogeneración usando Biomasa Forestal en el Departamento de Antioquia, Colombia," *Inf. tecnológica*, vol. 30, no. 1, pp. 63–74, 2019.
- [89] DANE, "DANE (2020). Estadísticas por tema - Información para todos," 2020. [Online]. Available: <https://www.dane.gov.co/index.php/estadisticas-por-tema>).
- [90] J. M. Lopez Lezama, F. Villada, and N. Muñoz Galeano, "Effects of Incentives for Renewable Energy in Colombia," *Ing. y Univ.*, vol. 21, no. 2, pp. 257–272, 2017.
- [91] X. Song and Z. Guo, "Production of synthesis gas by co-gasifying coke and natural gas in a fixed bed reactor," *Energy*, vol. 32, no. 10, pp. 1972–1978, 2007.
- [92] H. E. Díez, I. N. Gómez, and J. F. Pérez, "Mass, energy, and exergy analysis of the microgasification process in a top-lit updraft reactor: Effects of firewood type and forced primary airflow," *Sustain. Energy Technol. Assessments*, vol. 29, pp. 82–91, 2018.

- [93] R. F. S. Paulino, A. M. Essiptchouk, and J. L. Silveira, "The use of syngas from biomedical waste plasma gasification systems for electricity production in internal combustion: Thermodynamic and economic issues," *Energy*, vol. 199, p. 117419, 2020.
- [94] G. Collodi, G. Azzaro, N. Ferrari, and S. Santos, "Demonstrating Large Scale Industrial CCS through CCU - A Case Study for Methanol Production," *Energy Procedia*, vol. 114, pp. 122–138, 2017.
- [95] Y. Byun, M. Cho, S. Hwang, and J. Chung, "Thermal plasma gasification of municipal solid waste," in *Gasification for practical applications*, Y. Yun, Ed. Rijeka, Croatia: InTech, 2012, pp. 183–210.
- [96] A. C. Medina Jimenez, R. P. Bereche, and S. Nebra, "Three municipal solid waste gasification technologies analysis for electrical energy generation in Brazil," *Waste Manag. Res.*, vol. 37, no. 6, pp. 631–642, 2019.
- [97] Congreso de Colombia, "Plan Nacional de Desarrollo 2018-2022 'Pacto por Colombia, Pacto por la Equidad.'" Bogotá, Colombia, 2018.
- [98] U.S. Energy Information Administration (EIA), "Natural gas weekly update," 2020. .
- [99] Unidad de planeación minero-energética (UPME), "Proyección de los precios de los energéticos para la generación eléctrica 2018-2040." .
- [100] International energy agency, "World energy outlook 2019," 2019. [Online]. Available: <https://www.iea.org/reports/world-energy-outlook-2019/electricity>. [Accessed: 03-Aug-2020].
- [101] XM S.A E.S.P, "Informe de operación del SIN y administración del mercado 2017," 2018. .
- [102] J. F. Pérez, A. F. Agudelo, and S. Ramos, "The impact of climate phenomenon 'el Niño' on energy cost and opportunities for bioenergy in Colombia," in *6th International Symposium of Energy from Biomass and Waste*, 2016.
- [103] BP plc, "68th edition of BP Statistical review of world energy," 2019. .
- [104] T. Atalla, J. Blazquez, L. C. Hunt, and B. Manzano, "Prices versus policy: An analysis of the drivers of the primary fossil fuel mix," *Energy Policy*, vol. 106, pp. 536–546, 2017.
- [105] Z. Shareefdeen, A. Elkamel, and S. Tse, "Review of current technologies used in municipal solid waste-to-energy facilities in Canada," *Clean Technol. Environ. Policy*, vol. 17, no. 7, pp. 1837–1846, 2015.
- [106] V. Zhovtyansky and V. Valincius, "Efficiency of Plasma Gasification Technologies for Hazardous Waste Treatment," in *Gasification for Low-grade Feedstock*, Y. Yun, Ed. London, UK: IntechOpen, 2018, pp. 165–189.

- [107] A. S. Valmundsson and I. Janajreh, "Plasma gasification process modeling and energy recovery from solid waste," in *5th International Conference on Energy Sustainability*, 2011, no. 54686, pp. 361–368.
- [108] R. Vecten, Simon; Herbert, Ben; Wilkinson, Michael; Shaw, Andrew; Bimbo, Nuno; Dawson, "Integrated plasma gasification and SOFC system simulation using Aspen Plus," in *13th European SOFC and SOE Forum*, 2018, pp. 1–10.
- [109] P. Breeze, "Energy from Waste," 1st ed., London: Academic Press, 2018, pp. 1–9.
- [110] A. Mountouris, E. Voutsas, and D. Tassios, "Plasma gasification of sewage sludge: Process development and energy optimization," *Energy Convers. Manag.*, vol. 49, no. 8, pp. 2264–2271, 2008.
- [111] I. B. Matveev, N. V. Washcilenko, S. I. Serbin, and N. A. Goncharova, "Integrated Plasma Coal Gasification Power Plant," *IEEE Trans. PLASMA Sci.*, vol. 41, no. 12, pp. 3195–3200, 2013.
- [112] A. Perna *et al.*, "From waste to electricity through integrated plasma gasification/fuel cell (IPGFC) system," *Energy Convers. Manag.*, vol. 36, no. 2, p. 100412, 2017.
- [113] T. Nakyai, S. Authayanun, Y. Patcharavorachot, and A. Arpornwichanop, "Exergoeconomics of hydrogen production from biomass air-steam gasification with methane co-feeding," *Energy Convers. Manag.*, vol. 140, pp. 228–239, 2017.
- [114] T. A. Jack and C. O. C. Oko, "Exergy and exergoeconomic analysis of a municipal waste-to-energy steam reheat power plant for Port Harcourt city," *Int. J. Ambient Energy*, vol. 39, no. 4, pp. 352–359, 2018.
- [115] A. Behzadi, E. Houshfar, E. Gholamian, M. Ashjaee, and A. Habibollahzade, "Multi-criteria optimization and comparative performance analysis of a power plant fed by municipal solid waste using a gasifier or digester," *Energy Convers. Manag.*, vol. 171, pp. 863–878, 2018.
- [116] Y. Casas Ledón, P. González, S. Concha, C. A. Zaror, and L. E. Arteaga-Pérez, "Exergoeconomic valuation of a waste-based integrated combined cycle (WICC) for heat and power production," *Energy*, vol. 114, pp. 239–252, 2016.
- [117] E. J. O. Promes, T. Woudstra, L. Schoenmakers, V. Oldenbroek, A. T. Thattai, and P. V Aravind, "Thermodynamic evaluation and experimental validation of 253 MW Integrated Coal Gasification Combined Cycle power plant in Buggenum , Netherlands," *Appl. Energy*, vol. 155, pp. 181–194, 2015.
- [118] M. Pérez-Fortes and A. D. Bojarski, "Syngas from waste: Emerging Technologies," 1st ed., L. Puigjaner, Ed. Barcelona: Springer, 2011, pp. 100–117.
- [119] Saddiq HA, Perry S, Ndagana SF, and Mohammed A, "Modelling of gas turbine and gas turbine exhaust

- and its utilisation as combined cycle in utility system," *Int. J. Sci. Eng. Res.*, vol. 6, no. 4, pp. 925–933, 2015.
- [120] Z. Liu and I. A. Karimi, "Simulating combined cycle gas turbine power plants in Aspen HYSYS," *Energy Convers. Manag.*, vol. 171, pp. 1213–1225, 2018.
- [121] Aspen Technology Inc., "Aspen physical property system - Physical Property Methods and Models 11.1," 2001.
- [122] A. F. Agudelo, "A thermoeconomic approach to CO₂ emissions from energy systems," Universidad de Zaragoza, 2011.
- [123] J. H. Turner, J. D. Mckenna, and W. M. Vatavuk, "Baghouses and Filters," *Particulate Matter Controls*, 1998. .
- [124] M. Pérez-Fortes, A. D. Bojarski, E. Velo, J. M. Nougués, and L. Puigjaner, "Conceptual model and evaluation of generated power and emissions in an IGCC plant," *Energy*, vol. 34, no. 10, pp. 1721–1732, 2009.
- [125] National Energy Technology Laboratory, "COS HYDROLYSIS." .
- [126] F. Banat, O. Younas, and I. Didarul, "Energy and exergetic dissection of a natural gas sweetening plant using methyldiethanol amine (MDEA) solution," *J. Nat. Gas Sci. Eng.*, vol. 16, pp. 1–7, 2014.
- [127] B. Suleiman, A. S. Abdulkareem, Y. O. Abdulsalam, U. Musa, A. S. Kovo, and I. A. Mohammed, "Thermoeconomic analysis of natural gas treatment process using triethanolamine (TEA) and diethanolamine (DEA) as gas sweeteners," *J. Nat. Gas Sci. Eng.*, vol. 36, pp. 184–201, 2016.
- [128] W. Lan, G. Chen, X. Zhu, X. Wang, C. Liu, and B. Xu, "Biomass gasification-gas turbine combustion for power generation system model based on ASPEN PLUS," *Sci. Total Environ.*, vol. 628–629, pp. 1278–1286, 2018.
- [129] M. P. Boyce, "Gas Turbine Engineering Handbook," Fourth Ed., Elsevier Science, 2012, pp. 427–490.
- [130] V. L. Eriksen and J. E. Schroeder, "Heat Recovery Steam Generator Technology," V. L. Eriksen, Ed. Woodhead Publishing, 2017, pp. 45–63.
- [131] P. Flohr and P. Stuttaford, "Modern Gas Turbine Systems," P. Jansohn, Ed. Woodhead Publishing, 2013, pp. 151–191.
- [132] M. P. Boyce, "Combined Cycle Systems for Near-Zero Emission Power Generation," A. D. Rao, Ed. Woodhead Publishing, 2012, pp. 44–102.

- [133] A. Valero and C. Torres, "Thermoeconomic Analysis," *Exergy, Energy Syst. Anal. Optim. - Encycl. Life Support Syst.*, pp. 1–32, 1994.
- [134] A. Valero *et al.*, "On the thermoeconomic approach to the diagnosis of energy system malfunctions. Part 2. Malfunction definitions and assessment," *Energy*, vol. 29, pp. 1889–1907, 2004.
- [135] A. Valero, M. Lozano, and L. Serra, "CGAM problem: Definition and conventional solution," *Energy*, vol. 19, no. 3, pp. 279–286, 1994.
- [136] M. Lozano and A. Valero, "Theory of exergetic cost," *Energy*, vol. 18, no. 9, pp. 939–960, 1993.
- [137] A. Agudelo, A. Valero, and C. Torres, "Allocation of waste cost in thermoeconomic analysis," *Energy*, vol. 45, no. 1, pp. 634–643, 2012.
- [138] A. Valero, M. Lozano, and M. Munoz, "A general theory of exergy saving. On the exergetic cost," in *Computer-Aided Engineering and Energy Systems Vol. 3: Second Law Analysis and Modelling*, R. A. Gaglioli, Ed. New York, USA: The American Society of Mechanical Engineers.
- [139] W. Eisermann, P. Johnson, and W. L. Conger, "Estimating thermodynamic properties of coal, char, tar and ash," *Fuel Process. Technol.*, vol. 3, no. 1, pp. 39–53, 1980.
- [140] C. Finet, "Heating Value of Municipal Solid Waste," *Waste Manag. Res.*, vol. 5, no. 1, pp. 141–145, 1987.
- [141] J. L. Silveira and C. E. Tuna, "Thermoeconomic analysis method for optimization of combined heat and power systems. Part I," *Prog. Energy Combust. Sci.*, vol. 29, no. 6, pp. 479–485, 2003.
- [142] J. F. Pérez, L. F. Osorio, and A. F. Agudelo, "A Technical-economic analysis of wood gasification for decentralized power generation in Colombian forest cores," *Int. J. Renew. energy Res.*, vol. 8, no. 2, pp. 1071–1083, 2018.
- [143] Banco de la República (Banco Central de Colombia), "Consumer Price Index." .
- [144] Empresas Varias de Medellín S.A. E.S.P, "Tarifas segundo semestre de 2019," 2019. .
- [145] F. Bellomare and M. Rokni, "Integration of a municipal solid waste gasification plant with solid oxide fuel cell and gas turbine," *Renew. Energy*, vol. 55, pp. 490–500, 2013.
- [146] S. O. Oyedepo, R. O. Fagbenle, S. S. Adefila, and M. M. Alam, "Thermoeconomic and thermoenviromonic modeling and analysis of selected gas turbine power plants in Nigeria," *Energy Sci. Eng.*, vol. 3, no. 5, pp. 423–442, 2015.
- [147] A. Almutairi, P. Pilidis, and N. Al-Mutawa, "Energetic and exergetic analysis of combined cycle power plant: Part-1 operation and performance," *Energies*, vol. 8, no. 12, pp. 14118–14135, 2015.

- [148] V. Mrzljak, T. Senčić, and B. Žarković, "Turbogenerator Steam Turbine Variation in Developed Power: Analysis of Exergy Efficiency and Exergy Destruction Change," *Model. Simul. Eng.*, vol. 2018, pp. 1–12, 2018.
- [149] Y. Jiang and D. Bhattacharyya, "Techno-economic analysis of direct coal-biomass to liquids (CBTL) plants with shale gas utilization and CO₂ capture and storage (CCS)," *Appl. Energy*, vol. 189, pp. 433–448, 2017.
- [150] A. Kazemi, M. Malayeri, A. Gharibi kharaji, and A. Shariati, "Feasibility study, simulation and economical evaluation of natural gas sweetening processes - Part 1: A case study on a low capacity plant in iran," *J. Nat. Gas Sci. Eng.*, vol. 20, pp. 16–22, 2014.
- [151] D. A. Bell, B. F. Towler, and M. Fan, *Coal Gasification and Its Applications*. Elsevier Science, 2010.
- [152] XM, "Precio de bolsa y escasez." .
- [153] A. Arsalis, "Thermoeconomic modeling and parametric study of hybrid SOFC-gas turbine-steam turbine power plants ranging from 1.5 to 10 MWe," *J. Power Sources*, vol. 181, no. 2, pp. 313–326, 2008.
- [154] C. A. Frangopoulos, "Application of the thermoeconomic functional approach to the CGAM problem," *Energy*, vol. 19, no. 3, pp. 323–342, 1994.
- [155] J. Manninen and X. X. Zhu, "Optimal flowsheeting synthesis for power station design considering overall integration," *Energy*, vol. 24, no. 6, pp. 451–478, 1999.
- [156] M. L. N. M. Carneiro and M. S. P. Gomes, "Energy, exergy, environmental and economic analysis of hybrid waste-to-energy plants," *Energy Convers. Manag.*, vol. 179, pp. 397–417, 2019.
- [157] H. Dominic, "Costs for Municipal Waste Management in the UE," 2002.